Spring 5-15-2018

Correlated Variability and Adaptation in Orbitofrontal Cortex during Economic Choice

Katherine E. Conen
Washington University in St. Louis

WASHINGTON UNIVERSITY IN ST. LOUIS

Division of Biology and Biomedical Sciences
Neurosciences

Dissertation Examination Committee:
Camillo Padoa-Schioppa, Chair
Martha Bagnall
Todd Braver
Timothy Holy
Lawrence Snyder

Correlated Variability and Adaptation in Orbitofrontal Cortex during Economic Choice

by
Katherine Conen

A dissertation presented to
The Graduate School
of Washington University in
partial fulfillment of the
requirements for the degree
of Doctor of Philosophy

May 2018
St. Louis, Missouri

Table of Contents

List of Figures

List of Tables

Acknowledgments

The work leading to this dissertation was made possible by the outstanding support and mentorship of my adviser, Dr. Camillo Padoa-Schioppa. Comments from my thesis committee provided valuable advice and feedback during all stages of this project. Thanks to members of the Padoa-Schioppa lab for providing helpful discussion and making the lab an intellectually exciting place to be. Special gratitude goes to to our lab manager, Heide Schocknecht, who consistently made the lab environment run more smoothly. Additional thanks go to the Neuroscience Program Directors, past and present; and to Sally Vogt, whose incomparable help as Program Coordinator made it possible to navigate the graduate school process from beginning to end.

The research presented in this document was funded by NIH grants F31-MH107111 and T32-GM008151.

Special thanks to the Washington University Graduate School for allowing us to use their dissertation and thesis template as a starting point for the development of this document.

Katherine Conen

Washington University in St. Louis

May 2018

ABSTRACT OF THE DISSERTATION

Correlated Variability and Adaptation in Orbitofrontal Cortex during Economic Choice

for Arts & Sciences Graduate Students

by

Katherine Conen

Doctor of Philosophy in Biology and Biomedical Sciences

Neurosciences

Washington University in St. Louis, 2018

Professor Camillo Padoa-Schioppa, Chair

Economic decision-making requires the computation and comparison of subjective values. Several lines of evidence suggest that these processes are mediated by circuits in orbitofrontal cortex (OFC). Neurons in OFC encode the subjective values of choice options and outcomes, and damage to this area leads to selective deficits in value-guided behavior. To understand the nature of choice more thoroughly, it is useful to consider the features of OFC circuits that can limit or enhance information processing. In this document, I present work examining two factors that influence encoding in OFC: noise correlation and value adaptation. In the first study, I show that noise correlations in OFC are small but non-negligible, and that the structure of these correlations constrains the resolution of value representation in OFC. I go on to show that correlation structure predicts a weak relationship between single-neuron variability and decision outcomes in the context of a uniform linear model of decision making. These findings are

consistent with empirical data and support the hypothesis that OFC mediates value-based decision-making. In the second study, I investigate how neurons in OFC adapt to changes in the value distribution. I show that neurons adapt to both maximum and minimum available values, but that the dynamic range does not completely remap across conditions. While intermediate adaptation is sub-optimal, it indicates that OFC neurons can partially compensate for changes in the scale of decisions, allowing increased resolution of value encoding in high-magnitude conditions. In summary, decision-making may be limited by correlated noise, but the effect of this constraint is relatively small. Moreover, variability introduced by noise correlation may be partially ameliorated by adaptation to the value range.

Chapter 1: Limitation and Enhancement of Information Coding in Valuation Circuits

Throughout their lives, people regularly face decisions that rely on their subjective evaluation of different options. These choices, known as economic decisions, can cover a wide variety of contexts, ranging from the trivial (*what socks should I wear today?*) to the life-changing (*should I move to Europe?*). To make a choice, the subject must identify relevant options, compute each option's value, and compare these values to select the best outcome. The effectiveness of these processes depends on the nature of the neural systems that mediate them. In this work, I investigate the properties of neurons in macaque orbitofrontal cortex (OFC), a region associated with value-based decision making. I examine two factors that influence the efficiency of neural encoding: noise correlation and range adaptation. Noise correlation limits the information that can be encoded in neural circuits, potentially impairing economic choice. In contrast, adaptation can improve the resolution of value representation across contexts, reducing the effects of noise.

I will begin this chapter with an overview of the work linking OFC to economic choice. Next, I introduce the concept of noise correlation and discuss its relationship to information encoding. Finally, I discuss neuronal adaptation and its features in various neural circuits. In Chapters 2-3, I describe two studies analyzing these principles in the context of decision-related networks in orbitofrontal cortex (OFC). Chapter 2 presents an analysis of noise correlation and choice probability (previously published in Conen and Padoa-Schioppa 2015). Chapter 3 describes an experiment measuring how neurons in OFC adapt to changes in the recent value distribution. I will revisit these concepts in Chapter 4, where I bring together concepts from the first three

chapters, relating noise correlations and adaptation in OFC to behavioral performance during value-based decision making.

1.0 Contributions and Copyright Information

The studies described in Chapter 2-3 were designed in consultation with my thesis adviser, Dr. Camillo Padoa-Schioppa. Chapter 2 presents a study analyzing data from previous experiments. Data in these experiments were collected by Camillo Padoa-Schioppa at Harvard Medical School and were first published in (Padoa-Schioppa and Assad 2006) and (Padoa-Schioppa and Assad 2008). I collected the data for the experiment presented in Chapter 3 and conducted all analyses for both experiments.

Chapter 2 was previously published in the Journal of Neurophysiology (Conen and Padoa-Schioppa 2015). It is reproduced here with permission from the co-author. Its inclusion here is consistent with American Physiological Society guidelines, which allow the use of published articles in dissertations and thesis repositories.

1.1 Orbitofrontal Cortex and Economic Choice

Several lines of evidence suggest that value computation and comparison occur in OFC. OFC receives anatomical inputs across a wide range of sensory and limbic regions (Ongur and Price 2000), making it well-situated to integrate sensory inputs and motivational state (Padoa-Schioppa and Conen 2017). In human patients, lesions in OFC and the neighboring ventromedial prefrontal cortex (vmPFC) are associated with inconsistency in preferences and a lack of sensitivity to value feedback (Fellows and Farah 2007; Camille et al. 2011; Fellows 2011). In rodents and primates, lesions of OFC impair behavior in a reinforcer devaluation task, a goal-directed behavior that relies on the subjects' ability to modulate value computations based on

their current state (Gallagher et al. 1999; Izquierdo 2004; Rudebeck and Murray 2011; West et al. 2011). Deficits in devaluation suggest that OFC-lesioned animals rely on fixed values that have been stored in memory; they cannot compute values online.

Additional evidence for the role of OFC in economic choice comes from primate neurophysiology. Several experiments in primates have found that responses in OFC encode the value of choice options and outcomes (Padoa-Schioppa and Assad 2006; Abe and Lee 2011; Padoa-Schioppa 2013). Imaging studies have extended these results to humans, observing BOLD correlates of value in OFC and vmPFC (Cox and Kable 2014; Howard et al. 2015; Zhang et al. 2017). Notably, responses in OFC reflect the subjective nature of value, not objective characteristics of the reward (Padoa-Schioppa and Assad 2006; Raghuraman and Padoa-Schioppa 2014), and they integrate multiple features of the reward (Roesch and Olson 2005; Raghuraman and Padoa-Schioppa 2014). Studies from our group have found that different groups of neurons encode different variables during a juice choice task, namely the value of particular options (*offer value*), the value of the chosen option (*chosen value*), and the identity of the choice (*chosen juice*) (Padoa-Schioppa 2013). These categories remain consistent even when the set of available offers changes (Xie and Padoa-Schioppa 2016), suggesting a that there is a stable circuit for decision-making in OFC. Theoretical work supports the plausibility of such a circuit. Several distinct models of choice predict neural responses that closely resemble the three groups of cells identified empirically (Solway and Botvinick 2012; Rustichini and Padoa-Schioppa 2015; Friedrich and Lengyel 2016; Song et al. 2017). Taken together, this body of work provides strong support for the hypothesis that OFC plays a central role in value-based decision making.

1.2 Noise Correlations and Information Processing

The responses of an individual neuron vary widely, even under identical behavioral conditions. Researchers often compensate for this fact by averaging neural activity across trials. However, while this enables clean analysis of neural tuning, it misses a key feature of neuronal variability: namely, that activity fluctuations are correlated across the population. This phenomenon is generally called "noise correlation." Importantly, it refers to correlations in the residual activity from trial to trial, not similarities in the mean response function.

Noise correlations have been observed across a wide range of brain regions (Zohary et al. 1994; Lee et al. 1998; Constantinidis and Goldman-Rakic 2002; Averbeck and Lee 2003; Romo et al. 2003; Cohen and Maunsell 2009; Cohen and Kohn 2011; Gu et al. 2011; Jeanne et al. 2013; Smith and Sommer 2013). In sensory regions, pairs of neurons often have correlations on the order of 0.1-0.2, though some experiments suggest that these values are artificially high, reflecting either task demands or use of anesthesia (Ecker et al. 2010, 2014). Nevertheless, even when pairwise correlations are weak, the overall network state can be substantially affected by this shared variability (Schneidman et al. 2006). Furthermore, the effect of correlations on information encoding depends more on the pattern of correlation than its absolute magnitude (Abbott and Dayan 1999; Moreno-Bote et al. 2014).

Interest in noise correlations has consistently been tied to the question of population information. One of the first studies of noise correlations sought to explain why monkeys' psychophysical performance on a motion detection task was no better (and was in fact sometimes worse) than the performance derived for the best individual neurons in MT (Britten et al. 1992; Zohary et al. 1994). They reasoned that noise correlations between similarly tuned neurons could not be

removed by averaging across the population, thereby limiting the benefit of pooling across cells. Notably, this limitation would only exist if correlations were higher for cells with similar preferred directions, a correlation structure known as “limited-range correlation” (Kohn et al. 2016). Building on this principle, (Abbott and Dayan 1999) proved that limited-range correlations cause information to saturate in neural populations even as the size of the network increased. More recent work has demonstrated that this is only true when tuning functions are homogenous across a population. In networks where tuning curves vary in shape or amplitude, information continues to increase with population size, although for any given network size it may still be reduced by correlation (Ecker et al. 2011). Notably, a correlation structure known as “differential correlation” does cause information saturation even in heterogenous networks (Moreno-Bote et al. 2014). Differential correlation describes noise correlation that is proportional to the derivative of the tuning functions of pairs of neurons. Measuring these patterns empirically is challenging, but they can be detected in large simultaneously-recorded data sets using a decoding method (Moreno-Bote et al. 2014), and information-limiting correlations have been identified in vestibular coding using this approach (Pitkow et al. 2015).

The work described above addresses theoretical upper limits on population information. Frequently, these analyses assume that the decoding mechanism makes optimal use of the population structure and pattern of correlations to interpret neuronal activity (Ecker et al. 2010; Haefner et al. 2013). This assumption may not be realistic. When it does not hold, the practical impact of noise correlations increases (Beck et al. 2011; Ecker et al. 2011; Moreno-Bote et al. 2014; Pitkow et al. 2015). In this scenario, it is somewhat imprecise to attribute the information loss to noise; it is more accurately described as the results of an algorithmic suboptimality (Beck et al. 2012). However, these suboptimalities amplify the effects of noise in the circuit, so that

reducing noise – or noise correlation – leads to measurable improvements in performance. Indeed, several studies have observed a robust relationship between decreases in noise correlation and increases in behavioral performance mediated by learning and attention (Cohen and Maunsell 2009; Gu et al. 2011; Jeanne et al. 2013; Ni et al. 2018).

It is worth noting that suboptimality in decoding may be unavoidable. Optimal decoding requires a complete representation of the statistical structure of the environment, which may be too computationally complex to specify and to implement (Beck et al. 2011). When this is the case, changes in noise correlation, tuning slope, and overall variability provide more accessible mechanisms for behavioral improvement. Nevertheless, the assumption that noise correlations are always detrimental should be viewed with caution. Depending on the nature of the decoder, correlations may even increase behavioral efficiency in certain contexts (da Silveira et al. 2014; Haefner et al. 2016).

Interestingly, the relationship between single-neuron responses and behavioral choice can reveal information loss that arises from either suboptimal decoding or information-limiting correlations (Haefner et al. 2013; Pitkow et al. 2015). Studies in several sensory regions have observed a correlation between the variability in single neurons and the animal's choice in a perceptual decision (Britten et al. 1996; Romo et al. 2002; Nienborg and Cumming 2006; Liu et al. 2013). This relationship, termed choice probability or choice correlation, depends on the existence of noise correlations (Shadlen et al. 1996; Cohen and Maunsell 2009; Haefner et al. 2013). Choice probabilities can arise either from information-limiting correlations under an optimal read-out or from a non-limiting correlation structure with a suboptimal decoder. Distinguishing between these scenarios provides valuable information about the types of computations a network performs, as the weights of different neurons in decoding are substantially different under

optimal vs. correlation-blind decoders (Haefner et al. 2013; Pitkow et al. 2015). Notably, different decoding strategies predict different patterns of choice probability as a function of noise correlation (Haefner et al. 2013; Pitkow et al. 2015). Thus, the pattern and magnitude of choice probabilities can be used to assess the nature of the choice decoder. Moreover, even when the ability to infer decoding strategies is limited, the presence of choice probabilities in a network reveals the existence of correlation-related loss of information.

In Chapter 2, I present the results from an analysis of noise correlations and choice probabilities in OFC. I find that correlations are small, but range-limited – i.e. they are higher for neurons with the same preferred value. I relate noise correlations to empirically measures of choice probability, finding that the levels of choice probability we observe are consistent with a simple pooling model population decoding. Importantly, while range-limited correlations are not information-limiting in the context of optimal decoding, they do constrain population information when activity is read out in a uniform way (Ecker et al. 2011; Haefner et al. 2013). The pattern of noise correlations and choice probabilities I observe suggests that noise correlations and suboptimal choice decoding interact to limit value information in OFC.

1.3 Neuronal Adaptation

1.3.1 Sensory Adaptation and Efficient Coding

Neuronal responses properties are influenced by recent history. This phenomenon has been observed across all levels of the nervous system and occurs across a wide range of time scales, from milliseconds to hours or days (Fairhall et al. 2001; Kohn 2007; Hengen et al. 2013; Haak et al. 2014; Liu et al. 2016). In sensory systems, adaptation allows neurons to adjust to the current stimulus environment. Classic studies of sensory adaptation primarily examined suppression of

responses following exposure to an adaptor, frequently producing a horizontal shift in the response function (Ohzawa et al. 1982; Dean 1983; Hammond et al. 1988; Bonds 1991). These effects were mediated by changes in the gain and threshold of neuronal response functions, often through cell-intrinsic mechanisms (Sanchez-Vives and McCormick 2000; Sanchez-Vives et al. 2000; Ladenbauer et al. 2014), and could occur independently across different levels of the processing hierarchy (Kohn and Movshon 2003). Later experiments grew interested in adaptation to the distribution of stimuli (Fairhall et al. 2001; Nagel and Doupe 2006; Díaz-Quesada and Maravall 2008; Gutnisky and Dragoi 2008; Solomon and Kohn 2014; Liu et al. 2016). Adaptation of this sort requires both enhancement and suppression of responses across the stimulus distribution, and it frequently involves circuit-level mechanism as well as cell-intrinsic effects (Hô and Destexhe 2000; Wainwright et al. 2001; Chance et al. 2002; Carandini and Heeger 2011; Solomon and Kohn 2014; Natan et al. 2017).

Adaptation to the response distribution relates closely to the concept of efficient coding (Fairhall et al. 2001; Wark et al. 2007; Barlow 2012). The efficient coding hypothesis proposes that the purpose of adaptation is to maximize the transmission of sensory information (Louie and Glimcher 2012). It predicts that the dynamic range of responses should remap in to match the cumulative density function of the stimulus distribution (Wark et al. 2007). Interestingly, this process not only maximizes the resolution of sensory encoding, but also leads to a constant mean response level across different stimulus distributions, a feature that maintains network homeostasis (Benucci et al. 2013). Efficient coding reduces the redundancy of representations, and in principle it should improve behavior in perceptual tasks (Louie and Glimcher 2012). However, only a few experiments have directly related neuronal adaptation to behavioral improvement (Krekelberg et al. 2006; Liu et al. 2016). Furthermore, efficient coding is

inconsistent with other forms of functionally beneficial adaptation, such the improved novelty detection associated with repetition suppression (Boehnke et al. 2011; Malmierca et al. 2015). In general, the efficient coding hypothesis is most applicable in contexts that benefit from maximize information across all stimuli. Its predictions should be viewed with caution when this assumption does not apply.

1.3.2 Adaptation in Value-Encoding Regions

While most research on adaptation has focused on sensory systems, several studies have found evidence of adaptive coding in value-related responses as well. An early experiment recording from primate OFC found that the responses of individual neurons to the same reward-associated stimulus varied depending on whether that reward was the better or worse option in the current condition (Tremblay and Schultz 1999). These results provided the first suggestion that the gain of response functions in OFC might vary with the distribution of available rewards. However, this study could not distinguish between adaptation in the gain of encoding versus remapping to a new preferred stimulus under different reward contexts. When the role of OFC in value encoding was more clearly established, the possibility of value adaptation was tested more explicitly. An analysis by (Padoa-Schioppa 2009) found that neurons encoding the values of offers and chosen options during a juice choice task had a steeper encoding slope in conditions with a narrower range of available offers. A separate experiment found that the gain of value-encoding neurons adapted to changes in the variance of the reward distribution, again showing steeper encoding during narrower range conditions (Kobayashi et al. 2010). Imaging studies extended these results to human subjects, finding adaptation in BOLD correlates of value across several brain regions, including (Breiter et al. 2001; Nieuwenhuis et al. 2005; Cox and Kable 2014; Burke et al. 2016).

These results were analogous to findings in sensory systems finding adaptation to the variance of the stimulus distribution (Fairhall et al. 2001; Nagel and Doupe 2006; Díaz-Quesada and Maravall 2008; Liu et al. 2016), a necessary feature of efficient coding (Wark et al. 2007; Louie and Glimcher 2012). However, these studies left several open questions about the nature of value adaptation. First, changes in the range of value always entailed a corresponding change in the value maximum, making it impossible to determine which of these features neurons adapted to. Furthermore, these analyses looked at changes in the gain of value encoding but did not test for changes in activity levels overall. This limits their ability to detect whether the dynamic range was consistent across contexts, one prediction of the efficient coding hypothesis (Wark et al. 2007; Louie and Glimcher 2012). In chapter 3, I present an experiment that addresses these questions in value-encoding cells in OFC. I show that while neurons do adapt to the range of values, as determined by both the maximum and minimum, they do not completely remap their dynamic range, violating predictions of both the traditional efficient coding hypothesis (Wark et al. 2007; Barlow 2012) and a model of adaptation efficiency in value-based choice (Rustichini et al. 2017).

1.4 Summary

In the following chapters, I will present experimental results on the properties of noise correlation and value adaptation in the macaque OFC. In Chapter 2, I focus on noise correlations and their relationship to choice probability in OFC. The presence of these correlations imposes a limit on information coding in OFC. Chapter 3 describes adaptation to the maximum and minimum values during a juice choice task. I find that adaptation does not involve complete remapping of the dynamic range of responses. Nevertheless, changes in both maximum and minimum values induce adaptation in the gain of encoding. In Chapter 4, I bring these concepts

together, presenting a brief discussion of how adaptation compensates for correlation-imposed noise in value-encoding networks, potentially facilitating decision-making across a wide variety of scales.

1.5 References

Abbott LF, **Dayan P**. The Effect of Correlated Variability on the Accuracy of a Population Code. *Neural Comput* 11: 91–101, 1999.

Abe H, **Lee D**. Distributed Coding of Actual and Hypothetical Outcomes in the Orbital and Dorsolateral Prefrontal Cortex. *Neuron* 70: 731–741, 2011.

Averbeck BB, **Lee D**. Neural Noise and Movement-Related Codes in the Macaque Supplementary Motor Area [Online]. *J Neurosci* 23: 7630–7641, 2003. http://www.jneurosci.org/content/23/20/7630.short [21 Mar. 2014].

Barlow HB. Possible Principles Underlying the Transformations of Sensory Messages. In: *Sensory Communication*, p. 216–234.

Beck JM, **Latham PE**, **Pouget A**. Marginalization in Neural Circuits with Divisive Normalization. *J Neurosci* 31: 15310–15319, 2011.

Beck JM, **Ma WJ**, **Pitkow X**, **Latham PE**, **Pouget A**. Not noisy, just wrong: the role of suboptimal inference in behavioral variability. *Neuron* 74: 30–9, 2012.

Benucci A, **Saleem AB**, **Carandini M**. Adaptation maintains population homeostasis in primary visual cortex. *Nat Neurosci* 16: 724–9, 2013.

Boehnke SE, **Berg DJ**, **Marino RA**, **Baldi PF**, **Itti L**, **Munoz DP**. Visual adaptation and novelty responses in the superior colliculus. *Eur J Neurosci* 34: 766–779, 2011.

Bonds AB. Temporal dynamics of contrast gain in single cells of the cat striate cortex. *Vis Neurosci* 6: 239–255, 1991.

Breiter HC, **Aharon I**, **Kahneman D**, **Dale A**, **Shizgal P**. Functional imaging of neural responses to expectancy and experience of monetary gains and losses. *Neuron* 30: 619–639, 2001.

Britten KH, **Newsome WT**, **Shadlen MN**, **Celebrini S**, **Movshon JA**. A relationship between behavioral choice and the visual responses of neurons in macaque MT. *Vis Neurosci* 13: 87–100, 1996.

Britten KH, **Shadlen MN**, **Newsome WT**, **Movshon J a**. The analysis of visual motion: a comparison of neuronal and psychophysical performance. *J Neurosci* 12: 4745–4765, 1992.

Burke CJ, **Baddeley M**, **Tobler PN**, **Schultz W**. Partial Adaptation of Obtained and Observed

Value Signals Preserves Information about Gains and Losses. *J Neurosci* 36: 10016–10025, 2016.

Camille N, **Griffiths CA**, **Vo K**, **Fellows LK**, **Kable JW**. Ventromedial Frontal Lobe Damage Disrupts Value Maximization in Humans. *J Neurosci* 31: 7527–7532, 2011.

Carandini M, **Heeger DJ**. Normalization as a canonical neural computation. *Nat Rev Neurosci* 13: 51–62, 2011.

Chance FS, **Abbott L.**, **Reyes AD**. Gain Modulation from Background Synaptic Input. *Neuron* 35: 773–782, 2002.

Cohen MR, **Kohn A**. Measuring and interpreting neuronal correlations. *Nat Neurosci* 14: 811–9, 2011.

Cohen MR, **Maunsell JHR**. Attention improves performance primarily by reducing interneuronal correlations. *Nat Neurosci* 12: 1594–600, 2009.

Constantinidis C, **Goldman-Rakic PS**. Correlated discharges among putative pyramidal neurons and interneurons in the primate prefrontal cortex. *J Neurophysiol* 88: 3487–97, 2002.

Cox KM, **Kable JW**. BOLD Subjective Value Signals Exhibit Robust Range Adaptation. *J Neurosci* 34: 16533–16543, 2014.

Dean AF. Adaptation-induced alteration of the relation between response amplitude and contrast in cat striate cortical neurones. *Vision Res* 23: 249–256, 1983.

Díaz-Quesada M, **Maravall M**. Intrinsic mechanisms for adaptive gain rescaling in barrel cortex. *J Neurosci* 28: 696–710, 2008.

Ecker AS, **Berens P**, **Cotton RJ**, **Subramaniyan M**, **Denfield GH**, **Cadwell CR**, **Smirnakis SM**, **Bethge M**, **Tolias AS**. State dependence of noise correlations in macaque primary visual cortex. *Neuron* 82: 235–248, 2014.

Ecker AS, **Berens P**, **Keliris GA**, **Bethge M**, **Logothetis NK**, **Tolias AS**. Decorrelated neuronal firing in cortical microcircuits. *Science* 327: 584–7, 2010.

Ecker AS, **Berens P**, **Tolias AS**, **Bethge M**. The effect of noise correlations in populations of diversely tuned neurons. *J Neurosci* 31: 14272–83, 2011.

Fairhall AL, **Lewen GD**, **Bialek W**, **De Ruyter van Steveninck RR**. Efficiency and ambiguity in an adaptive neural code. *Nature* 412: 787–792, 2001.

Fellows LK. Orbitofrontal contributions to value-based decision making: Evidence from humans with frontal lobe damage. *Ann N Y Acad Sci* 1239: 51–58, 2011.

Fellows LK, **Farah MJ**. The role of ventromedial prefrontal cortex in decision making: Judgment under uncertainty or judgment per se? *Cereb Cortex* 17: 2669–2674, 2007.

Friedrich J, **Lengyel M**. Goal-Directed Decision Making with Spiking Neurons. *J Neurosci* 36:

1529–1546, 2016.

Gallagher M, **McMahan RW**, **Schoenbaum G**. Orbitofrontal cortex and representation of incentive value in associative learning. *J Neurosci* 19: 6610–6614, 1999.

Gu Y, **Liu S**, **Fetsch CR**, **Yang Y**, **Fok S**, **Sunkara A**, **DeAngelis GC**, **Angelaki DE**. Perceptual learning reduces interneuronal correlations in macaque visual cortex. *Neuron* 71: 750–61, 2011.

Gutnisky DA, **Dragoi V**. Adaptive coding of visual information in neural populations. *Nature* 452: 220–4, 2008.

Haak KV, **Fast E**, **Bao M**, **Lee M**, **Engel SA**. Four Days of Visual Contrast Deprivation Reveals Limits of Neuronal Adaptation. *Curr Biol* 24: 2575–2579, 2014.

Haefner RM, **Berkes P**, **Fiser J**. Perceptual Decision-Making as Probabilistic Inference by Neural Sampling. *Neuron* 90: 649–660, 2016.

Haefner RM, **Gerwinn S**, **Macke JH**, **Bethge M**. Inferring decoding strategies from choice probabilities in the presence of correlated variability. *Nat Neurosci* 16: 235–42, 2013.

Hammond P, **Mouat GS V**, **Smith AT**. Neural correlates of motion after-effects in cat striate cortical neurones: monocular adaptation [Online]. *Exp Brain Res* 72: 1–20, 1988. https://link.springer.com/content/pdf/10.1007/BF00248495.pdf [23 Feb. 2018].

Hengen KB, **Lambo ME**, **Van Hooser SD**, **Katz DB**, **Turrigiano GG**. Firing Rate Homeostasis in Visual Cortex of Freely Behaving Rodents. *Neuron* 80: 335–342, 2013.

Hô N, **Destexhe A**. Synaptic Background Activity Enhances the Responsiveness of Neocortical Pyramidal Neurons. *J Neurophysiol* 84: 1488–1496, 2000.

Howard JD, **Gottfried JA**, **Tobler PN**, **Kahnt T**. Identity-specific coding of future rewards in the human orbitofrontal cortex. *Proc Natl Acad Sci* 112: 5195–5200, 2015.

Izquierdo A. Bilateral Orbital Prefrontal Cortex Lesions in Rhesus Monkeys Disrupt Choices Guided by Both Reward Value and Reward Contingency. *J Neurosci* 24: 7540–7548, 2004.

Jeanne JM, **Sharpee TO**, **Gentner TQ**. Associative learning enhances population coding by inverting interneuronal correlation patterns. *Neuron* 78: 352–63, 2013.

Kobayashi S, **Pinto de Carvalho O**, **Schultz W**. Adaptation of reward sensitivity in orbitofrontal neurons. *J Neurosci* 30: 534–544, 2010.

Kohn A. Visual Adaptation: Physiology, Mechanisms, and Functional Benefits. *J Neurophysiol* 97: 3155–3164, 2007.

Kohn A, **Coen-Cagli R**, **Kanitscheider I**, **Pouget A**. Correlations and Neuronal Population Information. *Annu Rev Neurosci* 39: 237–256, 2016.

Kohn A, **Movshon JA**. Neuronal adaptation to visual motion in area MT of the macaque.

Neuron 39: 681–691, 2003.

Krekelberg B, **van Wezel RJA**, **Albright TD**. Adaptation in Macaque MT Reduces Perceived Speed and Improves Speed Discrimination. *J Neurophysiol* 95: 255–270, 2006.

Ladenbauer J, **Augustin M**, **Obermayer K**. How adaptation currents change threshold, gain, and variability of neuronal spiking. *J Neurophysiol* 111: 939–953, 2014.

Lee D, **Port NL**, **Kruse W**, **Georgopoulos AP**. Variability and Correlated Noise in the Discharge of Neurons in Motor and Parietal Areas of the Primate Cortex [Online]. *J Neurosci* 18: 1161–1170, 1998. http://www.jneurosci.org/content/18/3/1161.short [21 Mar. 2014].

Liu B, **Macellaio M V.**, **Osborne LC**. Efficient sensory cortical coding optimizes pursuit eye movements. *Nat Commun* 7: 12759, 2016.

Liu S, **Gu Y**, **DeAngelis GC**, **Angelaki DE**. Choice-related activity and correlated noise in subcortical vestibular neurons. *Nat Neurosci* 16: 89–97, 2013.

Louie K, **Glimcher PW**. Efficient coding and the neural representation of value. *Ann N Y Acad Sci* 1251: 13–32, 2012.

Malmierca MS, **Anderson LA**, **Antunes FM**. The cortical modulation of stimulus-specific adaptation in the auditory midbrain and thalamus: a potential neuronal correlate for predictive coding. *Front Syst Neurosci* 9: 19, 2015.

Moreno-Bote R, **Beck J**, **Kanitscheider I**, **Pitkow X**, **Latham P**, **Pouget A**. Information-limiting correlations. *Nat Neurosci* 17: 1410–1417, 2014.

Nagel KI, **Doupe AJ**. Temporal Processing and Adaptation in the Songbird Auditory Forebrain. *Neuron* 51: 845–859, 2006.

Natan RG, **Rao W**, **Geffen MN**. Cortical Interneurons Differentially Shape Frequency Tuning following Adaptation. *Cell Rep* 21: 878–890, 2017.

Ni AM, **Ruff DA**, **Alberts JJ**, **Symmonds J**, **Cohen MR**. Learning and attention reveal a general relationship between population activity and behavior. *Science* 359: 463–465, 2018.

Nienborg H, **Cumming BG**. Macaque V2 neurons, but not V1 neurons, show choice-related activity. *J Neurosci* 26: 9567–78, 2006.

Nieuwenhuis S, **Heslenfeld DJ**, **von Geusau NJA**, **Mars RB**, **Holroyd CB**, **Yeung N**. Activity in human reward-sensitive brain areas is strongly context dependent. *Neuroimage* 25: 1302–1309, 2005.

Ohzawa I, **Sclar G**, **Freeman RD**. Contrast gain control in the cat visual cortex. *Nature* 298: 266–268, 1982.

Ongur D, **Price J**. The Organization of Networks within the Orbital and Medial Prefrontal Cortex of Rats, Monkeys and Humans. *Cereb Cortex* 10: 206–219, 2000.

Padoa-Schioppa C. Range-Adapting Representation of Economic Value in the Orbitofrontal Cortex By Camillo Padoa-Schioppa Supplementary Figures. *J Neu* 29: 1404–14014, 2009.

Padoa-Schioppa C. Neuronal origins of choice variability in economic decisions. *Neuron* 80: 1322–1336, 2013.

Padoa-Schioppa C, **Assad JA**. Neurons in the orbitofrontal cortex encode economic value. *Nature* 441: 223–6, 2006.

Padoa-Schioppa C, **Conen KE**. Orbitofrontal Cortex: A Neural Circuit for Economic Decisions. *Neuron* 96: 736–754, 2017.

Pitkow X, **Liu S**, **Angelaki DE**, **DeAngelis GC**, **Pouget A**. How Can Single Sensory Neurons Predict Behavior? *Neuron* 87: 411–423, 2015.

Raghuraman AP, **Padoa-Schioppa C**. Integration of Multiple Determinants in the Neuronal Computation of Economic Values. *J Neurosci* 34: 11583–11603, 2014.

Roesch MR, **Olson CR**. Neuronal Activity in Primate Orbitofrontal Cortex Reflects the Value of Time. *J Neurophysiol* 94: 2457–2471, 2005.

Romo R, **Hernández A**, **Zainos A**, **Lemus L**, **Brody CD**. Neuronal correlates of decision-making in secondary somatosensory cortex. *Nat Neurosci* 5: 1217–25, 2002.

Romo R, **Hernández A**, **Zainos A**, **Salinas E**. Correlated Neuronal Discharges that Increase Coding Efficiency during Perceptual Discrimination. *Neuron* 38: 649–657, 2003.

Rudebeck PH, **Murray EA**. Dissociable effects of subtotal lesions within the macaque orbital prefrontal cortex on reward-guided behavior. *J Neurosci* 31: 10569–10578, 2011.

Rustichini A, **Conen KE**, **Cai X**, **Padoa-Schioppa C**. Optimal coding and neuronal adaptation in economic decisions. *Nat Commun* 8, 2017.

Rustichini A, **Padoa-Schioppa C**. A neuro-computational model of economic decisions. *J Neurophysiol* 114: 1382–1398, 2015.

Sanchez-Vives M V., **McCormick DA**. Cellular and network mechanisms of rhytmic recurrent activity in neocortex. *Nat Neurosci* 3: 1027–1034, 2000.

Sanchez-Vives M V, **Nowak LG**, **McCormick DA**. Membrane mechanisms underlying contrast adaptation in cat area 17 in vivo. *J Neurosci* 20: 4267–4285, 2000.

Schneidman E, **Berry MJ**, **Segev R**, **Bialek W**. Weak pairwise correlations imply strongly correlated network states in a neural population. *Nature* 440: 1007–12, 2006.

Shadlen M, **Britten K**, **Newsome W**, **Movshon J**. A computational analysis of the relationship between neuronal and behavioral responses to visual motion [Online]. *J Neurosci* 16: 1486–1510, 1996. http://www.jneurosci.org/content/16/4/1486.short [21 Mar. 2014].

da Silveira RA, **Berry MJ**, **II**. High-fidelity coding with correlated neurons. *PLoS Comput Biol*

10: e1003970, 2014.

Smith MA, **Sommer MA**. Spatial and temporal scales of neuronal correlation in visual area V4. *J Neurosci* 33: 5422–32, 2013.

Solomon SG, **Kohn A**. Moving Sensory Adaptation beyond Suppressive Effects in Single Neurons. *Curr Biol* 24: R1012–R1022, 2014.

Solway A, **Botvinick MM**. Goal-directed decision making as probabilistic inference: A computational framework and potential neural correlates. *Psychol Rev* 119: 120–154, 2012.

Song HF, **Yang GR**, **Wang X-J**. Reward-based training of recurrent neural networks for cognitive and value-based tasks. *Elife* 6, 2017.

Tremblay L, **Schultz W**. Relative reward preference in primate orbitofrontal cortex. *Nature* 398: 704–8, 1999.

Wainwright MJ, **Schwartz O**, **Simoncelli EP**. Natural Image Statistics and Divisive Normalization: Modeling Nonlinearities and Adaptation in Cortical Neurons. *Stat. Theor. brain.* .

Wark B, **Lundstrom BN**, **Fairhall A**. Sensory adaptation. *Curr. Opin. Neurobiol.* 17: 423–429, 2007.

West EA, **DesJardin JT**, **Gale K**, **Malkova L**. Transient Inactivation of Orbitofrontal Cortex Blocks Reinforcer Devaluation in Macaques. *J Neurosci* 31: 15128–15135, 2011.

Xie J, **Padoa-Schioppa C**. Neuronal remapping and circuit persistence in economic decisions. *Nat. Neurosci.* 2016.

Zhang Z, **Fanning J**, **Ehrlich DB**, **Chen W**, **Lee D**, **Levy I**. Distributed neural representation of saliency controlled value and category during anticipation of rewards and punishments. *Nat Commun* 8, 2017.

Zohary E, **Shadlen MN**, **Newsome WT**. Correlated neuronal discharge rate and its implications for psychophysical performance. *Nature* 370: 140–3, 1994.

Abbott LF, **Dayan P**. The Effect of Correlated Variability on the Accuracy of a Population Code. *Neural Comput* 11: 91–101, 1999.

Abe H, **Lee D**. Distributed Coding of Actual and Hypothetical Outcomes in the Orbital and Dorsolateral Prefrontal Cortex. *Neuron* 70: 731–741, 2011.

Averbeck BB, **Lee D**. Neural Noise and Movement-Related Codes in the Macaque Supplementary Motor Area [Online]. *J Neurosci* 23: 7630–7641, 2003. http://www.jneurosci.org/content/23/20/7630.short [21 Mar. 2014].

Barlow HB. Possible Principles Underlying the Transformations of Sensory Messages. In: *Sensory Communication*, p. 216–234.

Beck JM, **Latham PE**, **Pouget A**. Marginalization in Neural Circuits with Divisive

Normalization. *J Neurosci* 31: 15310–15319, 2011.

Beck JM, **Ma WJ**, **Pitkow X**, **Latham PE**, **Pouget A**. Not noisy, just wrong: the role of suboptimal inference in behavioral variability. *Neuron* 74: 30–9, 2012.

Benucci A, **Saleem AB**, **Carandini M**. Adaptation maintains population homeostasis in primary visual cortex. *Nat Neurosci* 16: 724–9, 2013.

Boehnke SE, **Berg DJ**, **Marino RA**, **Baldi PF**, **Itti L**, **Munoz DP**. Visual adaptation and novelty responses in the superior colliculus. *Eur J Neurosci* 34: 766–779, 2011.

Bonds AB. Temporal dynamics of contrast gain in single cells of the cat striate cortex. *Vis Neurosci* 6: 239–255, 1991.

Breiter HC, **Aharon I**, **Kahneman D**, **Dale A**, **Shizgal P**. Functional imaging of neural responses to expectancy and experience of monetary gains and losses. *Neuron* 30: 619–639, 2001.

Britten KH, **Newsome WT**, **Shadlen MN**, **Celebrini S**, **Movshon JA**. A relationship between behavioral choice and the visual responses of neurons in macaque MT. *Vis Neurosci* 13: 87–100, 1996.

Britten KH, **Shadlen MN**, **Newsome WT**, **Movshon J a**. The analysis of visual motion: a comparison of neuronal and psychophysical performance. *J Neurosci* 12: 4745–4765, 1992.

Burke CJ, **Baddeley M**, **Tobler PN**, **Schultz W**. Partial Adaptation of Obtained and Observed Value Signals Preserves Information about Gains and Losses. *J Neurosci* 36: 10016–10025, 2016.

Camille N, **Griffiths CA**, **Vo K**, **Fellows LK**, **Kable JW**. Ventromedial Frontal Lobe Damage Disrupts Value Maximization in Humans. *J Neurosci* 31: 7527–7532, 2011.

Carandini M, **Heeger DJ**. Normalization as a canonical neural computation. *Nat Rev Neurosci* 13: 51–62, 2011.

Chance FS, **Abbott L.**, **Reyes AD**. Gain Modulation from Background Synaptic Input. *Neuron* 35: 773–782, 2002.

Cohen MR, **Kohn A**. Measuring and interpreting neuronal correlations. *Nat Neurosci* 14: 811–9, 2011.

Cohen MR, **Maunsell JHR**. Attention improves performance primarily by reducing interneuronal correlations. *Nat Neurosci* 12: 1594–600, 2009.

Constantinidis C, **Goldman-Rakic PS**. Correlated discharges among putative pyramidal neurons and interneurons in the primate prefrontal cortex. *J Neurophysiol* 88: 3487–97, 2002.

Cox KM, **Kable JW**. BOLD Subjective Value Signals Exhibit Robust Range Adaptation. *J Neurosci* 34: 16533–16543, 2014.

Dean AF. Adaptation-induced alteration of the relation between response amplitude and contrast in cat striate cortical neurones. *Vision Res* 23: 249–256, 1983.

Díaz-Quesada M, **Maravall M**. Intrinsic mechanisms for adaptive gain rescaling in barrel cortex. *J Neurosci* 28: 696–710, 2008.

Ecker AS, **Berens P**, **Cotton RJ**, **Subramaniyan M**, **Denfield GH**, **Cadwell CR**, **Smirnakis SM**, **Bethge M**, **Tolias AS**. State dependence of noise correlations in macaque primary visual cortex. *Neuron* 82: 235–248, 2014.

Ecker AS, **Berens P**, **Keliris GA**, **Bethge M**, **Logothetis NK**, **Tolias AS**. Decorrelated neuronal firing in cortical microcircuits. *Science* 327: 584–7, 2010.

Ecker AS, **Berens P**, **Tolias AS**, **Bethge M**. The effect of noise correlations in populations of diversely tuned neurons. *J Neurosci* 31: 14272–83, 2011.

Fairhall AL, **Lewen GD**, **Bialek W**, **De Ruyter van Steveninck RR**. Efficiency and ambiguity in an adaptive neural code. *Nature* 412: 787–792, 2001.

Fellows LK. Orbitofrontal contributions to value-based decision making: Evidence from humans with frontal lobe damage. *Ann N Y Acad Sci* 1239: 51–58, 2011.

Fellows LK, **Farah MJ**. The role of ventromedial prefrontal cortex in decision making: Judgment under uncertainty or judgment per se? *Cereb Cortex* 17: 2669–2674, 2007.

Friedrich J, **Lengyel M**. Goal-Directed Decision Making with Spiking Neurons. *J Neurosci* 36: 1529–1546, 2016.

Gallagher M, **McMahan RW**, **Schoenbaum G**. Orbitofrontal cortex and representation of incentive value in associative learning. *J Neurosci* 19: 6610–6614, 1999.

Gu Y, **Liu S**, **Fetsch CR**, **Yang Y**, **Fok S**, **Sunkara A**, **DeAngelis GC**, **Angelaki DE**. Perceptual learning reduces interneuronal correlations in macaque visual cortex. *Neuron* 71: 750–61, 2011.

Gutnisky DA, **Dragoi V**. Adaptive coding of visual information in neural populations. *Nature* 452: 220–4, 2008.

Haak KV, **Fast E**, **Bao M**, **Lee M**, **Engel SA**. Four Days of Visual Contrast Deprivation Reveals Limits of Neuronal Adaptation. *Curr Biol* 24: 2575–2579, 2014.

Haefner RM, **Berkes P**, **Fiser J**. Perceptual Decision-Making as Probabilistic Inference by Neural Sampling. *Neuron* 90: 649–660, 2016.

Haefner RM, **Gerwinn S**, **Macke JH**, **Bethge M**. Inferring decoding strategies from choice probabilities in the presence of correlated variability. *Nat Neurosci* 16: 235–42, 2013.

Hammond P, **Mouat GS V**, **Smith AT**. Neural correlates of motion after-effects in cat striate cortical neurones: monocular adaptation [Online]. *Exp Brain Res* 72: 1–20, 1988. https://link.springer.com/content/pdf/10.1007/BF00248495.pdf [23 Feb. 2018].

Hengen KB, **Lambo ME**, **Van Hooser SD**, **Katz DB**, **Turrigiano GG**. Firing Rate Homeostasis in Visual Cortex of Freely Behaving Rodents. *Neuron* 80: 335–342, 2013.

Hô N, **Destexhe A**. Synaptic Background Activity Enhances the Responsiveness of Neocortical Pyramidal Neurons. *J Neurophysiol* 84: 1488–1496, 2000.

Howard JD, **Gottfried JA**, **Tobler PN**, **Kahnt T**. Identity-specific coding of future rewards in the human orbitofrontal cortex. *Proc Natl Acad Sci* 112: 5195–5200, 2015.

Izquierdo A. Bilateral Orbital Prefrontal Cortex Lesions in Rhesus Monkeys Disrupt Choices Guided by Both Reward Value and Reward Contingency. *J Neurosci* 24: 7540–7548, 2004.

Jeanne JM, **Sharpee TO**, **Gentner TQ**. Associative learning enhances population coding by inverting interneuronal correlation patterns. *Neuron* 78: 352–63, 2013.

Kobayashi S, **Pinto de Carvalho O**, **Schultz W**. Adaptation of reward sensitivity in orbitofrontal neurons. *J Neurosci* 30: 534–544, 2010.

Kohn A. Visual Adaptation: Physiology, Mechanisms, and Functional Benefits. *J Neurophysiol* 97: 3155–3164, 2007.

Kohn A, **Coen-Cagli R**, **Kanitscheider I**, **Pouget A**. Correlations and Neuronal Population Information. *Annu Rev Neurosci* 39: 237–256, 2016.

Kohn A, **Movshon JA**. Neuronal adaptation to visual motion in area MT of the macaque. *Neuron* 39: 681–691, 2003.

Krekelberg B, **van Wezel RJA**, **Albright TD**. Adaptation in Macaque MT Reduces Perceived Speed and Improves Speed Discrimination. *J Neurophysiol* 95: 255–270, 2006.

Ladenbauer J, **Augustin M**, **Obermayer K**. How adaptation currents change threshold, gain, and variability of neuronal spiking. *J Neurophysiol* 111: 939–953, 2014.

Lee D, **Port NL**, **Kruse W**, **Georgopoulos AP**. Variability and Correlated Noise in the Discharge of Neurons in Motor and Parietal Areas of the Primate Cortex [Online]. *J Neurosci* 18: 1161–1170, 1998. http://www.jneurosci.org/content/18/3/1161.short [21 Mar. 2014].

Liu B, **Macellaio M V.**, **Osborne LC**. Efficient sensory cortical coding optimizes pursuit eye movements. *Nat Commun* 7: 12759, 2016.

Liu S, **Gu Y**, **DeAngelis GC**, **Angelaki DE**. Choice-related activity and correlated noise in subcortical vestibular neurons. *Nat Neurosci* 16: 89–97, 2013.

Louie K, **Glimcher PW**. Efficient coding and the neural representation of value. *Ann N Y Acad Sci* 1251: 13–32, 2012.

Malmierca MS, **Anderson LA**, **Antunes FM**. The cortical modulation of stimulus-specific adaptation in the auditory midbrain and thalamus: a potential neuronal correlate for predictive coding. *Front Syst Neurosci* 9: 19, 2015.

Moreno-Bote R, **Beck J**, **Kanitscheider I**, **Pitkow X**, **Latham P**, **Pouget A**. Information-limiting correlations. *Nat Neurosci* 17: 1410–1417, 2014.

Nagel KI, **Doupe AJ**. Temporal Processing and Adaptation in the Songbird Auditory Forebrain. *Neuron* 51: 845–859, 2006.

Natan RG, **Rao W**, **Geffen MN**. Cortical Interneurons Differentially Shape Frequency Tuning following Adaptation. *Cell Rep* 21: 878–890, 2017.

Ni AM, **Ruff DA**, **Alberts JJ**, **Symmonds J**, **Cohen MR**. Learning and attention reveal a general relationship between population activity and behavior. *Science* 359: 463–465, 2018.

Nienborg H, **Cumming BG**. Macaque V2 neurons, but not V1 neurons, show choice-related activity. *J Neurosci* 26: 9567–78, 2006.

Nieuwenhuis S, **Heslenfeld DJ**, **von Geusau NJA**, **Mars RB**, **Holroyd CB**, **Yeung N**. Activity in human reward-sensitive brain areas is strongly context dependent. *Neuroimage* 25: 1302–1309, 2005.

Ohzawa I, **Sclar G**, **Freeman RD**. Contrast gain control in the cat visual cortex. *Nature* 298: 266–268, 1982.

Ongur D, **Price J**. The Organization of Networks within the Orbital and Medial Prefrontal Cortex of Rats, Monkeys and Humans. *Cereb Cortex* 10: 206–219, 2000.

Padoa-Schioppa C. Range-Adapting Representation of Economic Value in the Orbitofrontal Cortex By Camillo Padoa-Schioppa Supplementary Figures. *J Neu* 29: 1404–14014, 2009.

Padoa-Schioppa C. Neuronal origins of choice variability in economic decisions. *Neuron* 80: 1322–1336, 2013.

Padoa-Schioppa C, **Assad JA**. Neurons in the orbitofrontal cortex encode economic value. *Nature* 441: 223–6, 2006.

Padoa-Schioppa C, **Conen KE**. Orbitofrontal Cortex: A Neural Circuit for Economic Decisions. *Neuron* 96: 736–754, 2017.

Pitkow X, **Liu S**, **Angelaki DE**, **DeAngelis GC**, **Pouget A**. How Can Single Sensory Neurons Predict Behavior? *Neuron* 87: 411–423, 2015.

Raghuraman AP, **Padoa-Schioppa C**. Integration of Multiple Determinants in the Neuronal Computation of Economic Values. *J Neurosci* 34: 11583–11603, 2014.

Roesch MR, **Olson CR**. Neuronal Activity in Primate Orbitofrontal Cortex Reflects the Value of Time. *J Neurophysiol* 94: 2457–2471, 2005.

Romo R, **Hernández A**, **Zainos A**, **Lemus L**, **Brody CD**. Neuronal correlates of decision-making in secondary somatosensory cortex. *Nat Neurosci* 5: 1217–25, 2002.

Romo R, **Hernández A**, **Zainos A**, **Salinas E**. Correlated Neuronal Discharges that Increase

Coding Efficiency during Perceptual Discrimination. *Neuron* 38: 649–657, 2003.

Rudebeck PH, **Murray EA**. Dissociable effects of subtotal lesions within the macaque orbital prefrontal cortex on reward-guided behavior. *J Neurosci* 31: 10569–10578, 2011.

Rustichini A, **Conen KE**, **Cai X**, **Padoa-Schioppa C**. Optimal coding and neuronal adaptation in economic decisions. *Nat Commun* 8, 2017.

Rustichini A, **Padoa-Schioppa C**. A neuro-computational model of economic decisions. *J Neurophysiol* 114: 1382–1398, 2015.

Sanchez-Vives M V., **McCormick DA**. Cellular and network mechanisms of rhytmic recurrent activity in neocortex. *Nat Neurosci* 3: 1027–1034, 2000.

Sanchez-Vives M V, **Nowak LG**, **McCormick DA**. Membrane mechanisms underlying contrast adaptation in cat area 17 in vivo. *J Neurosci* 20: 4267–4285, 2000.

Schneidman E, **Berry MJ**, **Segev R**, **Bialek W**. Weak pairwise correlations imply strongly correlated network states in a neural population. *Nature* 440: 1007–12, 2006.

Shadlen M, **Britten K**, **Newsome W**, **Movshon J**. A computational analysis of the relationship between neuronal and behavioral responses to visual motion [Online]. *J Neurosci* 16: 1486–1510, 1996. http://www.jneurosci.org/content/16/4/1486.short [21 Mar. 2014].

da Silveira RA, **Berry MJ**, **II**. High-fidelity coding with correlated neurons. *PLoS Comput Biol* 10: e1003970, 2014.

Smith MA, **Sommer MA**. Spatial and temporal scales of neuronal correlation in visual area V4. *J Neurosci* 33: 5422–32, 2013.

Solomon SG, **Kohn A**. Moving Sensory Adaptation beyond Suppressive Effects in Single Neurons. *Curr Biol* 24: R1012–R1022, 2014.

Solway A, **Botvinick MM**. Goal-directed decision making as probabilistic inference: A computational framework and potential neural correlates. *Psychol Rev* 119: 120–154, 2012.

Song HF, **Yang GR**, **Wang X-J**. Reward-based training of recurrent neural networks for cognitive and value-based tasks. *Elife* 6, 2017.

Tremblay L, **Schultz W**. Relative reward preference in primate orbitofrontal cortex. *Nature* 398: 704–8, 1999.

Wainwright MJ, **Schwartz O**, **Simoncelli EP**. Natural Image Statistics and Divisive Normalization: Modeling Nonlinearities and Adaptation in Cortical Neurons. *Stat. Theor. brain.* .

Wark B, **Lundstrom BN**, **Fairhall A**. Sensory adaptation. *Curr. Opin. Neurobiol.* 17: 423–429, 2007.

West EA, **DesJardin JT**, **Gale K**, **Malkova L**. Transient Inactivation of Orbitofrontal Cortex Blocks Reinforcer Devaluation in Macaques. *J Neurosci* 31: 15128–15135, 2011.

Xie J, **Padoa-Schioppa C**. Neuronal remapping and circuit persistence in economic decisions. *Nat. Neurosci.* 2016.

Zhang Z, **Fanning J**, **Ehrlich DB**, **Chen W**, **Lee D**, **Levy I**. Distributed neural representation of saliency controlled value and category during anticipation of rewards and punishments. *Nat Commun* 8, 2017.

Zohary E, **Shadlen MN**, **Newsome WT**. Correlated neuronal discharge rate and its implications for psychophysical performance. *Nature* 370: 140–3, 1994.

Chapter 2: Neuronal Variability in Orbitofrontal Cortex during Economic Decisions

Neuroeconomic models assume that economic decisions are based on the activity of *offer value* cells in the orbitofrontal cortex (OFC), but testing this assertion has proven difficult. In principle, the decision made on a given trial should correlate with the stochastic fluctuations of these cells. However, this correlation, measured as a choice probability (CP), is small. Importantly, a neuron's CP reflects not only its individual contribution to the decision (termed read-out weight), but also the intensity and the structure of correlated variability across the neuronal population (termed noise correlation). A precise mathematical relation between CPs, noise correlations and read-out weights was recently derived by Haefner and colleagues (2013) for a linear decision model. In this framework, concurrent measurements of noise correlations and CPs can provide quantitative information on how a population of cells contributes to a decision. Here we examined neuronal variability in the OFC of rhesus monkeys during economic decisions. Noise correlations had similar structure but considerably lower strength compared to those typically measured in sensory areas during perceptual decisions. In contrast, variability in the activity of individual cells was high and comparable to that recorded in other cortical regions. Simulation analyses based on Haefner's equation showed that noise correlations measured in the OFC combined with a plausible read-out of *offer value* cells reproduced the experimental measures of CPs. In other words, the results obtained for noise correlations and those obtained for CPs taken together support the hypothesis that economic decisions are primarily based on the activity of *offer value* cells.

2.1 Introduction

The discharges of individual neurons in cortical and subcortical areas are highly variable, but fluctuations in the activity of different cells within a given area are often correlated (Cohen and Maunsell 2009; Jeanne et al. 2013; Lee et al. 1998; Liu et al. 2013; Poort and Roelfsema 2009; Romo et al. 2003; Shadlen and Newsome 1998; Smith and Kohn 2008; Smith and Sommer 2013; Zohary et al. 1994). This phenomenon, termed noise correlation, can provide deep insights into the functions of a particular brain region (Cohen and Maunsell 2009; Jeanne et al. 2013). The analysis of noise correlations is particularly informative in the context of decision making because certain patterns of correlated variability can induce a systematic relation between the fluctuations in the activity of individual cells and the decision made by the subject. This relation is quantified as a choice probability (CP), which is the probability with which an ideal observer would correctly predict the upcoming decision based on the activity of one cell (Britten et al. 1992; Britten et al. 1996). In studies of perceptual decisions, significant CPs have historically been interpreted as evidence that a particular sensory area participates in the decision process (Britten et al. 1996; Cohen and Newsome 2009; Liu et al. 2013; Nienborg and Cumming 2014; 2006; Romo et al. 2002), although CPs can also be produced by top-down feed-back (Nienborg and Cumming 2009). Importantly, a neuron's CP reflects not only its individual contribution to the decision (termed read-out weight), but also the intensity and the structure of noise correlations within the entire network (Britten et al. 1996; Cohen and Newsome 2009; Nienborg and Cumming 2009; Shadlen and Newsome 1998). A precise mathematical relation between CPs, noise correlations and read-out weights was recently derived by Haefner and colleagues for a linear decision model (Haefner et al. 2013). Within this framework, concurrent measurements of noise correlations and CPs can provide quantitative information on how a population of cells

contributes to a decision. These principles – originally developed for perceptual decisions – were applied here to the domain of economic choice.

An individual executing an economic choice assigns a subjective value to each of the available offers and then makes a decision by comparing values. This behavior is selectively disrupted by lesions of the orbitofrontal cortex (OFC) (Camille et al. 2011; Gallagher et al. 1999; Gremel and Costa 2013; Rudebeck et al. 2013). Furthermore, neural activity in this area encodes the values subjects assign to offered and chosen goods while choosing between them (Padoa-Schioppa 2011; Wallis 2011). Current models posit that economic decisions are based on values computed in the OFC (Kable and Glimcher 2009; Padoa-Schioppa 2011; Rangel and Hare 2010; Rushworth et al. 2012). In previous work, we examined the neuronal activity of monkeys choosing between different juices. We identified three groups of neurons: *offer value* cells encoding the value of one of the two juices, *chosen value* cells encoding the value of the chosen juice, and *chosen juice* cells encoding the choice outcome in a binary way (Padoa-Schioppa and Assad 2006; 2008). Thus according to current views, *offer value* cells would provide the primary input to the decision process. Testing this hypothesis, however, has proven difficult. Furthermore, we recently found that CPs of *offer value* cells are substantially lower (Padoa-Schioppa 2013) than normally measured in sensory areas during perceptual decisions (Britten et al. 1996; Nienborg and Cumming 2014; 2006; Romo et al. 2002). One possible explanation for this result is that *offer value* cells influence decisions less than previously thought. Alternatively, CPs of *offer value* cells may be low because noise correlations in the OFC are low, or perhaps because noise correlations are "balanced" (i.e., independent of whether two *offer value* cells are associated to the same good or to different goods) (Haefner et al. 2013; Nienborg et al. 2012).

To address these issues, we examined noise correlations in the primate OFC during a juice-choice task. Noise correlations had similar structure but considerably lower strength compared to those typically reported for sensory areas. Applying Haefner's mathematical framework, we found that CPs measured in the OFC arise from the distribution of noise correlations given a plausible linear read-out of *offer value* cells. Specifically, the empirical mean(CP) fell between the values predicted by a uniform-pooling model and that predicted by an optimal linear decoder.

2.2 Materials & Methods

2.2.1 Data set

We analyzed neuronal data from two experiments previously described in detail (Padoa-Schioppa and Assad 2006; 2008). In both experiments, two rhesus monkeys (one male, one female) chose between juices offered in varying amounts. The two experiments differed only in the number of juices available in each session. In experiment 1, two juices were offered in each session (A and B). In experiment 2, three juices were offered in each session (A, B and C), two juices were offered in each trial, and trials with the three juice pairs were presented in pseudo-random order. In both experiments, an "offer type" was defined by two offers (e.g. [1A:2B]) and a "trial type" was defined by an offer type and a choice (e.g. [1A:2B,A]). The spatial contingencies (left/right) were counterbalanced across trials and different offer types were pseudo-randomly interleaved. Each offer type was usually presented ≥20 times. Neuronal recordings were performed from orbitofrontal cortex (OFC) and four electrodes were typically used in each session.

All analyses were conducted in Matlab (MathWorks, Inc). The neuronal classification was described in previous studies. Briefly, we defined seven time windows: pre-offer (0.5 s before

the offer), post-offer (0.5 s after the offer), delay (0.1-1 s after the offer), pre-go (0.5 s before the go cue), reaction time (RT; from the go to the saccade onset), pre-juice (0.5 s before juice delivery) and post-juice (0.5 s after juice delivery). A "neuronal response" was defined as the activity of one cell in one time window as a function of the trial type. Task-related responses were identified by a 1-way ANOVA (factor [trial type]; $p<0.001$). In preliminary analyses, we tested the neuronal population against a large number of variables. Procedures of variable selection identified *offer value, chosen value* and *chosen juice* as the three variables encoded by the neuronal population (Padoa-Schioppa and Assad 2006). The encoding of these variables was categorical and generally consistent across time windows, indicating that neurons formed three distinct groups (Padoa-Schioppa 2013). A variable was said to explain a response if a linear regression of the response onto that variable had a non-zero slope ($p<0.05$). For each neuron, the group was identified by the variable that provided the highest sum R^2 across all seven time windows. Cells whose responses were not explained by any of these variables were defined as *null*. The data set thus included 252 *offer value* cells, 288 *chosen value* cells, 252 *chosen juice* cells and 692 *null* cells. Table 2.1 indicates the number of cell pairs recorded for each pair type.

2.2.2 Analysis of single cell variability

For each cell, we analyzed the power-law relation between the mean spike count (μ) and its standard deviation (σ). In essence, we performed the regression $\log(\sigma) = \alpha \log(\mu) + \beta$, where each data point represented one trial type. Our analysis relied on systematic changes in μ with the trial type and was thus carried out only on time windows in which the neuron was tuned (i.e., when the neuronal response was explained by the encoded variable). The analysis presupposed a monotonic relationship between μ and σ. Thus we excluded neuronal responses that did not present any correlation between these measures across trial types ($p>0.1$; 10% of time windows

Table 2.1 Number of simultaneously recorded cell pairs. Pair types are labeled as follows: (1) [*offer value*, *offer value*]; (2) [*chosen value*, *chosen value*]; (3) [*chosen juice*, *chosen juice*]; (4) [*offer value*, *chosen value*]; (5) [*offer value*, *chosen juice*]; (6) [*chosen value*, *chosen juice*]; (7) [*offer value*, *null*]; (8) [*chosen value*, *null*]; (9) [*chosen juice*, *null*]; (10) [*null*, *null*]. See also Fig.2.5a. For pair types 1-3, cell pairs are further broken down depending on whether the two neurons had the same polarity or different polarity (see main text).

Pair Type	*1*	*2*	*3*	*4*	*5*	*6*	*7*	*8*	*9*	*10*	*Total*
Same Electrode											
Total	40	53	46	62	62	53	104	98	75	270	863
Same polarity	(23)	(33)	(25)	--	--	--	--	--	--	--	--
Different polarity	(17)	(27)	(21)	--	--	--	--	--	--	--	--
Different Electrode											
Total	73	116	70	148	106	194	362	463	421	623	2,576
Same polarity	(42)	(62)	(34)	--	--	--	--	--	--	--	--
Different polarity	(31)	(54)	(36)	--	--	--	--	--	--	--	--

excluded). Also, to minimize the effects of measurement noise, we restricted the analysis to trial types with ≥10 trials (~4% of trials excluded). These criteria reduced the number of extreme values in the analysis, but did not substantially alter the median values obtained for α and β across the population.

For each neuronal response, we determined the values of α and β using Deming's regression (Glaister 2001). Simple linear regressions assume that the x-variable is measured exactly and that only the y-variable is affected by error. In contrast, Deming's regression finds the best linear fit

for the case when both x and y are measured with error and the ratio between error in x and error in y is known. Error in log(μ) and log(σ) were derived by propagation of uncertainty from the standard error of the mean (SEM) and the standard error of the standard deviation (SESD). We used an approximation of SESD (Ahn and Fessler 2003) that is highly accurate (within 3%) for n>10 observations:

$$\mathrm{SESD} \approx \frac{\sigma}{\sqrt{2(n-1)}}$$

From here, we calculated the ratio of error (λ) for each trial type in a time window.

$$\lambda = \frac{2(n-1)\,\mu^2}{n\,\sigma^2}$$

We used the mean λ across trial types to obtain α_w and β_w for each time window. Values of α_w and β_w were then averaged across time windows to obtain overall values of α and β for each cell.

The Fano factor and coefficient of variation were measured separately for each cell, each time window and each trial type. Measures were then averaged across trial types. The time course of individual-cell variability was calculated using a 200 ms sliding window with 25 ms intervals.

2.2.3 Analysis of noise correlations

Noise correlation (r_{noise}) was defined as Pearson's correlation between the trial-to-trial activity of two simultaneously recorded neurons. For each cell, trial type and time window, we computed the mean firing rate and standard deviation (SD) across trials. We z-scored the firing rate in each trial accordingly and obtained a normalized activity fluctuation. To minimize the effect of outliers, we removed trials for which either neuron's firing rate was >3 SD away from the mean for that trial type (Smith and Kohn 2008), although this procedure did not have a measurable

impact on the results. We then computed Pearson's correlation between normalized activity fluctuations for every pair of simultaneously recorded cells.

All statistical comparisons of noise correlations across pair types based on tuning, distance and time window were done after applying Fisher's r-to-z transformation. The significance of individual noise correlations was tested by computing correlations on trial-shuffled data. This method captures the range of correlations expected by chance for a pair of cells with given activity profiles. The trial order was randomly permuted for one of the two cells in a pair and Pearson's correlation was calculated on permuted data. This procedure was repeated 1,000 times for each pair and used to generate a confidence interval. Pairs with r_{noise} outside of their 95% confidence interval were considered statistically significant.

For the sliding time window analysis, we calculated r_{noise} around the offer, go signal and juice delivery using 200 ms sliding time windows with 25 ms increments. For all other analyses, separate values of r_{noise} were obtained for the seven time windows throughout the trial. The overall r_{noise} for a cell pair was defined as the average r_{noise} across time windows. All time windows were 500 ms long except RT (typically 250-400 ms). Restricting the analysis to time windows in which both neurons were tuned ($p<0.1$) did not measurably alter the effects of distance, timing, cell type, or polarity described in the main text. Similarly, repeating calculations with shorter time windows slightly reduced r_{noise} but did not alter the effects of distance, timing, or cell type.

For certain analyses, we introduced the concept of neuronal polarity. In *offer value* cells, the encoded juice and the slope sign were always unambiguous. However, in *chosen juice* cells, the design of experiment 1 made it impossible to distinguish between a cell encoding juice A with a

positive slope and a cell encoding juice B with a negative slope (in both cases, the firing rate would be high/low for choices of juice A/B). We thus developed the concept of neuron polarity, which combined juice association and slope sign. The polarity was always +1 or -1. For experiment 1, the polarity was +1 when a higher firing rate of the cell corresponded to a higher probability of choosing juice A. By this convention, cells that encoded juice A with a positive slope (A+ cells) and cells that encoded juice B with a negative slope (B- cells) both had polarity = +1. In contrast, A- cells and B+ cells both had polarity = -1. The same convention held for experiment 2, except that cells encoding juice C were relabeled as encoding juice A (juice B) when paired with a cell encoding juice B (juice A). The definition of polarity applied to *offer value* and *chosen juice* cells; for *chosen value* cells, the polarity reduced to the sign of the encoding.

2.2.4 Computing choice probabilities and neuronal sensitivity

The methods used to calculate empirical CPs in *offer value* cells have been described previously (Padoa-Schioppa 2013), and were carried out here with minor alterations. Briefly, we focused on offer types in which the animal split its choices between the two juices, imposing that each juice be chosen in ≥3 trials. For each offer type, trials were divided based on the animal's choice. The two resulting distributions of firing rates were compared with a receiver operating characteristic analysis, from which we obtained the area under the curve (AUC). The CP for each cell was obtained averaging the AUC across offer types. By definition, an offer value cell presents CP>0.5 if, for given offers, the firing rate is higher in trials in which the animal chooses the juice encoded by the neuron. Thus an *offer value* cell with positive encoding presents CP>0.5 if its activity provides a direct contribution to the decision. Conversely, an *offer value* cell with negative encoding presents CP<0.5 if its activity provides a direct contribution to the decision

(because the cell is *less* active when the animal chooses the juice encoded by the neuron). To compute an overall mean(CP) across the population, we thus rectified CPs for cells with negative encoding by defining CP as 1-AUC for these neurons. This convention allowed us to pool cells with positive and negative encoding.

We examined the relation between neuronal sensitivity (d') and CP. This analysis focused on *offer value* cells and on the post-offer time window. For each neuronal response, we computed the standard deviation for each trial type and we averaged the result across trial types. The neuronal sensitivity was calculated dividing the tuning slope by the average standard deviation. Note that cells with negative encoding also have negative neuronal sensitivity. Thus to examine the relation between CP and d' we pooled *offer value A* cells and *offer value B* but we did not rectify CPs.

Unless otherwise indicated, all the CPs described in this study were calculated in the 500 ms after the offer (the same time window used to compute noise correlations). However, the simulation analyses on the relation between CPs and noise correlations (see below) were repeated using a shorter time window, 150-400 ms after the offer, as in a previous study (Padoa-Schioppa 2013). As illustrated in Fig.7cd, the results obtained with the two procedures were essentially identical.

2.2.5 Reconstructing choice probabilities from noise correlations

In a linear decision model, a binary decision between options X and Y is a linear read-out of a neural population. In formulas,

$$D = \sum_{i=1}^{n} \omega_i \varphi_i \qquad (1)$$

where φ_i is the activity of neuron *i* and ω_i is the weight given to that neuron in the decision. By convention, D>0 corresponds to choosing X and D<0 corresponds to choosing Y. Thus neurons with $\omega_i > 0$ support choosing X, while those with $\omega_i < 0$ support choosing Y. Haefner et al (2013) showed that the relationship between CPs, neuronal covariances and read-out weights is well approximated by the equation

$$CP_k = 0.5 + \frac{\sqrt{2}}{\pi} \frac{(\mathbf{X\omega})_k}{\sqrt{\mathbf{X}_{kk}\boldsymbol{\omega}^T\mathbf{X\omega}}} \quad (2)$$

where CP_k is the choice probability of cell *k,* **X** is the covariance matrix for the network, $\mathbf{X}_{kk}$ is the variance of cell *k,* and **ω** is the vector of read-out weights. Generally the covariance matrix for a cortical circuit is not fully known. However, it is still possible to calculate CP by using the overall trends in correlation data to construct **X.** Using Eq.2, we conducted a series of simulations to assess whether noise correlations measured in the OFC, taken together with a plausible read-out scheme of *offer value* cells, would induce a distribution of CPs close to that measured empirically. Specifically, we simulated CPs for a population of 10,000 *offer value* units. One half of the units had positive polarity (representing positive encoding of juice A or negative encoding of juice B) and the other half had negative polarity (representing negative encoding of juice A or positive encoding of juice B). Noise correlations used in the simulations were computed from the empirical data. Randomly sampling pairwise correlations does not generally produce a viable (positive definite) correlation matrix. In order to reconstruct CPs, we thus generated a viable and realistic correlation matrix from empirical data as follows.

First, we defined the constant *c* as the difference in mean(r_{noise}) for pairs of *offer value* cells with the same vs. opposite polarity based on data from the relevant time window. For "long-distance"

simulations, c was computed using only pairs of neurons recorded from different electrodes. For "mixed-distance" simulations, c was calculated separately for same-electrode pairs (c_{same}) and different-electrode pairs ($c_{different}$), and the final value was defined as $c = 0.9\ c_{different} + 0.1\ c_{same}$. This weighting of $c_{different}$ vs. c_{same} corresponds to a scenario in which neurons from the same electrode are representative of 10% of all cell pairs in the OFC. This scenario likely overestimates average noise correlations, since it assumes that correlations remain high for inter-neuronal distances up to 1 mm. Thus long-distance and mixed-distance simulations effectively provided a lower bound and an upper bound for mean(CP).

Second, we constructed a simplified correlation matrix **C**, where $C_{ij} = 1$ when i = j; $C_{ij} = c$ when i≠j and polarity(i) = polarity(j); and $C_{ij} = 0$ when polarity(i) ≠ polarity(j). To emulate the heterogeneity observed in empirical noise correlations, we added variability to the matrix using the method described by Hardin et al. (2013), in which the realistic correlation matrix **S** is:

$$S_{ij} = C_{ij} + \varepsilon \mathbf{u}_i^T \mathbf{u}_j, \quad i \neq j; \text{ otherwise } S_{ij} = C_{ij}$$

In this equation, ε is the maximum possible noise (defined so that $0<S_{ij}<1$ for all i,j) and $\mathbf{u}_i$ are random M-dimensional unit vectors. In the simulations, we used $\varepsilon = 0.9$ and $M = 100$. We thus obtained a realistic (positive definite) correlation matrix such that the variances of its elements were comparable to variances calculated from the empirical distribution of r_{noise}. For the uniform condition, this random factor does not affect the outcome, as CPs depend exclusively on the mean difference in correlation between pairs in the same pool vs. competing pools (Haefner et al. 2013). For the optimal condition, changing the parameters of the correlation matrix affects CP, but if **C**, M and ε are kept constant, values of CP are consistent across simulations. To verify this point, we repeated each simulation 30 times and found that mean(CP) varied by $<10^{-3}$.

In addition to an entry in the correlation matrix, each unit in the simulation was also assigned a standard deviation, which was drawn from the empirical distribution for *offer value* cells. The covariance matrix was computed from the noise correlation matrix and the standard deviations. For simulations based on Fisher's optimal read-out weights (Xanthopoulos et al. 2013), each unit was also assigned a slope, indicating how much its response changed with a small shift in offer value. Each slope was always paired with the same standard deviation, as these two parameters are empirically related in our data.

In the case of uniform read-out, weights were set equal to +1 or -1 based on the polarity of each unit. In the calculation of CP, weights are normalized (see Eq.2). Thus the specific value of the uniform weight did not matter, as long as the absolute value was the same for all units. For simulations based on optimal read-out, weights were determined by Fisher's linear discriminant analysis (Xanthopoulos et al. 2013). Certain simulations included two "fictive" hysteresis units (one positive and one negative), meant to account for the effects of choice hysteresis (see below). These units were assigned weights equal to 0.161 times the total weight of the offer value pool. Their variance was defined as $var_{hyst} = p\ (1\text{-}p)\ \phi^2$, where ϕ is the mean firing rate modulation of *offer value* cells (see below). Positive and negative hysteresis units were uncorrelated with offer value units and perfectly anti-correlated with each other.

2.2.6 Derivation of read-out weights for hysteresis units

We previously quantified the effect of choice hysteresis with a logistic analysis (Padoa-Schioppa 2013). Briefly, we constructed a model:

$$\begin{aligned} &choice\ B = 1/\left(1+\exp\left(-X\right)\right) \\ &X = a_0 + a_1 \log\left(\#B/\#A\right) + a_2\left(\delta_{n-1,B} - \delta_{n-1,A}\right) \end{aligned} \qquad (3)$$

The variable choice B was equal to 1 if the animal chose juice B and 0 otherwise. #A and #B were, respectively, the quantities of juices A and B offered to the animal. The current trial was labeled as trial n. The variable $\delta_{n-1,\,J}$ was equal to 1 if the animal received juice J in the previous trial and 0 otherwise. Notably, the difference ($\delta_{n-1,\,B}$ - $\delta_{n-1,\,A}$) was equal to 1, -1 or 0 depending on whether the previous trial ended with receipt of juice B, juice A or otherwise (for example with receipt of the third juice in experiment 2). The logistic regression provided an estimate for a_0, a_1 and a_2. By construction, $a_1>0$. In the simplified model with $a_2 = 0$, a_1 was the inverse temperature and a measure of choice variability, while the indifference point was provided by $\exp(-a_0/a_1)$. Choice hysteresis corresponded to $a_2>0$. Eq.3 may be re-written as follows:

$$\begin{aligned} X &= a_0 + a_1\left(\log\frac{\#B}{\#A} + a_2/a_1\left(\delta_{n-1,B} - \delta_{n-1,A}\right)\right) \\ X &= a_0 + a_1\log\left(\frac{\#B}{\#A}\exp\left((a_2/a_1)\left(\delta_{n-1,B} - \delta_{n-1,A}\right)\right)\right) \\ X &= a_0 + a_1\log\left(\frac{\#B}{\#A}\frac{\exp\left((a_2/a_1)\,\delta_{n-1,B}\right)}{\exp\left((a_2/a_1)\,\delta_{n-1,A}\right)}\right) \\ X &= a_0 + a_1\log\left(\frac{\#B\left(1+\varepsilon\,\delta_{n-1,B}\right)}{\#A\left(1+\varepsilon\,\delta_{n-1,A}\right)}\right) \end{aligned} \qquad (4)$$

In the last passage, we defined ε such that $\exp(a_2/a_1) = 1 + \varepsilon$ and we used the relation:

$$\exp\left((a_2/a_1)\,\delta_{n-1,B}\right) = 1 + \delta_{n-1,B}\left(\exp\left(a_2/a_1\right) - 1\right) = 1 + \varepsilon\,\delta_{n-1,B} \qquad (5)$$

The final formulation indicates that the effect of choosing juice B (juice A) in the previous trial is equivalent to that of multiplying the quantity of juice B (juice A) by a factor $1 + \varepsilon = \exp(a_2/a_1)$. The logistic regression was performed for each session in the data set. Averaging across sessions, we obtained $\text{mean}(\exp(a_2/a_1)) = 1.161$, and thus $\text{mean}(\varepsilon) = 0.161$.

Consider this result in the context of a linear decision model. In the absence of hysteresis:

$$D = \sum_{i=1}^{2k} \omega_i \ \phi_i \qquad \text{if D>0 choose A; if D<0 choose B} \qquad (6)$$

Here, 2*k* is the total number of *offer value* cells, ω_i is the read-out weight of neuron *i* and ϕ_i is its firing rate modulation (i.e., the firing rate minus the intercept corresponding to zero value). *Offer value* cells do not reflect choice hysteresis, but they encode value in a linear way. Thus choice hysteresis can be modeled *as if* it affected the firing rates of offer value cells. More precisely, the effect of choosing juice B (juice A) in the previous trial is equivalent to that of multiplying the firing rate of *offer value B* cells (*offer value A* cells) by a factor 1 + ε. In formulas:

$$\begin{aligned} D &= D_A + D_B = \sum_{i=1}^{k} \omega_i^A \ \phi_i^A + \sum_{i=1}^{k} \omega_i^B \ \phi_i^B \\ D_A &= \sum_{i=1}^{k} \omega_i^A \ \phi_i^A \left(1 + \varepsilon \ \delta_{n-1,A}\right) \\ D_A &= \sum_{i=1}^{k} \omega_i^A \ \phi_i^A + \sum_{i=1}^{k} \omega_i^A \ \phi_i^A \ \varepsilon \ \delta_{n-1,A} \end{aligned} \qquad (7)$$

We now consider only cases in which, $\omega_i^A = 1/k$ and $\omega_i^B = -1/k$ (uniform weights). If so,

$$\begin{aligned} D_A &= \sum_{i=1}^{k} \omega_i^A \ \phi_i^A + \varepsilon \ \delta_{n-1,A} \frac{1}{k} \sum_{i=1}^{k} \phi_i^A \\ D_A &= \sum_{i=1}^{k} \omega_i^A \ \phi_i^A + \varepsilon \ \delta_{n-1,A} \overline{\phi^A} \end{aligned} \qquad (8)$$

The first term is the simple contribution of the first pool of neurons independent of choice hysteresis. The second term can now be interpreted as one additional unit with firing rate equal to the average firing rate of *offer value A* cells and read-out weight of ε. The same holds for D_B except that the read-out weight for the additional unit has a minus sign.

Elements of the covariance matrix related to the two hysteresis units are computed as follows. First, the two hysteresis units are perfectly anti-correlated with each other. Second, since trial-by-trial fluctuations in the activity of *offer value* cells are independent of choice hysteresis, the correlation between the hysteresis units and other *offer value* cells equals zero. Third, with respect to the variance of the hysteresis units, we note that $\overline{\phi^J}$ in Eq.8 is an average across cells, not across trials. However, since trial-by-trial fluctuations in the activity of *offer value* cells are independent of choice hysteresis, $\overline{\phi^J}$ does not fluctuate across trials and only depends on the mean activity of *offer value* cells for given offer. Therefore, if p is the proportion of trials in which the animal chooses juice J, the variance of the hysteresis unit is:

$$\mathrm{var}_{hyst}^{J} \approx p(1-p)\left(\overline{\phi^J}\right)^2$$

For the simulations, we calculated $\overline{\phi^J}$ based on the activity of *offer value* cells that were tuned during the post-offer time window (N = 144). For each cell, we identified offer types for which the animal split its choices between juices A and B (i.e., the offer types for which CPs were defined) and we averaged the spike count modulation across trials. Values of *p* were determined separately for each session. We thus computed var_{hyst} separately for each cell. The variance of the hysteresis units in the simulation was then computed by averaging var_{hyst} across *offer value* cells. Numerically, we found mean(var_{hyst}) = 3.96 $(\mathrm{sp/s})^2$.

2.3 Results

The purpose of this study was to quantify noise correlations in OFC and to examine the relation between noise correlations and CPs measured in this area during economic decisions. The Results are organized as follows. In the first section, we describe the neuronal variability

measured for individual cells. In the following three sections, we describe the correlation in neuronal variability for pairs of cells (a.k.a., noise correlation), its time course during a trial, and its dependence on the variables encoded by the two neurons. In the last two sections, we summarize the empirical results obtained for CPs, and we examine the relation between noise correlations and CPs in the framework of a linear decision model. The latter analysis is based on a series of computer simulations.

2.3.1 Firing rates of individual neurons are highly variable

In the experiments, two animals chose between different juices offered in varying quantity (Fig.2.1a). We recorded and analyzed the activity of 1,484 cells in seven time windows (see Materials & Methods). Preliminary analyses identified three distinct groups of cells, namely *offer value* cells (N = 252; Fig.2.1bc), *chosen value* cells (N = 288; Fig.2.1d) and *chosen juice* cells (N = 252; Fig.2.1e). For each group, the encoding could be positive (increasing firing rate for increasing values) or negative (decreasing firing rate for increasing values). Cells in these three groups were collectively referred to as "tuned" cells. Other neurons, whose activity was not modulated by the offers and/or was not explained by any of the three variables, were referred to as *null* cells (N = 692).

We first examined the variability in the firing rate of individual neurons across trials. For each cell, we analyzed the relation between the mean spike count (μ) and its standard deviation (σ). We began with the general assumption that σ and μ are related by a power law:

$$\sigma = \beta \cdot \mu^{\alpha} \tag{9}$$

$$\log(\sigma) = \alpha \log(\mu) + \log(\beta) \tag{10}$$

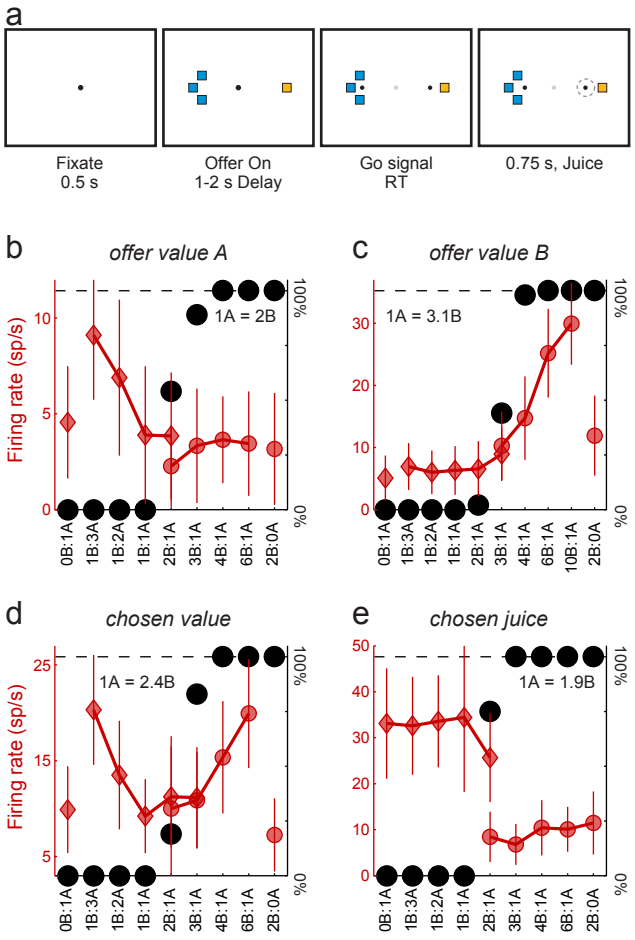

Figure 2.1 Behavioral task and cell groups. a. Juice choice task. At the beginning of each trial, the animal fixated on the center of a screen. Two sets of colored squares, representing the two offers, appeared after 0.5 s. For each offer, the color indicated the juice identity and the number of squares indicated the juice quantity. The animal maintained center fixation for a randomly variable delay (1-2 s), after which the fixation point disappeared and two saccade targets appeared by the offers (go cue). The animal indicated its choice with a saccade and maintained peripheral fixation for 0.75 s before juice delivery. b. Neuron encoding the offer value A. The x-axis represents different offer types ranked by the ratio #B: #A. Black symbols represent the percent of "B" choices. Red symbols represent the neuronal firing rate (diamonds and circles indicate, respectively, choices of juice A and juice B). To highlight the variability in firing rates, thinner error bars here indicate the SD and thicker error bars indicate the SEM. c. Neuron encoding the offer value B. d. Neuron encoding the chosen value. e. Neuron encoding the chosen juice. All conventions in panels cde are as in panel b.

where α and β are constants. To estimate α and β, we took advantage of the fact that neuronal responses in OFC vary depending on the trial type. We computed μ and σ for each tuned cell, each time window, and each trial type. For each cell and each time window, we fit Eq.10 using

Deming's regression (see Materials & Methods) and we obtained α_w and β_w (Fig.2.2a). We then averaged α_w and β_w across time windows to obtain an overall value of α and β for each cell. Across the population we found mean(α) = 0.679 ± 0.008 (Fig.2.2b) and mean(β) = 1.12 ± 0.01. The measures of α and β were significantly correlated (Fig.2.2c) and comparable to findings in visual cortex (Dean 1981; Vogels et al. 1989).

One important metric for individual cells is provided by the relation between neuronal variability and firing rate. As apparent in Eq.10, both α and β contribute to the variability, and both parameters are only defined for tuned cells. Therefore, to quantify this relation in all cells (including *null* cells), we analyzed the Fano factor and the coefficient of variation in relation to the baseline firing rate (pre-offer time window). Population analyses revealed that the Fano factor varied only mildly with the baseline firing rate (Fig.2.2d), whereas the coefficient of variation had a strong inverse relationship with the baseline firing rate (Fig.2.2e).

Finally, we analyzed the time course of neuronal variability. We computed the Fano factor in 200 ms sliding time windows and averaged it across the entire population (Fig.2.2f). The Fano factor dropped shortly after the offer and returned to baseline in the next 500-700 ms. It decreased again and more modestly after the go signal, remained depressed around juice delivery, and returned to baseline gradually in the 1 s following juice delivery. An analysis of the coefficient of variation provided a similar picture (not shown). This result resonates with previous reports (Churchland et al. 2010), although neuronal variability in the OFC was

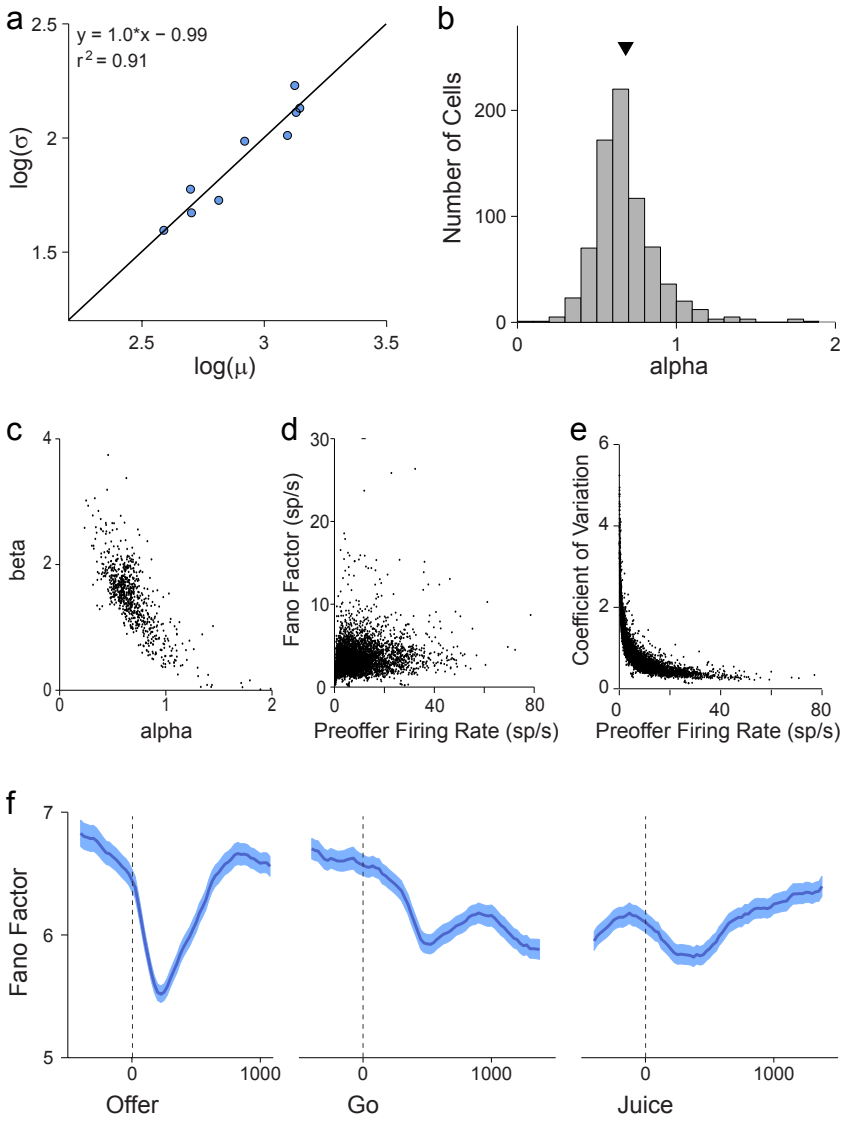

Figure 2.2 Neuronal variability in the OFC. a. Relation between mean firing rate (μ) and variance (σ) for one representative offer value cell (post-offer time window). Data are plotted in log scale and each data point represents one trial type. The line is obtained from Deming's regression. For this response, αw = 1.0 and βw = -0.99. For each tuned cell (763 cells total), α and β were obtained averaging αw and βw across time windows. b. Distribution of α. Across the population, mean(α) = 0.679 ± 0.008 (± SEM). c. Relation between α and β. Each data point represents one neuron and the two quantities are strongly anti-correlated. One outlier (0.1%) fell outside the range shown. d. Relation between the Fano factor and the baseline activity. Baseline activity was defined as the firing rate in the pre-offer time window. Each data point represents one neuron. Across the population, mean(Fano factor) = 1.8. e. Relation between coefficient of variation (cv) and baseline activity. The two quantities are strongly anti-correlated. Across the population, mean(cv) = 1.0. f. Time course of neuronal variability. Dark lines and shaded regions represent, respectively, the mean Fano factor and the corresponding SEM (in sp/s). The Fano factor was calculated in 200 ms sliding windows. Neuronal variability dropped sharply shortly after the offer onset; it returned to the initial levels 500-700 ms after the offer; it decreased again and more mildly following the go signal and remained depressed until the trial end. The coefficient of variation presented a similar time course (not shown).

previously found to drop only after juice delivery, whereas we observed the largest effect shortly after the offer. This discrepancy presumably reflects the fact that previous work focused on classical conditioning whereas our monkeys were engaged in a choice task.In summary, the firing rate of individual neurons in OFC was highly variable, and this variability was comparable to that typically measured in sensory areas.

2.3.2 Noise correlations in orbitofrontal cortex are low

Our data set included 3,439 pairs of cells recorded simultaneously. Of these, 863 pairs were recorded from the same electrode and 2,576 pairs were recorded from different electrodes placed at ≥1 mm distance. We computed the noise correlation (r_{noise}) for each of cell pair. Across the population, r_{noise} ranged from -0.59 to 0.87, with mean(r_{noise}) = 0.019 ± 0.001 (average computed pooling time windows; Fig.2.3a). Noise correlation strongly depended on inter-neuronal distance ($p<10^{-10}$, one-way ANOVA). Pairs recorded from the same electrode had mean(r_{noise}) = 0.054 ± 0.004, while pairs at ≥1 mm distance had mean(r_{noise}) = 0.008 ± 0.001. To look at the effects of distance more closely, we binned pairs into five groups based on distance (Fig.2.3b). Pairs recorded from the same electrode had significantly higher noise correlations than pairs at any of the greater distances (all $p <10^{-10}$, Tukey-Kramer test). Noise correlations did not decrease further at higher distances (all p>0.05, Tukey-Kramer test). Importantly, mean(r_{noise}) was significantly above zero in each time window, both at short distance (same electrode) and at long distance (different electrodes; all $p<10^{-3}$; t test).

Notably, our measures of noise correlations were substantially smaller than those found in many previous studies of sensory and motor areas (Fig.2.3a) (Gutnisky and Dragoi 2008; Kohn and Smith 2005; Lee et al. 1998; Liu et al. 2013; Nienborg and Cumming 2006; Poort and Roelfsema 2009; Smith and Kohn 2008; Smith and Sommer 2013; Zohary et al. 1994) (but see

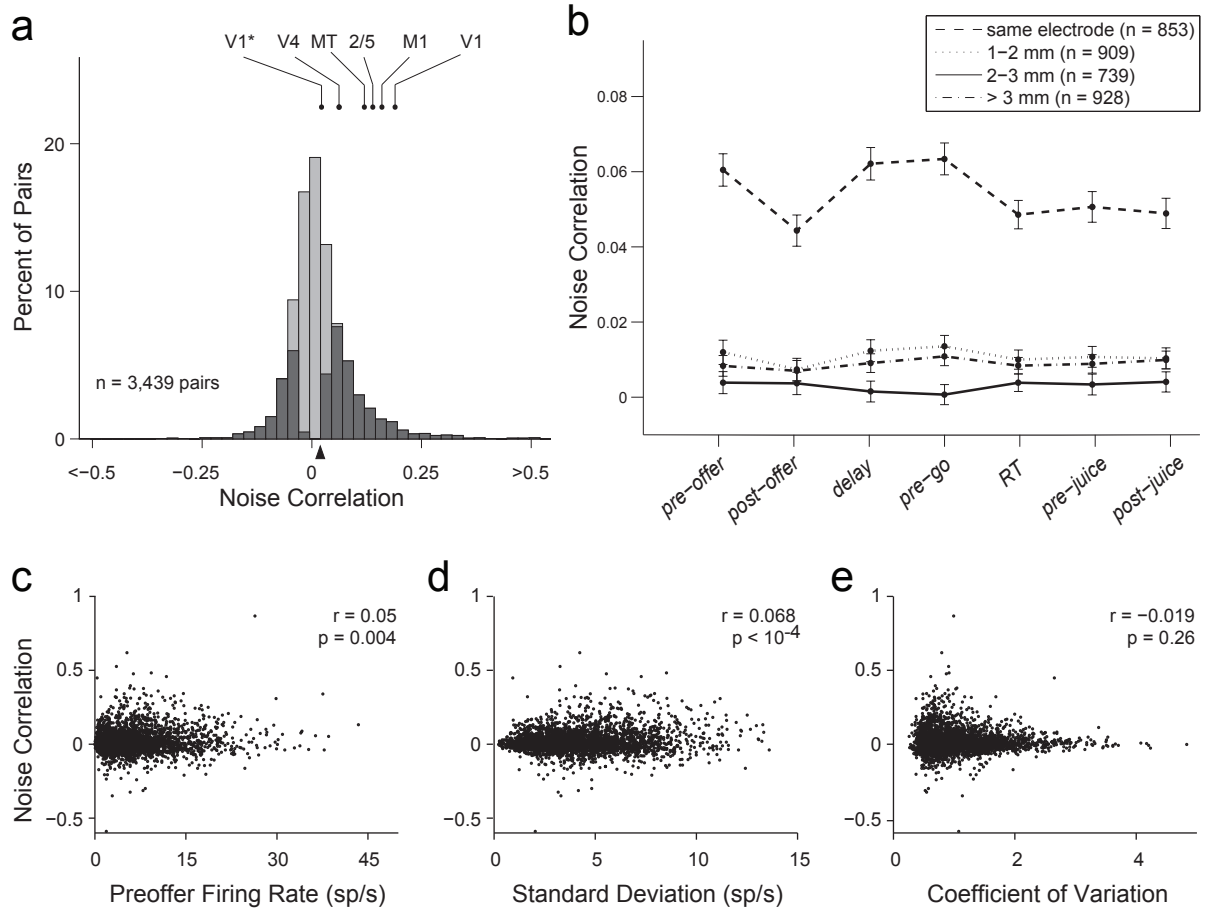

Figure 2.3 Noise correlation (rnoise) between pairs of neurons in OFC. a. Overall distribution of rnoise. In this plot, we pooled all cell pairs and all time windows. Cell pairs with significant rnoise are indicated in dark. The rnoise differed significantly from zero for 1,592/3,439 (46%) cell pairs ($p<0.05$; bootstrap analysis; see Materials & Methods). The black triangle below the x-axis marks the population average. For comparison, we indicate measures of noise correlation previously reported for MT (Zohary et al. 1994), parietal areas 2/5 (Lee et al. 1998), M1 (Lee et al. 1998), V4 (Mitchell et al. 2009) and V1. For V1, the higher data point shown here is from (Poort and Roelfsema 2009) and comparable measures were reported in (Gutnisky and Dragoi 2008; Kohn and Smith 2005; Nienborg and Cumming 2006; Smith and Kohn 2008); the lower data point is from (Ecker et al. 2010) and a comparable measure was reported in (Ecker et al. 2014). b. Values of rnoise grouped by inter-electrode distance. The x-axis represents different time windows (see Materials & Methods). For all time windows, rnoise was significantly higher when the two cells were recorded from the same electrode. Notably, rnoise did not decrease beyond values measured at 1 mm distance. Error bars indicate SEM. c. Noise correlation as a function of the geometric mean of baseline firing rates. The geometric mean averaged across the population was 5.85 ± 0.09 sp/s (mean ± SEM). Across the population, noise correlations were weakly but significantly correlated with the geometric mean of baseline firing rates ($r = 0.05$, $p<0.005$; Spearman rank correlation). d. Noise correlation as a function of the geometric mean of standard deviations. Population mean ± SEM = 4.20 ± 0.04 sp/s. e. Noise correlation as a function of the geometric mean of the coefficients of variation. Population mean ± SEM = 1.048 ± 0.009. Data for panels cde were taken from the pre-offer time window. Note that values of rnoise for individual cell pairs fluctuate throughout the course of the trial and are negatively correlated with firing rate across time windows (see Fig.4).

(Averbeck and Lee 2003; Ecker et al. 2014; Ecker et al. 2010; Mitchell et al. 2009; Miura et al. 2012). We thus examined several factors that might have artificially biased our estimates of noise correlation. First, since correlated activity may have variable timing, it is possible to underestimate noise correlations if the time windows for calculations are too small. However, the time windows used here (200-500 ms) were comparable to those used in many other studies and would capture the majority of correlated activity even if the timing of spikes varied stochastically over ~100 ms (Cohen and Kohn 2011). For an additional control, we doubled the size of the time windows to 1 s and found that r_{noise} increased only by 15%. Second, imperfect spike sorting can bias measurements of r_{noise}. Specifically, when multiple cells are recorded on the same electrode, mis-assignment of spikes can create spurious correlations. However, this type of error would only apply to cells from the same electrode, and it would tend to inflate rather than reduce r_{noise}. Conversely, discarding meaningful spikes or mistakenly splitting spikes from one cell into several clusters could artificially lower r_{noise}. However, in order to decrease r_{noise} from 0.1 to the levels we observed in OFC, it would be necessary to discard >75% of spikes or to mis-identify a single neuron as more than six separate cells (Cohen and Kohn 2011), which seems implausible. Third, firing rates in OFC are lower than in many other cortical areas (see below), and noise correlations tend to increase with firing rate (de la Rocha et al. 2007). Thus one possibility is that the discrepancy in r_{noise} reflected a genuine difference between areas, but was entirely due to the properties of individual cells as opposed to the network organization. However, additional analyses cast doubts on this view. Indeed, values of r_{noise} were comparable for pairs of tuned and *null* cells, despite the fact that *null* cells had lower firing rates throughout the trial. Furthermore, although the geometric mean of the firing rates was significantly related to r_{noise} in our dataset, this correlation was weak (Fig.2.3c). Finally, our results can be compared to the predictions of a

model relating noise correlation to firing rate (Cohen and Kohn 2011). The model predicts r_{noise} > 0.15 when both neurons have a firing rate of 1 sp/s. In our dataset, 90% of pairs had a baseline firing rate >1 sp/s for both neurons, while only 5% of pairs had r_{noise} > 0.15. In conclusion, differences in firing rates between OFC and sensory areas cannot fully explain the lower noise correlations found in OFC.

2.3.3 Time course of noise correlations

We next examined how noise correlations varied over the course of a trial. A first analysis was based on seven large time windows. A repeated-measures ANOVA revealed that the strength of noise correlations varied systematically across time windows ($p<10^{-5}$; Fig.2.3b). A post-hoc analysis indicated that r_{noise} was significantly lower during the post-offer time window compared to the pre-offer, delay and pre-go time windows ($p<0.005$; Tukey-Kramer test). Intermediate r_{noise} occurred during RT, pre-juice and post-juice time windows.

To analyze the time course of r_{noise} at higher resolution, we calculated r_{noise} in 200 ms sliding time windows. As illustrated in Fig.2.4a, the mean(r_{noise}) dropped immediately after the offer presentation and returned to baseline levels ~700 ms after the offer. It dropped again, but to a lesser extent, after the go signal, remained depressed until juice delivery, and returned to baseline gradually in the subsequent 1 s. Interestingly, the time profile measured for the correlated variability (Fig.2.4a) closely resembled that measured for the variability of individual cells (Fig.2.2e) and was inversely related to neuronal firing rate over the course of the trial (Fig.2.4b). One concern might be whether transient decreases in noise correlation are caused by increases in firing rates. To address this issue, we restricted the analysis to cells whose firing rate *decreased* after the offer, and found that mean(r_{noise}) dropped after the offer even for these cells. Thus the drop in r_{noise} observed in Fig.2.4a was not simply a byproduct of higher firing rates.

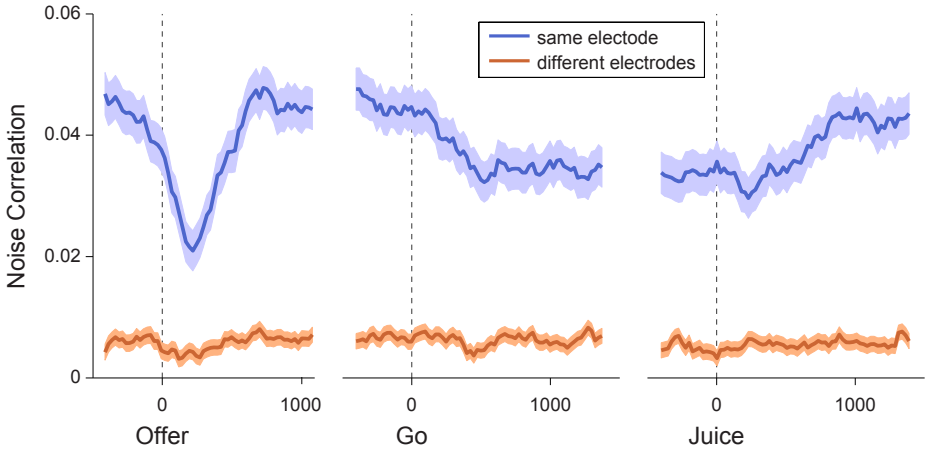

Figure 2.4 Time course of noise correlation and firing rate. a. Noise correlation. Values of rnoise were computed in 200 ms time windows slid by 25 ms intervals around offer presentation (left panel), go signal (middle panel) and juice delivery (right panel). In the figure, each data point is placed on the x-axis in the center of the corresponding time window. Dark lines and shaded regions indicate mean(rnoise) and SEM, respectively. Noise correlations¬ dropped sharply and transiently after the offer. This effect, most evident when neurons were recorded from the same electrode, was also observed when neurons were recorded from different electrodes. A second and more modest decrease in rnoise occurred after the go signal. This second drop was pronounced only in same-electrode pairs. Noise correlations gradually returned to baseline levels after juice delivery. The figure includes all cell pairs in the data set (863 same-electrode pairs, dark gray; 2,576 different-electrode pairs, light gray). b. Firing rate. The figure illustrates the firing rate averaged across all tuned cells (763 cells). All conventions as in panel a.

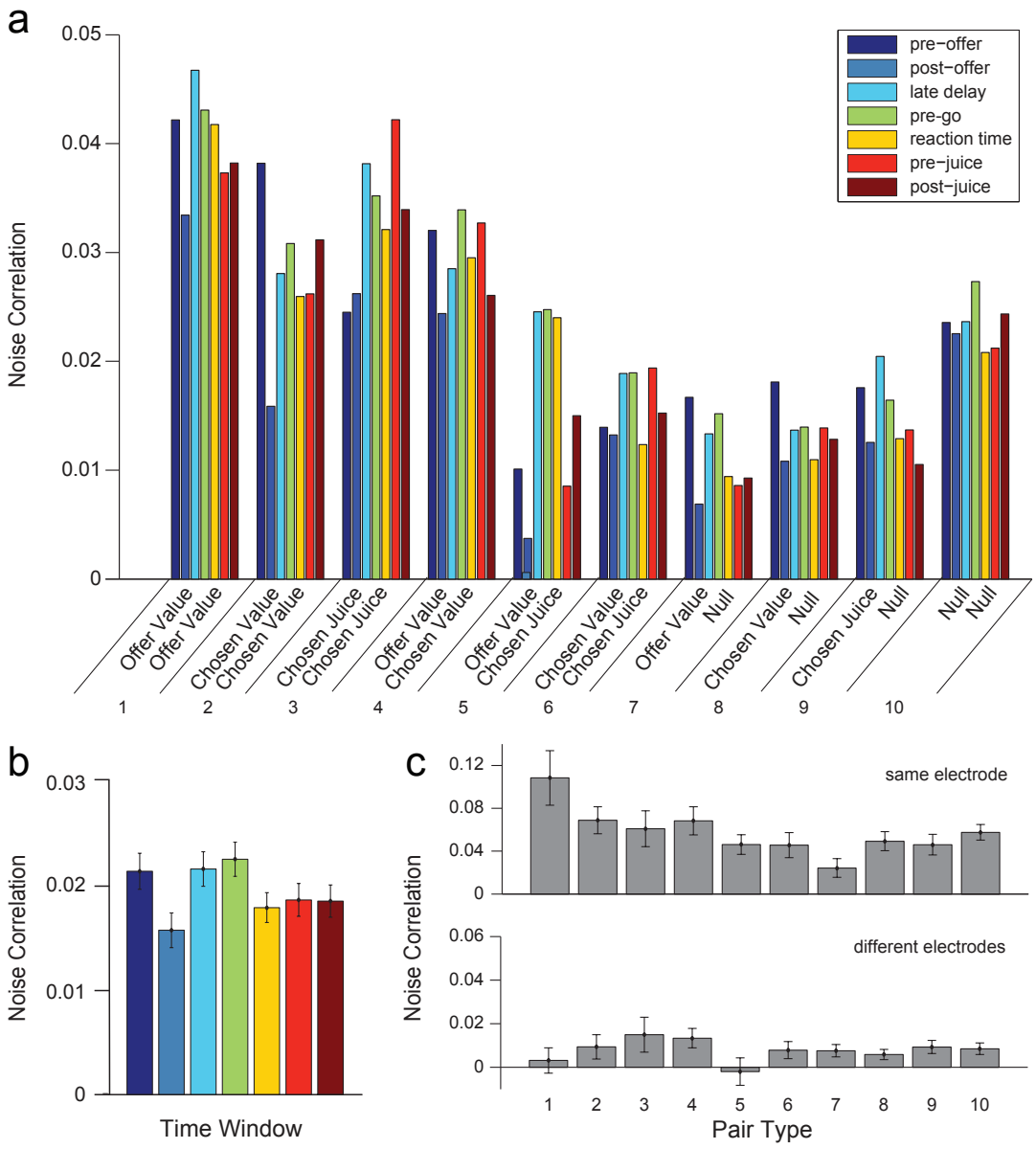

Figure 2.5 Noise correlations for different pair types. a. Mean rnoise recorded for ten pair types and seven time windows. The number of pairs for each pair type is indicated in Table 1 and colors indicate different time windows. Starting from the pre-offer time window (baseline), rnoise decreased in the post-offer time window (9/10 pair types). It then increased in the delay and pre-go time windows compared to the post-offer (10/10 pair types). It decreased again in the RT time window (10/10 pair types) and remained roughly stable for the rest of the trial. Notably, null cells had much lower firing rates compared to tuned cells. The fact that noise correlations between pairs of null cells (pair type 10) were lower than, but comparable to those between tuned neurons confirmed that firing rate was not the primary factor in rnoise. b. Mean rnoise for pair types 1-3, divided by juice polarity (see Materials & Methods). Pairs of neurons with the same polarity are on the left of each panel, while those with opposite polarities are on the right. For chosen juice pairs with opposite polarity, residual activity from the previous trial leads to negative noise correlations in the pre-offer time window. c. Mean rnoise by pair type. Data from different time windows are averaged separately for cell pairs recorded from the same electrode (top) and from different electrodes (bottom). All error bars indicate SEM.

We next examined the time course of noise correlations as a function of the variables encoded by the two cells. Neurons in our data set fell into four groups – *offer value, chosen value, chosen juice* and *null*. These groups led to ten pair types (Table 2.1). Fig.2.5a summarizes the values of r_{noise} observed for every pair type and time window. The time course of noise correlations was roughly consistent across pair types. In almost all cases, r_{noise} decreased in the post-offer time window compared to baseline, increased in the delay and pre-go time windows, decreased again after the go signal and remained stable for the rest of the trial. Pairs of *chosen juice* neurons (pair type 3) presented an exception to this pattern. For these pairs, r_{noise} was lowest in the pre-offer time window, with a non-significant increase after the offers were presented. This time course reflects a distinct feature of *chosen juice* neurons. Unlike other groups of neurons, *chosen juice* cells show in the pre-offer time window a tail activity related to the outcome of the previous trial (Padoa-Schioppa 2013). Thus if two *chosen juice* cells have opposite juice preference, the tail activity introduces a negative correlation in the pre-offer time window. This point can be observed in Fig.2.5b (far right), where pairs of chosen juice cells were divided based on whether they encoded the same juice (same polarity) or different juices (opposite polarity). Note that for pairs of *chosen* juice cells with the same polarity, the time course across time windows is similar to that observed for other pair types.

2.3.4 Noise correlations depend on the variables encoded by the two cells

A primary goal of the study was to assess how noise correlations depend on the variables encoded by the two cells. To examine this issue, we first pooled data across time windows for each pair type (see Fig.2.5a) and examined the entire population. A one-way ANOVA showed a significant effect of the pair type ($p < 3*10^{-4}$). Mean(r_{noise}) was generally highest when two cells encoded the same variable (pair types 1-3) or were both *null* (pair type 10). However, r_{noise} was

also relatively high for pairs of [*offer value*, *chosen value*] cells (pair type 4). Post-hoc tests showed several significant differences in line with these patterns (type 1 > types 6-10; type 2 > types 7-9; type 3 > types 6-8; type 4 > types 7-9; type 10 > types 7-8; $p<0.05$, Tukey's LSD). We then broke down cell pairs depending on the distance between the two neurons (Fig.2.5c). In these conditions, the pair type had a significant effect on r_{noise} when cells were from the same electrode (one-way ANOVA, $p = 0.006$). For cell pairs recorded on different electrodes, there was no significant effect of pair type (one-way ANOVA, $p = 0.7$). This finding suggests that the systematic pattern seen in Fig.2.5a was influenced by the spatial distribution of cells. Indeed, the proportion of pairs found on the same electrode was about twice as high for pair types 1-4 and pair type 10 than it was for pair types 6-9 (see Table 2.1), leading to greater mean(r_{noise}) in these pair types.

We further analyzed noise correlations between cells in the same group (*offer value*, *chosen value*, *chosen juice*). Specifically, we examined how r_{noise} depended on whether the two cells encoded the same juice or different juices, and how r_{noise} depended on the slope signs (positive or negative encoding). For *offer value* cells, the encoded juice and the slope sign were always unambiguous. For *chosen juice* cells, the design of experiment 1 made it impossible to distinguish between a cell encoding juice A with a positive slope and a cell encoding juice B with a negative slope (in both cases, the firing rate would be high/low for choices of juice A/B). We thus developed the concept of neuron polarity, which combined juice association and slope sign (see Materials & Methods). In essence, two cells had the same/opposite polarity if they "supported" the same/opposite decision. Our analyses showed that noise correlations were generally higher when two cells in the same group had the same polarity (Fig.2.5b, Fig.2.6ab). This pattern could be observed in both pairs from the same electrode and pairs from different

electrodes (same electrode, $p<10^{-4}$; different electrode, $p < 0.003$; separate two-way ANOVAs with factors [pair type x polarity]).

In the most granular analysis, we divided pairs of *offer value* cells in eight pools depending on whether the cells were recorded from the same or different electrodes, on whether the cells encoded the same juice or different juices, and on whether the sign of the encoding (positive or negative) was the same or different (Fig.2.6cd). At this level, there were no statistical differences between groups (t test, all $p > 0.05$). However, the patterns are interesting to note, since they are responsible for the differences in juice polarity shown in Fig.2.6ab which are used in the remainder of the paper. Noise correlations were highest when the two cells encoded the same juice with the same sign and progressively lower when the two cells encoded different juices with opposite signs, different juices with the same sign, and the same juice with opposite signs.

When two *offer value* cells encoded the same variable (same juice, same sign) and were recorded from the same electrode, mean(r_{noise}) was comparable to values seen in many sensory areas (Cohen and Kohn 2011). However, unlike neurons in sensory regions, *offer value* cells did not appear to cluster based on the encoded variable. Such a clustering would make it more likely to encounter pairs of *offer value* cells encoding the same variable (same juice, same sign) when two neurons are recorded from the same electrode compared to when two neurons are recorded ≥1 mm apart. In contrast, considering all pairs of *offer value* cells, 15/40 (38%) encoded the same variable when the two neurons were recorded from the same electrode, while 26/73 (34%) encoded the same variable when the two neurons were recorded from different electrodes (Fig.2.6cd).

We do not know how sharply r_{noise} decays with distance, but it appears clear that the decay fully

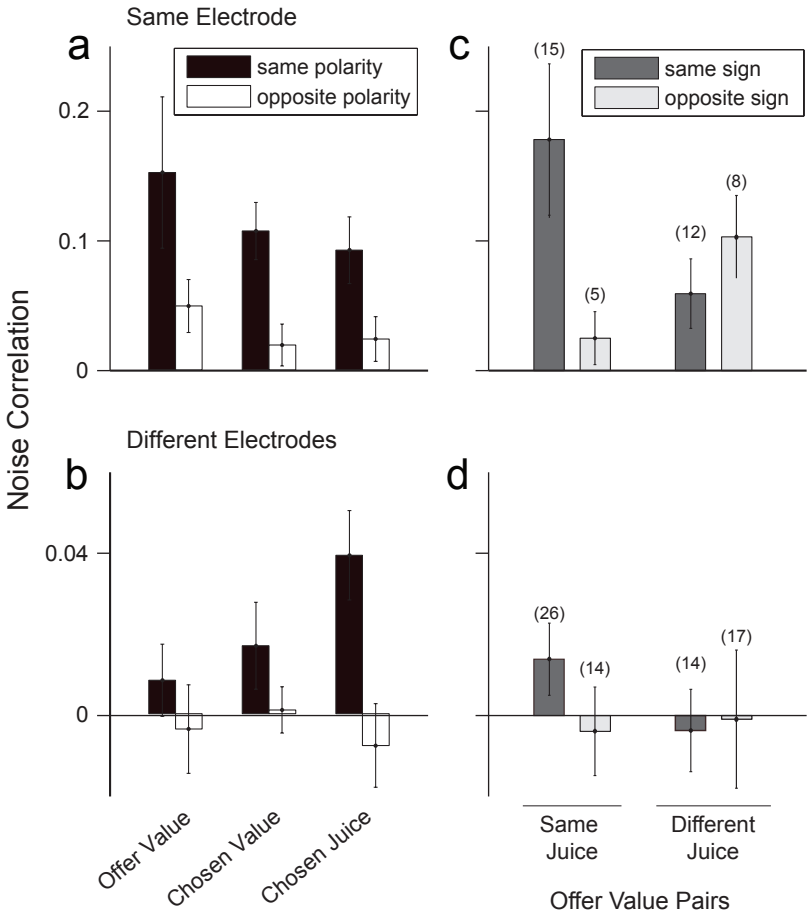

Figure 2.6 Noise correlations depend on the polarity of the two cells. Top (bottom) panels refer to cell pairs from the same electrode (different electrodes). ab. Noise correlations between cells in the same group (offer value, chosen value and chosen juice). Black (white) bars refer to pairs of cells with the same (opposite) polarity. For each cell group, rnoise was higher when the two neurons had the same polarity. This observation was true both at short and long distance. cd. Noise correlations between pairs of offer value cells. Pairs were divided in 8 pools depending on whether the two cells were recorded from the same or different electrode (top, bottom), on whether the two neurons encoded the same juice or different juices (left, right), and on whether the sign of the encoding for the two cells was the same or different (dark gray, light gray). In general, rnoise was highest when two cells encoded the same juice with the same sign. Values of rnoise show the average across all time windows. Numbers in parentheses indicate the number of neurons in each pool. All error bars indicate SEM.

occurs within 1 mm (Fig.2.3b). Since the area of OFC examined in our studies is relatively large (10-20 mm^2 of cortex), most pairs of *offer value* cells are ≥1 mm apart. Hence, the results shown in Fig.2.6d likely represent the typical r_{noise} for the majority of *offer value* cell pairs. Among these pairs, mean(r_{noise}) was highest when neurons encoded the same juice with the same sign. This gives rise to the difference in juice polarity seen in Fig.2.6ab and is particularly important for the remainder of the paper. If noise correlations within and between pools of *offer value* cells were balanced, stochastic fluctuations in different pools of neurons would be equal on average and their effects onto the decision would cancel. As a consequence, CPs would be at chance (Haefner et al. 2013; Nienborg et al. 2012). Thus the extent to which CPs of *offer value* cells differ from chance level is tightly related to the differences between the values shown in Fig.2.6d.

2.3.5 Choice probabilities in orbitofrontal cortex

Current models posit that economic decisions are based on values computed in the OFC. In other words, *offer value* cells would provide the primary input to the decision. Consider a neuron that contributes to a decision process. In principle, stochastic fluctuations in the activity of the cell might be correlated with the decision made on any given trial. This correlation is quantified as a choice probability (CP), which is essentially the probability with which an ideal observer would infer the decision outcome based only on the activity of the cell (Britten et al. 1996). At chance, CP = 0.5 and by convention CP>0.5 (CP<0.5) for neurons with positive (negative) encoding. We thus examined CP for *offer value* cells. To obtain an overall estimate for the population, we pooled neurons associated with the two juices (A and B) and we rectified the CP of *offer value* cells with negative encoding (see Materials & Methods). The distribution of CPs measured in the 500 ms after the offer was broad, with mean(CP) = 0.513 ± 0.007 (Fig.2.7a). This value was

higher than, but not statistically different from 0.5 ($p = 0.08$; t test). Importantly, CPs may be partly or fully explained by post-decision feed-back. In principle, feed-forward and feed-back components of CPs can be disentangled based on a precise estimate of the decision time, which can be obtained in perceptual decisions using dynamic stimuli (Nienborg and Cumming 2009). However, economic decisions are not equally amenable to this approach because "stimuli" (i.e., offers) are entirely and unambiguously revealed as soon as they appear on the monitor. Importantly, when we quantified CPs focusing on an earlier and shorter time window (150-400 ms after the offer, as in a previous study (Padoa-Schioppa 2013)), we obtained a measure that was smaller but still >0.5 (mean(CP) = 0.507 ± 0.007). All *offer value* cells associated to a given juice carry the same signal (they encode the same variable). But from a decoding perspective, it would make sense if neurons with higher signal-to-noise ratio (higher neuronal sensitivity) had greater influence on the decision (higher CP). Indeed, a correlation between CP and neuronal sensitivity has been observed in sensory areas during perceptual decisions (Britten et al. 1996; Liu et al. 2013). We thus examined the relation between the CP and the neuronal sensitivity of individual cells across the population (Fig.2.7b). For each *offer value* cell, the neuronal sensitivity was calculated dividing the tuning slope by the average standard deviation. In this analysis, we pooled cells associated with the two juices (A and B), but we did not rectify cells with negative encoding (neuronal sensitivity < 0). CP and neuronal sensitivity were significantly correlated ($r = 0.20$, $p < 0.003$, Spearman rank correlation). We further quantified the relation between CP and sensitivity with a linear fit ($y = a_0 + a_1 x$; Fig.2.7b, red line), which provided a linear term significantly greater than zero ($a_1 = 0.14$; 95% confidence interval = [0.06, 0.21]). To assess distortions from linearity, we also performed a fit using a third order polynomial ($y = a_0 + a_1 x + a_2 x^2 + a_3 x^3$; Fig.2.7b, blue line). We found that terms a_0 and a_1 were significantly greater

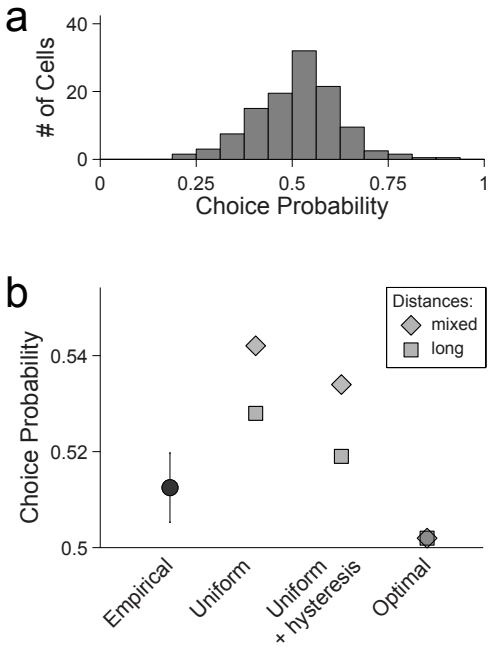

Figure 2.7 Choice probabilities and noise correlations. a. Empirical distribution of CPs measured in the 500 ms after offer onset (N = 229 cells). Cells with positive and negative encoding were pooled (see Materials & Methods). Across the population, mean(CP) = 0.513 ± 0.007 (± SEM). b. Relation between choice probability and neuronal sensitivity. Each data point in the figure represents one offer value cell. For each neuron, the neuronal sensitivity was calculated dividing the tuning slope by the average standard deviation. Cells encoding the two juices (A and B) were pooled, but cells with a negative encoding were not rectified here (sensitivity < 0). Color lines indicate the result of a linear fit (a0 + a1 x; red line) and the result of a fit based on a third-order polynomial (a0 + a1 x + a2 x2 + a3 x3; blue line). In the latter, terms a0 and a1 were significantly >0, while terms a2 and a3 were indistinguishable from 0, indicating that the read-out of offer value cells was close to optimal (Haefner et al. 2013). Two outliers (gray dots) were not included in the regressions, but adding them to the data set did not alter any of the significance results. cd. Reconstructing choice probabilities from noise correlations. Each data point represents the mean(CP) obtained empirically or from a simulation (see Results). The error bars shown for the empirical measure indicate SEM. For each read-out scheme, long-distance and mixed-distance simulations provided, respectively, a lower bound and an upper bound for mean(CP) (see Materials & Methods). Empirical and simulated CP were calculated during the post-offer time window (c) and the window 150-400ms following offer onset (d).

than zero (95% confidence interval) while terms a_2 and a_3 were statistically indistinguishable from zero (95% confidence interval). For a control, we repeated these analyses based on polarity (i.e., separating neurons associated with the two juices) and we obtained similar results. These analyses essentially fulfill the optimality test of Haefner et al (2013). The results indicate that the read-out of *offer value* cells does not differ significantly from an optimal scheme.

As previously noted (Padoa-Schioppa 2013), mean(CP) measured for *offer value* cells was substantially lower than the equivalent measure obtained for neurons in the middle temporal (MT) area during perceptual decisions (Britten et al. 1996; Cohen and Newsome 2009). At the same time, noise correlations between pairs of *offer value* cells were 5-10 times smaller than those measured in area MT under comparable conditions (Fig.2.6cd). Importantly, a precise mathematical relation links noise correlations, CPs and the read-out weights of individual cells in a population. Within this computational framework, concurrent measures of noise correlations and CPs gave us the opportunity to investigate quantitatively the contribution of *offer value* cells to economic decisions.

2.3.6 Reconstructing choice probabilities from noise correlations

Using Haefner's equation (Eq.2), we conducted a series of simulations to assess whether noise correlations measured in the OFC, taken together with a plausible read-out scheme of *offer value* cells, would induce a distribution of CPs close to that measured empirically. Specifically, we simulated CPs for a population of 10,000 *offer value* units. One half of the units had positive polarity (representing positive encoding of juice A or negative encoding of juice B) and the other half had negative polarity (representing negative encoding of juice A or positive encoding of juice B). Noise correlations used in the simulations were computed from the empirical distributions measured for pairs of *offer value* cells during the post-offer time window (see

Materials & Methods). We examined several read-out schemes (see below). For each scheme, we considered two noise correlation matrices, referred to as "long-distance" and "mixed-distance", which effectively provided a lower bound and an upper bound for mean(CP) (see Materials & Methods).

Fig.2.7c summarizes the results of six simulations. First, we considered the simple case in which all units have equal magnitude weights (all $\omega_i = \pm 1$). CPs obtained from these simulations (long-distance mean(CP) = 0.528; mixed-distance mean(CP) = 0.542) were clearly above the empirical measure. Importantly, these simulations ignored a known source of choice variability, namely choice hysteresis (Padoa-Schioppa 2013). In essence, when two offers have similar values, monkeys were mildly biased towards the juice they chose in the previous trial. Choice hysteresis was quantified using a logistic analysis and its effect was equivalent to multiplying the quantity of the previously chosen juice by 1.161. Most importantly, choice hysteresis was not reflected in the activity of *offer value* cells (Padoa-Schioppa 2013) and could thus be interpreted as an independent input to the decision. To account for choice hysteresis in the simulation, we incorporated two "fictive" units, one positive and one negative, corresponding to a previous choice of juice A or juice B, respectively. The relative weight of the two hysteresis units was derived mathematically starting from the estimate obtained from the logistic analysis, and was equal to ±0.161 times the cumulative weight of *offer value* units (see Materials & Methods). CPs obtained from these simulations (long-distance mean(CP) = 0.519; mixed-distance mean(CP) = 0.534; Fig.2.7c) were closer to, but still above, the empirical measure.

Imposing uniform read-out weights may be overly simplistic, since the brain could certainly take advantage of the heterogeneity in neuronal responses encoding a given offer value (Ecker et al. 2011). Indeed, the linear relation between CP and neuronal sensitivity across the population

(Fig.2.7b) suggests that the read-out of *offer value* cells is close to optimal (Haefner et al. 2013). Thus to complement our simulation analyses, we calculated the mean(CP) for a population of *offer value* units under the assumption of an optimal linear read-out. Optimal read-out weights were computed using Fisher's linear discriminant analysis, which finds the set of weights that best separates two conditions – in this case, choice A versus choice B. These weights took into account the slope of the encoding measured for each neuron, as well as the response covariance measured across neurons. We thus computed the optimal read-out weights for the population of *offer value* cells. CPs obtained from these simulations (long-distance mean(CP) = 0.502; mixed-distance mean(CP) = 0.502; Fig.2.7c) were essentially at chance level and well below the empirical measure.

We repeated these analyses using a shorter and earlier time window (150-400ms after offer onset) (Fig.2.7d). Noise correlations, empirical CPs and simulated CPs were all lower in this time window. Notably, the empirical measure of mean(CP) was very close to that obtained from the simulation using uniform weights and accounting for choice hysteresis (empirical = 0.507, simulated = 0.506).

To summarize, the CPs of *offer value* cells were lower than those typically measured in sensory areas during perceptual decisions. However, CPs were quantitatively as expected given the structure and the strength of noise correlations measured for pairs of *offer value* cells in OFC. The results obtained focusing on an earlier and shorter time window strengthen this conclusion.

2.4 Discussion

2.4.1 Noise correlations in orbitofrontal cortex are low

Noise correlations in the OFC were on the order of 0.01. This measure is substantially lower than those reported for many cortical regions. Specifically, work in V1 (Gutnisky and Dragoi 2008; Kohn and Smith 2005; Nienborg and Cumming 2006) but see (Ecker et al. 2010), V2 (Nienborg and Cumming 2006), MT (Cohen and Newsome 2009; Zohary et al. 1994), somatosensory area S2 (Romo et al. 2003) and primary motor cortex (Lee et al. 1998) have found noise correlations ranging 0.1-0.25. Studies in V4 (Cohen and Maunsell 2009; Mitchell et al. 2009) have reported intermediate levels of correlation ($r_{noise} \approx 0.03$-0.07), which are closer to but still slightly higher than those observed here for OFC. In lateral prefrontal cortex, noise correlations were smaller, but about twice the size of those found here (Constantinidis and Goldman-Rakic 2002). Importantly, many of these measures were obtained in awake behaving monkeys (Cohen and Newsome 2009; Gutnisky and Dragoi 2008; Nienborg and Cumming 2014; 2006; Poort and Roelfsema 2009; Zohary et al. 1994). Notable exceptions are the studies of Ecker and colleagues, who recently reported measures of r_{noise} in V1 comparable to those described here, and raised the hypothesis that high noise correlations measured in earlier studies may reflect factors such as spatial attention or task strategy (Ecker et al. 2014; Ecker et al. 2010) see also (Gawne et al. 1996; Gawne and Richmond 1993). In this respect, it is worth emphasizing that our animals were actively engaged in a choice task. Moreover, since neurons in the OFC are not spatially tuned or associated with specific actions, factors such as spatial attention, action planning or minor stimulus variability are unlikely to affect r_{noise}. Thus noise correlations in the OFC seem genuinely lower than those measured in sensory areas under comparable conditions. How can we explain this discrepancy?

Possibly important is the fact that our offers were always unequivocally defined. In contrast, studies of perceptual decisions often used stochastic stimuli (Liu et al. 2013; Nienborg and Cumming 2006; Poort and Roelfsema 2009; Zohary et al. 1994). In principle, specific realizations of a stochastic stimulus could elicit systematic neuronal responses (Bair and Koch 1996), which could result in over-estimates of noise correlations (because noise correlations could partly reflect signal correlations). Independently of this consideration, at least two features distinguish OFC structurally and functionally from sensory areas. First, OFC lacks a clear position in a feed-forward processing stream and, instead, integrates converging inputs from multiple sensory and limbic regions (Ongur and Price 2000). In contrast, sensory systems typically present hierarchical processing streams and are, by definition, predominantly unimodal. Theoretical analysis has suggested that correlations arise naturally across sequential stages of feed-forward processing (Rosenbaum et al. 2010) and that hierarchical organization in itself may contribute to r_{noise} in many sensory areas. Consistent with this view, noise correlations in perirhinal cortex (Erickson et al. 2000) and in the supplemental motor area (SMA) (Averbeck and Lee 2003), both of which lack a clear hierarchical position, are low and comparable to those measured here. Second, aside from hierarchy, it remains unclear whether OFC has any topographic organization. As noted above, pairs of *offer value* cells encoding the same variable (same juice, same sign) were equally prevalent at short and long distances (Fig.2.6cd), indicating that any clustering is loose at best. At the same time, significant CPs are almost exclusively observed when the choice-relevant variable is topographically organized within a cortical area (Nienborg and Cumming 2014), suggesting that the circuit organization associated with a topographic map is a necessary condition to observe the patterns of noise correlation that induce high CPs. Interestingly, the rodent anterior piriform cortex (Miura et al. 2012), which also lacks

any clear topography, is one of the few areas where r_{noise} is comparable to that measured here. Conversely, noise correlations in SMA – an area with a clear topography – are low (Averbeck and Lee 2003), indicating that topography is necessary but not sufficient to induce high noise correlations.

Despite differences in strength, noise correlations measured in the OFC presented several traits that clearly resembled those observed in other brain regions. First, r_{noise} was strongly affected by distance, falling off within 1 mm. A similar effect of distance was found in other cortical areas, although the decay was less sharp in V1 (Smith and Kohn 2008) and V4 (Smith and Sommer 2013). Second, as observed in sensory areas (Cohen and Newsome 2008; Liu et al. 2013; Smith and Kohn 2008), r_{noise} in OFC was highest when two neurons had similar tuning (i.e., when they encoded the same juice with the same sign). Notably, it is the "differential" component of noise correlations that ultimately limits the information encoded by a neuronal population (Abbott and Dayan 1999; Moreno-Bote et al. 2014; Shadlen et al. 1996). Third, the time course of noise correlations within a trial – specifically the fact that r_{noise} drops immediately after presentation of a relevant stimulus – is a common phenomenon (Carnevale et al. 2012; Churchland et al. 2010; Kohn and Smith 2005). In conclusion, it appears that noise correlations measured in OFC differ in strength, but not in structure from those measured in other brain regions.

2.4.2 Noise correlations, choice probabilities and offer-value read-out

Current neuroeconomic models assume that decisions are based on subjective values computed in the OFC (Kable and Glimcher 2009; Padoa-Schioppa 2011; Rangel and Hare 2010; Rushworth et al. 2012). In the formalism of a linear decision model (Eq.1), this means that the normalized read-out weights of *offer value* cells should add to 1. Taking into account choice hysteresis, which provides a smaller but independent contribution to the decision, this

proposition can be amended stating that normalized read-out weights of each *offer value* pool should add to ~0.839. To test this hypothesis, one would ideally measure read-out weights directly, but this is not practically feasible. However, read-out weights are quantitatively related to noise correlations and CPs, both of which can be measured. Based on this theoretical framework, we showed that the distribution of CPs measured for *offer value* cells can be reconstructed from concurrent measures of noise correlations assuming a plausible scheme of read-out weights. More specifically, the empirical measure for mean(CP) fell between the values obtained with a uniform and with an optimal read-out.

Our results provide a plausibility argument in favor of the hypothesis that *offer value* cells provide the primary input to economic decisions. Importantly, the decision process is most likely affected also by other factors. For example, previous results indicated that decisions are partly biased by the initial state of the neural assembly, reflected in the "predictive activity" of *chosen juice* cells (Padoa-Schioppa 2013). This predictive activity is largely a tail activity from the previous trial and is thus related to the behavioral phenomenon of choice hysteresis. Thus our simulations accounted for this source of choice variability. At the same time, our simulations did not include other possible sources of variability such as residual fluctuations in the initial state of the decision circuit, trial-by-trial fluctuations in the relative value of the goods (Padoa-Schioppa 2013) or downstream noise (Haefner et al. 2013). Most importantly, since any of those factors would reduce CPs, simulation analyses that accounted for any of them would effectively strengthen our current conclusions. Conversely, the extent and implications of non-linearities in the decoder remain to be examined. Exploring the fine structure and the mechanisms of the neural circuit that generates value-based decisions is a major goal for future research.

2.5 References

Abbott LF, and Dayan P. The effect of correlated variability on the accuracy of a population code. *Neural Comput* 11: 91-101, 1999.

Ahn S, and Fessler JA. Globally convergent image reconstruction for emission tomography using relaxed ordered subsets algorithms. *IEEE Trans Med Imaging* 22: 613-626, 2003.

Averbeck BB, and Lee D. Neural noise and movement-related codes in the macaque supplementary motor area. *J Neurosci* 23: 7630-7641, 2003.

Bair W, and Koch C. Temporal precision of spike trains in extrastriate cortex of the behaving macaque monkey. *Neural Comput* 8: 1185-1202, 1996.

Britten KH, Newsome WT, and Saunders RC. Effects of inferotemporal cortex lesions on form-from-motion discrimination in monkeys. *Exp Brain Res* 88: 292-302, 1992.

Britten KH, Newsome WT, Shadlen MN, Celebrini S, and Movshon JA. A relationship between behavioral choice and the visual responses of neurons in macaque MT. *Vis Neurosci* 13: 87-100, 1996.

Camille N, Griffiths CA, Vo K, Fellows LK, and Kable JW. Ventromedial frontal lobe damage disrupts value maximization in humans. *J Neurosci* 31: 7527-7532, 2011.

Carnevale F, de Lafuente V, Romo R, and Parga N. Internal signal correlates neural populations and biases perceptual decision reports. *Proc Natl Acad Sci U S A* 109: 18938-18943, 2012.

Churchland MM, Yu BM, Cunningham JP, Sugrue LP, Cohen MR, Corrado GS, Newsome WT, Clark AM, Hosseini P, Scott BB, Bradley DC, Smith MA, Kohn A, Movshon JA, Armstrong KM, Moore T, Chang SW, Snyder LH, Lisberger SG, Priebe NJ, Finn IM, Ferster D, Ryu SI, Santhanam G, Sahani M, and Shenoy KV. Stimulus onset quenches neural variability: a widespread cortical phenomenon. *Nat Neurosci* 13: 369-378, 2010.

Cohen MR, and Kohn A. Measuring and interpreting neuronal correlations. *Nat Neurosci* 14: 811-819, 2011.

Cohen MR, and Maunsell JH. Attention improves performance primarily by reducing interneuronal correlations. *Nat Neurosci* 12: 1594-1600, 2009.

Cohen MR, and Newsome WT. Context-dependent changes in functional circuitry in visual area MT. *Neuron* 60: 162-173, 2008.

Cohen MR, and Newsome WT. Estimates of the contribution of single neurons to perception depend on timescale and noise correlation. *J Neurosci* 29: 6635-6648, 2009.

Constantinidis C, and Goldman-Rakic PS. Correlated discharges among putative pyramidal neurons and interneurons in the primate prefrontal cortex. *J Neurophysiol* 88: 3487-3497, 2002.

de la Rocha J, Doiron B, Shea-Brown E, Josic K, and Reyes A. Correlation between neural spike trains increases with firing rate. *Nature* 448: 802-806, 2007.

Dean AF. The variability of discharge of simple cells in the cat striate cortex. *Exp Brain Res* 44: 437-440, 1981.

Ecker AS, Berens P, Cotton RJ, Subramaniyan M, Denfield GH, Cadwell CR, Smirnakis SM, Bethge M, and Tolias AS. State dependence of noise correlations in macaque primary visual cortex. *Neuron* 82: 235-248, 2014.

Ecker AS, Berens P, Keliris GA, Bethge M, Logothetis NK, and Tolias AS. Decorrelated neuronal firing in cortical microcircuits. *Science* 327: 584-587, 2010.

Ecker AS, Berens P, Tolias AS, and Bethge M. The effect of noise correlations in populations of diversely tuned neurons. *J Neurosci* 31: 14272-14283, 2011.

Erickson CA, Jagadeesh B, and Desimone R. Clustering of perirhinal neurons with similar properties following visual experience in adult monkeys. *Nat Neurosci* 3: 1143-1148, 2000.

Gallagher M, McMahan RW, and Schoenbaum G. Orbitofrontal cortex and representation of incentive value in associative learning. *J Neurosci* 19: 6610-6614, 1999.

Gawne TJ, Kjaer TW, Hertz JA, and Richmond BJ. Adjacent visual cortical complex cells share about 20% of their stimulus-related information. *Cereb Cortex* 6: 482-489, 1996.

Gawne TJ, and Richmond BJ. How independent are the messages carried by adjacent inferior temporal cortical neurons? *J Neurosci* 13: 2758-2771, 1993.

Glaister P. Least squares revisited. *Math Gaz* 85: 104-107, 2001.

Gremel CM, and Costa RM. Orbitofrontal and striatal circuits dynamically encode the shift between goal-directed and habitual actions. *Nat Commun* 4: 2264, 2013.

Gutnisky DA, and Dragoi V. Adaptive coding of visual information in neural populations. *Nature* 452: 220-224, 2008.

Haefner RM, Gerwinn S, Macke JH, and Bethge M. Inferring decoding strategies from choice probabilities in the presence of correlated variability. *Nat Neurosci* 16: 235-242, 2013.

Hardin J, Garcia SR, and Golan DA. Method for generating realistic correlation matrices. *Ann Appl Stat* 7: 1733-1762, 2013.

Jeanne JM, Sharpee TO, and Gentner TQ. Associative learning enhances population coding by inverting interneuronal correlation patterns. *Neuron* 78: 352-363, 2013.

Kable JW, and Glimcher PW. The neurobiology of decision: consensus and controversy. *Neuron* 63: 733-745, 2009.

Kohn A, and Smith MA. Stimulus dependence of neuronal correlation in primary visual cortex of the macaque. *J Neurosci* 25: 3661-3673, 2005.

Lee D, Port NL, Kruse W, and Georgopoulos AP. Variability and correlated noise in the discharge of neurons in motor and parietal areas of the primate cortex. *J Neurosci* 18: 1161-1170, 1998.

Liu S, Gu Y, DeAngelis GC, and Angelaki DE. Choice-related activity and correlated noise in subcortical vestibular neurons. *Nat Neurosci* 16: 89-97, 2013.

Mitchell JF, Sundberg KA, and Reynolds JH. Spatial attention decorrelates intrinsic activity fluctuations in macaque area V4. *Neuron* 63: 879-888, 2009.

Miura K, Mainen ZF, and Uchida N. Odor representations in olfactory cortex: distributed rate coding and decorrelated population activity. *Neuron* 74: 1087-1098, 2012.

Moreno-Bote R, Beck J, Kanitscheider I, Pitkow X, Latham P, and Pouget A. Information-limiting correlations. *Nat Neurosci* 2014.

Nienborg H, Cohen MR, and Cumming BG. Decision-related activity in sensory neurons: correlations among neurons and with behavior. *Annu Rev Neurosci* 35: 463-483, 2012.

Nienborg H, and Cumming BG. Decision-related activity in sensory neurons may depend on the columnar architecture of cerebral cortex. *J Neurosci* 34: 3579-3585, 2014.

Nienborg H, and Cumming BG. Decision-related activity in sensory neurons reflects more than a neuron's causal effect. *Nature* 459: 89-92, 2009.

Nienborg H, and Cumming BG. Macaque V2 neurons, but not V1 neurons, show choice-related activity. *J Neurosci* 26: 9567-9578, 2006.

Ongur D, and Price JL. The organization of networks within the orbital and medial prefrontal cortex of rats, monkeys and humans. *Cereb Cortex* 10: 206-219, 2000.

Padoa-Schioppa C. Neurobiology of economic choice: a good-based model. *Annu Rev Neurosci* 34: 333-359, 2011.

Padoa-Schioppa C. Neuronal origins of choice variability in economic decisions. *Neuron* 80: 1322-1336, 2013.

Padoa-Schioppa C, and Assad JA. Neurons in orbitofrontal cortex encode economic value. *Nature* 441: 223-226, 2006.

Padoa-Schioppa C, and Assad JA. The representation of economic value in the orbitofrontal cortex is invariant for changes of menu. *Nat Neurosci* 11: 95-102, 2008.

Poort J, and Roelfsema PR. Noise correlations have little influence on the coding of selective attention in area V1. *Cereb Cortex* 19: 543-553, 2009.

Rangel A, and Hare T. Neural computations associated with goal-directed choice. *Curr Opin Neurobiol* 20: 262-270, 2010.

Romo R, Hernandez A, Zainos A, Lemus L, and Brody CD. Neuronal correlates of decision-making in secondary somatosensory cortex. *Nat Neurosci* 5: 1217-1225, 2002.

Romo R, Hernandez A, Zainos A, and Salinas E. Correlated neuronal discharges that increase coding efficiency during perceptual discrimination. *Neuron* 38: 649-657, 2003.

Rosenbaum RJ, Trousdale J, and Josic K. Pooling and correlated neural activity. *Front Comput Neurosci* 4: 9, 2010.

Rudebeck PH, Saunders RC, Prescott AT, Chau LS, and Murray EA. Prefrontal mechanisms of behavioral flexibility, emotion regulation and value updating. *Nat Neurosci* 16: 1140-1145, 2013.

Rushworth MF, Kolling N, Sallet J, and Mars RB. Valuation and decision-making in frontal cortex: one or many serial or parallel systems? *Curr Opin Neurobiol* 2012.

Shadlen MN, Britten KH, Newsome WT, and Movshon JA. A computational analysis of the relationship between neuronal and behavioral responses to visual motion. *J Neurosci* 16: 1486-1510, 1996.

Shadlen MN, and Newsome WT. The variable discharge of cortical neurons: implications for connectivity, computation, and information coding. *J Neurosci* 18: 3870-3896, 1998.

Smith MA, and Kohn A. Spatial and temporal scales of neuronal correlation in primary visual cortex. *J Neurosci* 28: 12591-12603, 2008.

Smith MA, and Sommer MA. Spatial and temporal scales of neuronal correlation in visual area V4. *J Neurosci* 33: 5422-5432, 2013.

Vogels R, Spileers W, and Orban GA. The response variability of striate cortical neurons in the behaving monkey. *Exp Brain Res* 77: 432-436, 1989.

Wallis JD. Cross-species studies of orbitofrontal cortex and value-based decision-making. *Nat Neurosci* 2011.

Xanthopoulos P, Pardalos P, and Trafalis T. Linear discriminant analysis. In: *Robust data mining*. New York: Springer, 2013, p. 27-33.

Zohary E, Shadlen MN, and Newsome WT. Correlated neuronal discharge rate and its implications for psychophysical performance. *Nature* 370: 140-143, 1994.

Chapter 3: Inefficient Adaptation to the Value Range during Economic Choice

Adaptation is a ubiquitous feature of neuronal responses. While it has been studied most frequently in sensory systems, studies have found adaptation to the subjective value distribution in several brain regions, including orbitofrontal cortex. While increases in the value range have been associated with decreases in the gain of neuronal responses, several features of value adaptation are poorly understood. In particular, previous studies of value adaptation did not dissociate the range of value from the value maximum, nor did they look for range-dependent changes in the offset of the dynamic range. Here we examine how value-encoding neurons in macaque orbitofrontal cortex adapt to changes in both maximum and minimum values. We find that neurons adapt to both the maximum and the minimum, but that adaptation is intermediate: the dynamic range does not remap completely to changes in range. Using a simulation of choice behavior, we showed that inefficiencies introduced by the change in offset may impair choice behavior and could partially limit improvements achieved through adaptation in the response gain.

3.1 Introduction

Neuronal adaptation occurs across all levels of perceptual, motor, and cognitive processing. Neural activity adapts to recent history on time scales ranging from milliseconds to hours or days (Kohn 2007; Wark et al. 2007; Hengen et al. 2013). It contributes to homeostatic regulation (Benucci et al. 2013; Hengen et al. 2013), enables efficient representation of stimuli (Adibi et al. date unknown; Dan et al. 1996; Lewicki 2002; Gutnisky and Dragoi 2008), and sharpens behavioral performance (Krekelberg et al. 2006; Liu et al. 2016).

While adaptation has been investigated most thoroughly in sensory systems, it has also been observed in value-encoding networks. Studies in non-human primates have found adaptive encoding of subjective value in several brain regions, including orbitofrontal cortex (OFC) (Padoa-Schioppa 2009; Kobayashi et al. 2010; Yamada et al. 2018), anterior cingulate cortex (Cai and Padoa-Schioppa 2014), amygdala (Saez et al. 2017), and midbrain dopamine neurons (Tobler et al. 2005). Experiments looking at BOLD activity in humans have reported value adaptation in ventromedial prefrontal cortex (vmPFC), cingulate cortex, ventral striatum, and elsewhere (Elliott et al. 2008; Cox and Kable 2014; Burke et al. 2016). Recently, studies have begun to explore the behavioral implications of value adaptation using a combination of experimental and theoretical approaches. This work suggests that value adaptation in different regions may modulate learning rates during reinforcement learning (Diederen et al. 2016) and reduce stochasticity in value-based decisions (Rustichini et al. 2017). At the same time, other studies suggest that value adaptation on a more rapid time scale may produce irrational decision-making patterns (Soltani et al. 2012; Yamada et al. 2018).

Despite this growing interest, gaps in our understanding of value adaptation limit our ability to predict and interpret its effects. Previous studies of value adaptation have not clearly distinguished between the range of values and the maximum value in a given context, making it difficult to determine which features ultimately drive responses to adapt (Padoa-Schioppa 2009; Kobayashi et al. 2010; Cox and Kable 2014). Furthermore, these studies focused exclusively on the gain of value encoding, ignoring overall changes in neuronal activity across conditions (Padoa-Schioppa 2009; Kobayashi et al. 2010; Cox and Kable 2014; Rustichini et al. 2017). In this study, we developed a task that allowed us to address these points. We focused on value encoding responses in OFC, a that has been linked value-based decision making in humans and other primates through both lesion studies (Fellows and Farah 2007; Fellows 2011; Rudebeck and Murray 2011) and neurophysiological experiments (FitzGerald et al. 2009; Peters and Büchel 2009; Kennerley et al. 2011; Raghuraman and Padoa-Schioppa 2014; Rich and Wallis 2016; Xie and Padoa-Schioppa 2016).

We analyzed the value adaptation in OFC neurons to changes in both the maximum and minimum of the value distribution. We recorded neural activity as monkeys performed a juice choice task, during which the value distribution of each juice could change in one of six ways: increase/decrease in maximum value, increase/decrease in minimum value, or increase/decrease in both. We found that value-encoding neurons adapted to both maximum and minimum values, but that responses did not remap completely to the new range of options. This intermediate adaptation was not a result of an unfinished process or of a mixture of adapting and non-adapting cells, but rather a consistent characteristic of the population. Partial adaptation could be characterized by an offset in the overall activity levels across different conditions. Simulating a simple decision network, we showed that the presence of this offset was sub-optimal, but that its effect was minor compared to the effect of narrowing the dynamic range.

3.2 Materials and Methods

3.2.1 Subjects

All experimental procedures conformed to the NIH Guide for the Care and Use of Laboratory Animals and were approved by the Animal Studies Committee at Washington University in St. Louis. Two adult male rhesus macaques (*Macaca mulatta;* D, 11.5 kg; F, 11.0 kg) were used in the study. Before training, a head-restraint device and a recording chamber were implanted on the skull under general anesthesia. The recording chamber (main axes, 50 x 30 mm) was centered on coordinates (A30, L0). Structural MRI scans were obtained before and after implantation and used to guide recording.

3.2.2 Range adaptation task

In this experiment, monkeys performed a variant of a juice choice task used in several previous studies (Padoa-Schioppa and Assad 2006; Cai and Padoa-Schioppa 2014; Xie and Padoa-Schioppa 2016). Monkeys were given a series of choices between two juices, A and B, offered in

varying quantities. Juice A was defined as the preferred juice (i.e. 1A was generally chosen over 1B). On each trial, the monkey began by fixating on a central point. After 1s, cues appeared on each side of the central fixation, indicating the current range of possible offers. The cues consisted of a set of filled and empty colored squares. The color of the squares indicated the types of juice, the total number of squares represented the maximum possible offer for that juice in the current block, and the filled squares represented the minimum possible offer in that block (Fig.3.1A). The cues remained on screen for 1s and were then replaced by a set of solid squares denoting the offers on the current trial. After a random 1-2s delay, the central fixation point disappeared and targets appeared next to each offer, signaling the monkey to indicate his choice with a saccade to one of the options. The monkey then received whichever offer he selected. If the monkey broke fixation before the go signal appeared or if he failed to fixate the target for 750ms after the saccade, the trial was aborted and the monkey received no reward.

Each session consisted of 2-3 blocks of ~250 trials. The quantity offered varied pseudo-randomly from trial to trial within a defined range. Within a block, the range of possible offers was kept consistent for each juice. The monkey could either learn the value range implicitly through experience or explicitly by use of the range cues. Between blocks, the range of available offers for each juice changed, with three possible ranges for each juice: “high” (2-5 units of juice A or 4-10 units of B), “low” (0-3 uA or 0-6 uB), and “wide” range (0-5 uA or 0-10 uB). Most range transitions consisted of an increase/decrease in the minimum value (V_{min}) while the maximum value (V_{max}) either remained constant or shifted in conjunction with the minimum. Note that when maximum and minimum values changed together, the difference between them was kept constant. We counterbalanced the type of range transition across sessions. In a smaller subset of

sessions, the maximum value increased/decreased while the minimum was kept at zero. The ranges of juice A and B could change in either the same or different directions in any session.

The task was run on custom-written software (http://www.monkeylogic.net/) based on Matlab (MathWorks). Eye position was monitored with an infrared video camera (Eyelink; SR Research).

3.2.3 Analysis of behavior

All analyses were conducted in Matlab. Unless otherwise noted, reported p-values were calculated using the Wilcoxon signed rank test.

Choice behavior was analyzed separately for each range block. We defined the choice pattern as the percent of trials in which the animal chose juice B for each offer value ratio (#B/#A). We fit the choice pattern to a sigmoid function using logistic regression:

$$P(\text{choice B}) = 1 / (1 + e^{-X})$$

$$X = a_0 + a_1 \log(\#B/\#A)$$

From this fit, we determined the relative value of the two juices (ρ) and the sigmoid steepness (η):

$$\rho = \exp(-a_0/a_1)$$

$$\eta = a_1$$

We looked for changes in ρ and η as a function of range type. To do this, we compared data for all pairs of blocks within a session. We recorded during 107 sessions, each of which included 2-3 range conditions, yielding a total of 236 unique block pairs. 31 block pairs were excluded from

analysis because the logistic regression separated choices perfectly in at least one of the blocks, preventing accurate estimation of fit parameters. For the remaining 205 block pairs, we computed a fractional difference in each parameter across different range types, where we defined fractional difference as an index variable equal to the difference in values divided by their sum. We tested whether the fractional difference deviated from zero (Wilcoxon signed rank test).

3.2.4 Electrophysiology

We recorded neuronal data from the central OFC of two monkeys, in a region approximately corresponding to area 13m (Ongur and Price 2000) (monkey D: A 31:36, L -6:-10; monkey F: A 31:37 L -6:-11 and 6:11). Recordings were obtained using tungsten electrodes (125 µm diameter; FHC) and 16-channel silicon V-probes (185 µm diameter, 100 µm spacing between electrodes; V-probe). Electrodes were lowered vertically into position each day using a custom-built microdrive (step size: 2.5 µm). Recording depth was determined ahead of time based on structural MRI. During experiments, the monkeys sat in an electrically insulated enclosure (Crist Instruments) with their head fixed.

Electrical signals were amplified (gain: 10,000) and band-pass filtered (low-pass cut-off: 300 Hz, high-pass cut-off: 6 kHz; Lynx 8, Neuralynx). Action potentials were detected on-line by setting a threshold during recording, and waveforms crossing the threshold were saved (40 kHz sampling rate; Power 1401, Cambridge Electronic Design). Spike sorting was conducted off-line using standard software (Spike 2, Cambridge Electronic Design). Neurons were included in the analysis if they remained stable and well-isolated in two range blocks for at least 120 trials per block. Responses that were not stably isolated for the full session were only analyzed for the trials in which they were stable. In the V-probe recordings, spikes from the same neuron were

occasionally picked up by two neighboring contacts. These were detected manually and one of the duplicates was excluded from analysis.

3.2.5 Response classification

We analyzed cell data in seven time windows following offer onset: post-offer (0.5 s after offer onset), late-delay (0.5-1.0 s after offer onset), pre-go (0.5 s before the go signal), reaction time (time from go cue to target acquisition, usually ~200ms), post-juice (0.5 s after juice delivery) and post-juice 2 (0.5 s to 1s after juice delivery). Data were analyzed independently for each range block. We defined a "trial type" as a set of two offers and the monkey's choice between them. For example, if the monkey chose B on a trial where he was offered 1A vs. 6B, the trial type would be [1A : 6B; B]. Task-based neuronal activity was calculated by taking the mean firing rate for each trial type in each time window. A "neuronal response" was defined as the activity of one cell in one time window across two range blocks. Since we were interested in the effects of adaptation at steady state, we discarded the first 16 trials of each block before analysis, thereby excluding trials where the monkey had not yet experienced the full range of values.

A response was considered task-related if it passed an ANOVA (factor: trial type; $p < 0.05$) in both of the two range blocks. To classify task-related responses, we regressed each response against the variables *offer value A, offer value B, chosen value,* and *chosen juice*. Regressions were performed separately for each of the two range blocks. We classified a response as encoding a variable if 1) the regression on that variable had a nonzero slope in both blocks and 2) that variable had highest total R^2 in the two blocks. Further analyses focused on *offer value* and *chosen value* responses. Responses were excluded from analysis if the ranges of the two blocks differed by <0.5 units of value for the encoded variable (132 responses) or if activity during the

fixation time window changed by a factor >1.6 (208 responses). Including these responses in the analysis added noise but did not qualitatively alter results.

3.2.6 Normalization of responses for averaging

Several figures show average traces of *offer value* response activity normalized so that value and response both range from 0-1. Unless otherwise specified, these responses were normalized such that:

$$R_{norm} = (R - R_{min,wide})/(R_{max,wide} - R_{min,wide})$$

$$V_{norm} = (V - V_{min,wide})/(V_{max,wide} - V_{min,wide})$$

for cases when either V_{max} or V_{min} change alone, and:

$$R_{norm} = (R - R_{min,low})/(R_{max,high} - R_{min,low})$$

$$V_{norm} = (V - V_{min,low})/(V_{max,high} - V_{min,low})$$

for cases where V_{max} and V_{min} shift concurrently. R_{norm} and V_{norm} denote normalized responses and values, R and V denote the non-normalized responses and values, and $R_{max,j}$ and $R_{min,j}$ indicate the response to V_{max} and V_{min} in range type j.

3.2.7 Metrics of Adaptation

Data were analyzed in Matlab (MathWorks). Unless otherwise noted, reported p-values were calculated using the Wilcoxon signed rank test.

Analysis of adaptation was restricted to *offer value A, offer value B,* and *chosen value* responses. We grouped responses into three types of range transition: change V_{max} only, change V_{min} only, and change both. Transition types could be divided further based on the direction of change

(increase/decrease). For *offer value* responses, we controlled the value range so that each transition type was consistent. Thus if we describe the offer value as a fraction of the wide value range ($\Delta V_{,wide}$), the normalized ranges are 0-0.6uV (low range), 0.4-1uV (high range), and 0-1 uV (wide range) for all *offer value* responses. *Chosen value* ranges depended on the choice pattern of the animal and varied across sessions. For the purposes of this experiment, we said that the maximum/minimum chosen value changed if the difference between was greater than >0.5 uB.

For each response, we regressed neural activity onto value independently in each range block. We obtained the slope of encoding (s) from each fit. Slopes were compared directly across range types, and the relationship between slope and range was tested more precisely using Adaptation Ratios:

$$AR_{max} = (s_1 V_{max,1}) / (s_2 V_{max,2})$$

$$AR_{range} = (s_1 \Delta V_1) / (s_2 \Delta V_{max,2})$$

$$AR_{none} = s_1 / s_2$$

Where $V_{max,i}$ is the maximum value in range i and ΔV_i is the range of values (maximum - minimum) in range i. For this experiment, we defined Range 1 = wide range for responses where V_{max} or V_{min} changed alone, and Range 1 = high value range for cases where both V_{max} and V_{min} changed.

In addition to the slope, we used the regression to calculate the responses to the minimum and maximum values (R_{min} and R_{max}) from the regression:

$$R_{min} = s * V_{min} + c$$

$$R_{max} = s * V_{max} + c$$

Where V_{min} and V_{max} are the minimum and maximum values in the current block and c is the y-intercept of the linear fit. We computed the normalized difference for conditions where either V_{min} or V_{max} change alone:

$$\Delta R_{min} = (R_{min,wide} - R_{min,narrow})/(R_{max,wide} - R_{min,wide})$$

$$\Delta R_{max} = (R_{max,wide} - R_{max,narrow})/(R_{max,wide} - R_{min,wide})$$

And for conditions where both change:

$$\Delta R_{min} = (R_{min,high} - R_{min,low})/(R_{max,high} - R_{min,low})$$

$$\Delta R_{max} = (R_{max,high} - R_{max,low})/(R_{max,high} - R_{min,low})$$

3.2.8 Analysis of time course

To study adaptation in early vs. late trials after the range transition, we separated trials from the first and second half of each range block and computed independent tuning functions for each half. Responses were excluded if the slope changed by a factor >5 in the first range block (2 responses excluded). Including these responses did not substantially affect results, but did add noise to the data, particularly for changes in Vmax. Plots of mean tuning curves in the first and second halves of each block were normalized to the first half of the wide range block.

3.2.9 Measuring nonlinearities in tuning

For each response, we fit neural activity in each block with independent second-order and third-order polynomials:

Quadratic fit: $R(V) = \beta_{0,q} + \beta_{1,q} V + \beta_{2,q} V^2$

Cubic fit: $R(V) = \beta_{0,c} + \beta_{1,c} V + \beta_{2,c} V^2 + \beta_{3,c} V^3$

Where V is each value, R is the average response to that value, and $\boldsymbol{\beta_q}$ and $\boldsymbol{\beta_c}$ are the fit coefficients for the quadratic and cubic fits respectively. We focused the analysis on $\beta_{2,q}$ and $\beta_{3,c}$ (hereafter called β_2 and β_3). To examine the effects of value range on the tuning curvature, we compared the distributions of β_2 and β_3 across each value range (Wilcoxon signed rank test). We also compared β_2 and β_3 for each response across blocks for all range transitions and computed the Pearson correlation for each coefficient across blocks.

The wide range condition contained a greater number of unique V than the high or low ranges, which may constrain the fit. In particular, if responses are roughly linear with a small, constant floor effect, the fit obtained for the wide range will appear more linear. In order to compare the ranges in a balanced way, we repeated the quadratic and cubic fits for the wide range using a subsampled set of values, equivalent to the value distribution in the low range. This procedure let us look at the effects of range on tuning curvature for equally constrained fits.

3.2.10 Simulation

We constructed a simple linear model of decision-making to explore the effect of baseline firing rates on choice behavior. The model consisted of a population of 10,000 simulated *offer A* and *offer B* neurons (5000 units per group). Each unit encoded *offer value* in a linear way, such that the response of unit *i* on trial *t* was:

$$R_{i.t} = V_t * (R_{max} - R_{BL}) + R_{BL} + c_{i,t}$$

where R_{BL} is the baseline activity, R_{max} is the maximum response of the unit, V_t is the value of the encoded juice on trial *t*, and $c_{i,t}$ is a noise term for unit *i* on trial *t*. Units of R and V are arbitrary.

Importantly, trial-to-trial variability was correlated across the population, reflecting the presence of noise correlations (r_{noise}) in OFC *offer value* neurons (Conen and Padoa-Schioppa 2015). We generated a realistic correlation matrix **Q** for the population as described previously (Hardin et al. 2013; Conen and Padoa-Schioppa 2015). We set mean(r_{noise}) = 0.01 for units encoding the same juice and mean(r_{noise}) = 0 for units encoding different juices. To generate the vector of noise terms $\mathbf{c_t}$ for the population on each trial, we generated values of uncorrelated noise $\mathbf{u_t} \sim$ N(0,1). This was multiplied by the correlation matrix and scaled according to the Fano factor (F) and the mean response for the current offer type ($\langle R_v \rangle$) to obtain $\mathbf{c_t}$:

$$\mathbf{c_t} = \mathbf{Q}\ \mathbf{u_t}\ \langle R_v \rangle\ (F)^{0.5}$$

the scaling factor $\langle R_v \rangle\ (F)^{0.5}$ accounts the observation that the variance in firing rate is proportional to the mean response.

Using this model, we simulated choice behavior for increasing values of R_{BL}. We considered two scenarios: 1) units had a fixed R_{max} or 2) units had a fixed activity range (R_{max} - R_{BL}). For convenience, we defined R_{max} = 1 for the first scenario and (R_{max} - R_{BL}) = 1 for the second. Each simulation consisted of 1000 trials, and the decision on each trial was determined by the difference in the net activity of the *offer value A* and *offer value B* units. The value of each juice for a given trial was a randomly chosen integer ranging from 0 to 10. In both scenarios, we simulated the choice pattern for the neural population as values of R_{BL} increased from 0 to 1. We repeated the simulation for five different values of F and ran the simulation 20 times for each value of F and R_{BL}. We defined the "reward fraction" as V_{chosen}/V_{best} for each trial, where V_{best} was the higher of the two offered values. Choice performance in each condition was assessed

based on the average reward fraction across trials. Note that chance value for the reward fraction is >0.5, since the lower value option on each trial still has $V > 0$.

3.3 Results

3.3.1 Value range influences choice behavior

To examine the features of value adaptation, we trained animals to perform a modified version of a juice choice task (Fig.3.1a). The task consisted of 2-3 blocks of ~250 trials. Within each block, the monkey was presented with a series of choices between two juices, A and B. The quantity of juice offered varied pseudorandomly within a set range, defined by a minimum and maximum value (V_{min} and V_{max}). Each juice could be offered in a "high", "low", or "wide" range (see Methods). Between blocks, the range of available offers changed in one of six ways: V_{max} increase/decreased, the V_{min} increased/decreased, or V_{max} and V_{min} increased/decreased concurrently while (V_{max} - V_{min}). The range of the two juices could change in either the same or opposite directions.

We analyzed the animals' behavior separately in each range block. Using logistic regression, we fit the choice behavior with a sigmoid function, which provided a measure of behavioral steepness (η) and relative value (ρ) in each block (see Methods). The monkeys' decisions showed a quality-quantity tradeoff between the juices. The relative value of the juices (ρ) ranged from 1.1 to 5.0 across sessions, with mean(ρ) = 2.4. Within a session, ρ was strongly correlated across blocks (r = 0.73, p = 5.5E-35, Pearson correlation) (Fig.3.1b). Values of ρ increased slightly over the course of the session, reflecting the animal's increasing satiety (median $\Delta\rho$ = 0.07 across blocks; p = 0.01, Wilcoxon signed rank test). Choice behavior was moderately affected by the value range (Fig.3.1cd). Relative values were generally slightly greater in high and wide range

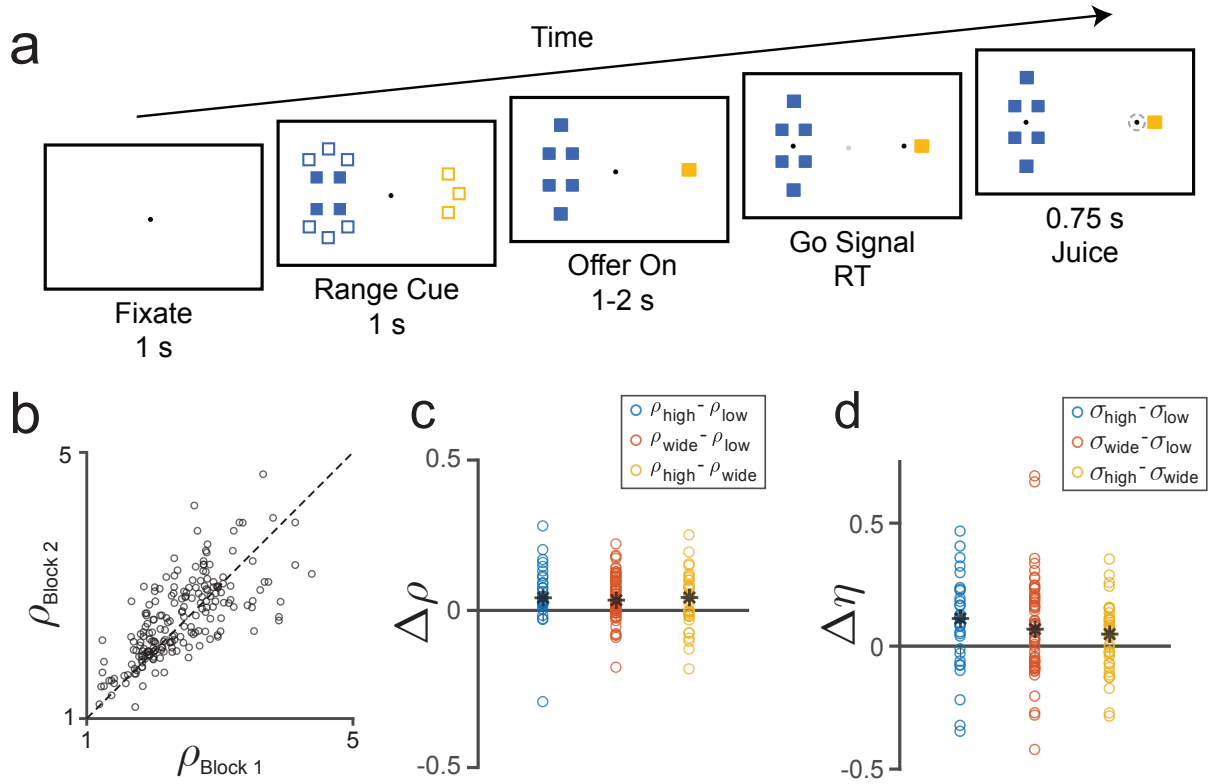

Figure 3.1 Range adaptation task and behavioral results. (A) Time course of a trial. The animal initiates the trial by fixating on a central point. After 1s, range cues appear on either side of the central fixation. Filled squares indicate the minimum possible offer for a given juice and total squares indicate the maximum. After 1s, the cues are replaced by two sets of filled squares representing the current offers. After a variable interval (1-2s), the central fixation disappears, and targets appear next to each offer, cuing the monkey to indicate his choice. The monkey then makes a saccade to one of the targets and holds fixation for 0.75s, after which he receives the selected juice. Each session consists of 2-3 range blocks, each with ~250 trials. Ranges remain constant across trials within each block. (B-D) Choice behavior across sessions. Each point represents the behavior from one pair of blocks in a session (n=205). (B) Relative value in the earlier vs. later block of a session. Values of ρ were strongly correlated across pairs of blocks in a session (r = 0.73 , p = 5.5E-35, c) and slightly elevated in later blocks (median $\Delta\rho = 0.07$; p = 0.01). (C) Fractional difference in ρ across range types. Median differences: ρhigh-ρlow = 0.040 (p = 2.3E-4), ρwide-ρlow = 0.032 (p = 8.3E-5), ρhigh-ρwide = 0.041 (p = 0.54). (D) Fractional difference in sigmoid steepness across range types. Median differences: ηhigh-ηlow = 0.11 (p = 7.7E-3), ηwide-ηlow = 0.069 (p = 4.2E-3), ηhigh-ηwide = 0.049 (p = 0.14). Black asterisks indicate median fractional differences. All p-values Wilcoxon signed rank test.

blocks compared to low (Fig.3.1c, p = 2.3E-4 and p = 8.3E-5, Wilcoxon signed rank). In addition, high and wide range blocks had steeper sigmoid functions than low range blocks (Fig.3.1d), indicating greater decision variability. High range blocks tended to have slightly steeper sigmoids than wide blocks, but this effect was not significant (p = 0.14).

3.3.2 Neural responses adapt to maximum and minimum values

We recorded 1262 cells from two monkeys as they performed the range adaptation task (monkey D, left hemisphere: 480 cells; monkey F, left hemisphere: 373 cells, right hemisphere: 409 cells). We analyzed the activity of these neurons in seven time windows after offer onset, and we defined a neuronal response as the activity of one neuron in one time window across two range blocks. Modifying the approach used in previous studies (Padoa-Schioppa and Assad 2006), we identified value-related responses and classified responses as encoding *offer value A, offer value B, chosen value*, or *chosen juice* (see Methods). 488 neurons encoded a decision-related response in at least one time window (monkey D: 248 cells, 51.7%; monkey F: 240 cells, 30.7%). We identified 1917 decision-related responses, 984 of which encoded the *offer value* or *chosen value* (Table 3.1). Out of these, a total of 644 value-encoding responses met inclusion criteria for our analysis of adaptation (see Methods).

We considered three basic hypotheses in our analysis of adaptation: 1) responses would adapt to V_{max} only, 2) responses would adapt to both V_{max} and V_{min}, or 3) responses would not adapt. In broad terms, responses adapt to a parameter if changing that parameter alters the tuning function. Changes of this sort could be seen in individual responses for all types of range transition (Fig.3.2). Responses across the population were highly variable (Fig.3.3a-c), but consistently showed adaptation to both maximum and minimum values. Notably, this adaptation does not

appear “complete”: the range of firing rates is different across range types, indicating that neural activity does not remap completely to different conditions. This is seen most clearly in (Fig.3.3d): although the three range types have distinct tuning curves, the minimum response is increased in the high range compared to the others. Likewise, the maximum response in the low range is decreased compared to low and high.

Table 3.1 Number of responses encoding each variable for Monkeys D and F. Later analyses focused on *offer value* and *chosen value* responses. Values in parenthesis indicate the number of responses that met inclusion criteria.

Response	**Monkey D**	**Monkey F**
Offer Value A	242 (160)	123 (75)
Offer Value B	116 (78)	88 (51)
Chosen Value	249 (173)	166 (107)
Chosen Juice	578	355

3.3.3 Activity ranges do not completely remap

To examine value adaptation quantitatively, we focused on three features of the response function: the slope of encoding (s), the response to V_{min} (R_{min}) and the response to V_{max} (R_{max}). We analyzed changes in the tuning slope (s) in two ways. First, we compared the slope directly across changes in V_{max}, V_{min}, or both (Fig.3.4a-c). On average, s was generally greater in high and low value ranges compared to the wide range, consistent with the hypothesis that neurons adapt to both maximum and minimum values (high vs. wide: p = 1.7E-7; high vs. low: p = 7.3E-8; Wilcoxon signed rank test). Responses also showed slightly higher slopes in the low range condition relative to the high (p = 4.3E-7, Wilcoxon signed rank test). While this is consistent

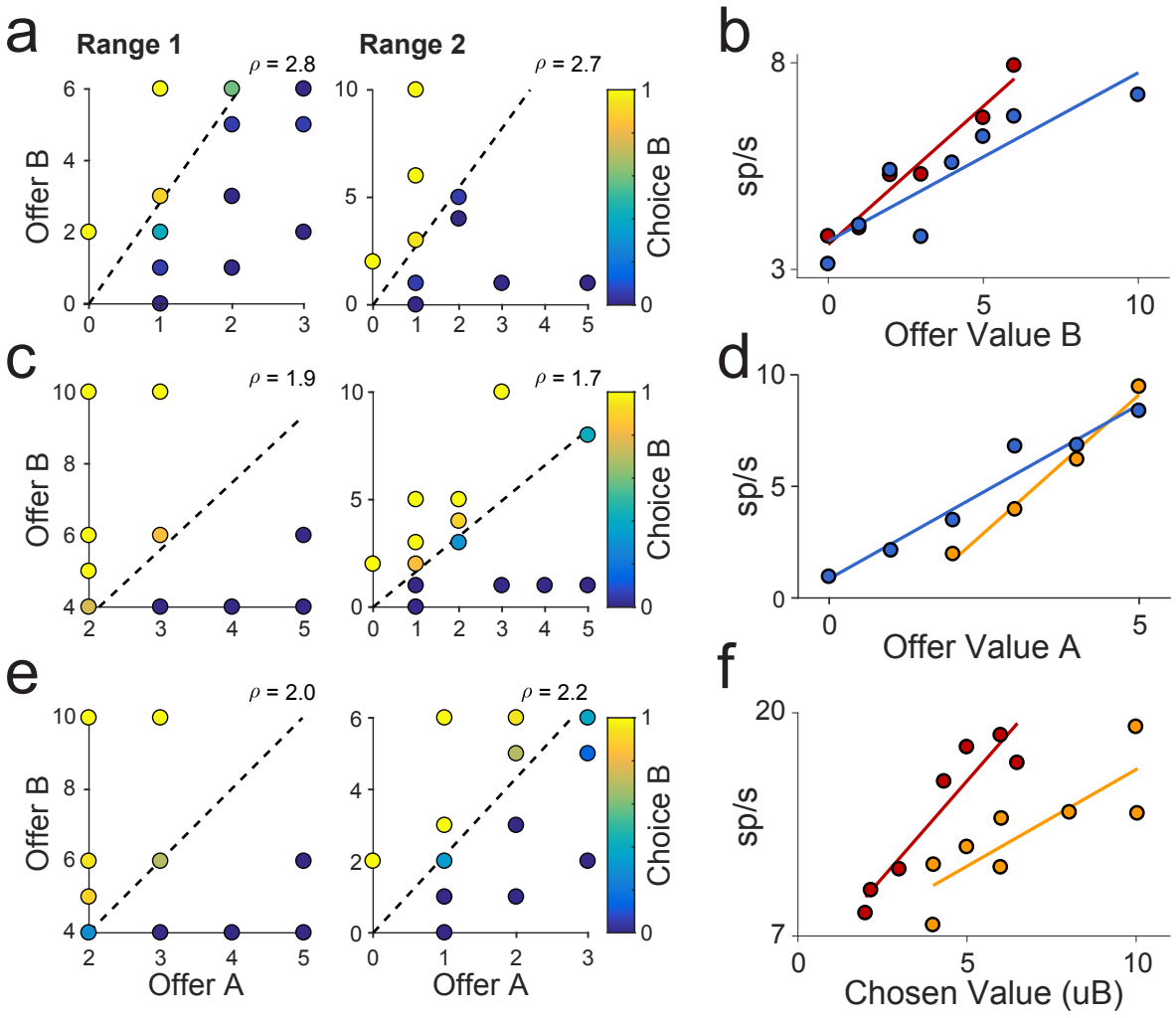

Figure 3.2 Examples of behavior and neuronal activity for three types of range transition. (A,B) Increase in maximum value. (C,D) Decrease in minimum value. (E,F) Decrease in both.(A,C,E) Choice behavior. Each point represents an offer type. Quantity of offer A is shown on the x-axis and quantity of offer B on the y-axis. The color of each point indicates the fraction of trials the animal chose juice B. (B,D,E) Neural activity across the two range blocks. Colors indicate range type (red = low range; blue = wide range; yellow = high range). Responses encode offer value B (B), offer value A (D), and chosen value.

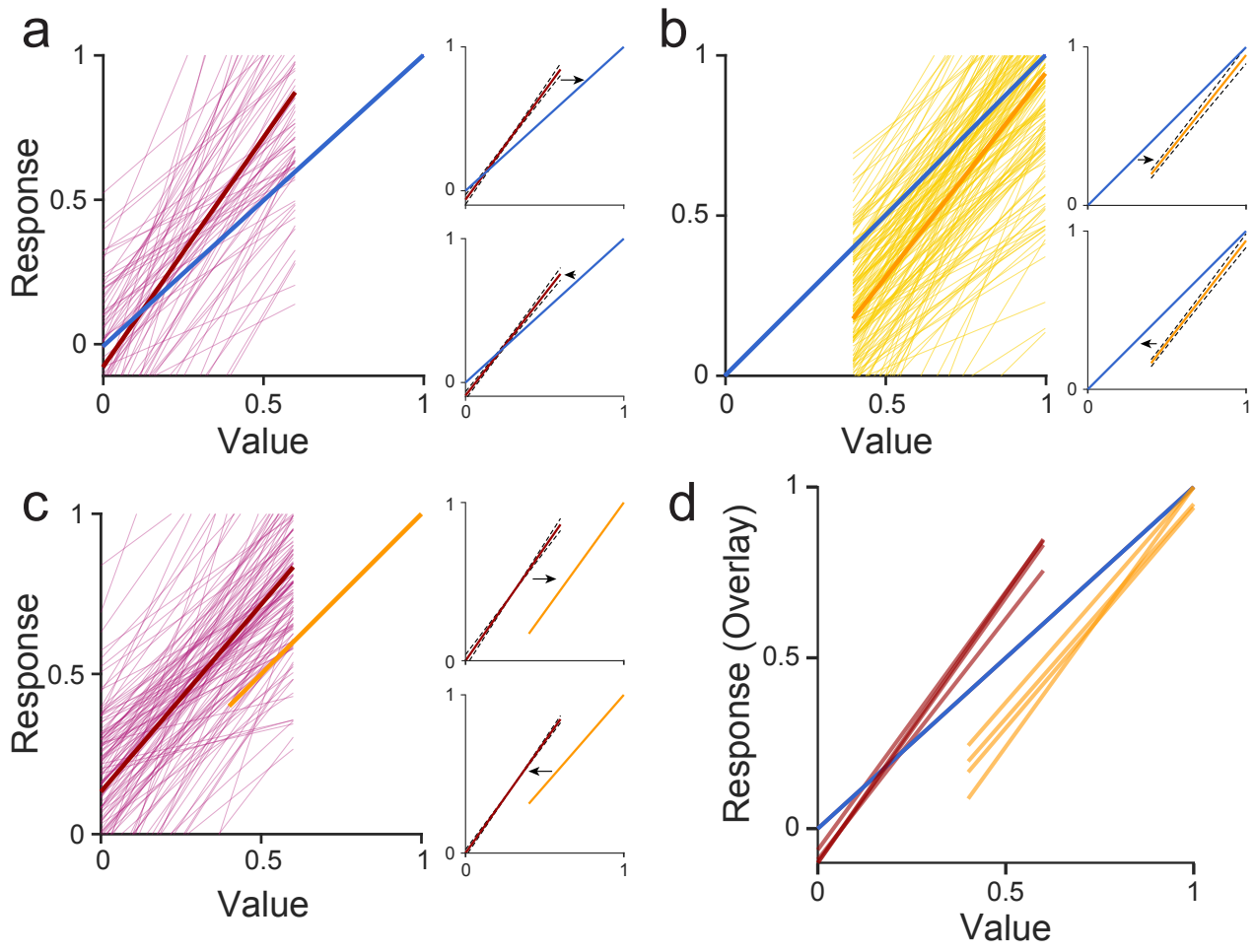

Figure 3.3 Adaptation in offer value responses across each type of range transition. (A-C) Individual responses (light lines) and population mean (dark line) for (A) change in maximum value (n = 72); (B) change in minimum value (n = 163); or (C) change in both (n = 129). Insets show average responses for transitions where Vmax and/or Vmin increase (top) or decrease (bottom). Dotted lines show ± SEM. Responses are normalized to the wide range (A,B) or high range (C). Insets in (C) are normalized to the Vmax(high) – Vmin(low).(D) Overlay of mean responses for all six types of range transition. Transitions from (A) and (B) are aligned to wide range. Transitions from (A) and (C) are aligned to the low range.

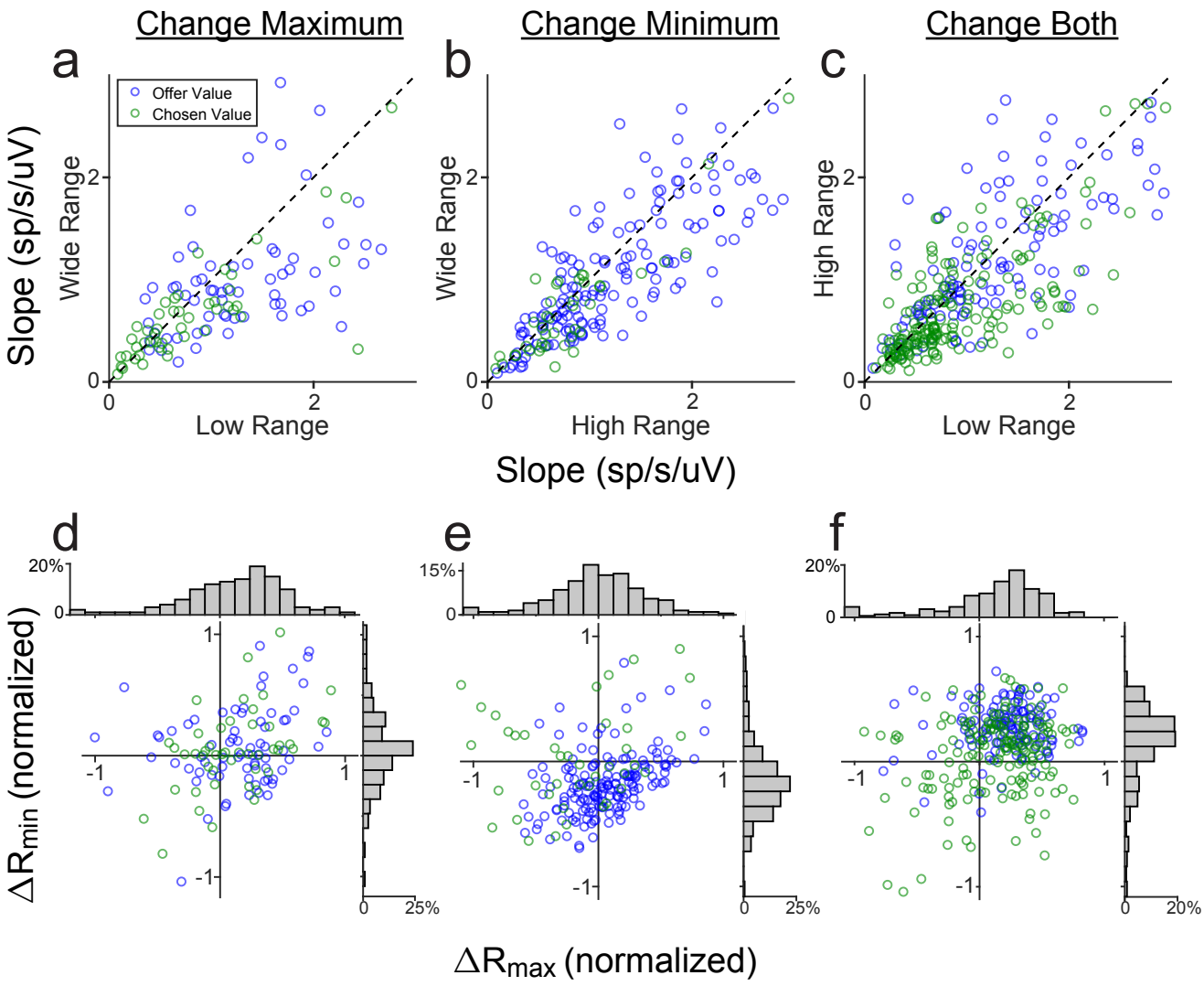

Figure 3.4 Metrics of value adaptation. (A-C) Changes in the slope of value encoding of offer value and chosen value responses. Transition type: (A) maximum value changes (n = 121), (B) minimum value changes (n = 206), (C) both change (n = 317 responses). For chosen value responses, a change in maximum/minimum values was defined as a difference of >0.5 uB. Dashed lines show y=x. Value encoding was generally steeper for low or high value ranges compared to the wide range, though the effect was more obvious for the low value range (high vs. wide: p = 1.7E-7; high vs. low: p = 7.3E-8; Wilcoxon signed rank test). When both maximum and minimum values changed, the encoding slope for high and low value ranges was close to the unity line, but slightly higher for the low value range (p = 4.3E-7, Wilcoxon signed rank test). (D-F) Changes in the response to the minimum and maximum values in following range transitions. Deviation from zero indicates a shift in the neural response range across blocks. Inset histograms show the distribution of ΔR¬min and Δ R¬max. (D) Rwide - Rnarrow, n = 121 response; 2 outliers not shown in plot. (E) Rwide - Rnarrow n = 206 responses; 4 outliers not shown in plot. (F) Rwide - Rnarrow, n = 317 responses; 8 outliers not shown in plot. Values were normalized to Rmax,wide - Rmin,wide for (D,E) and Rmax,high-Rmin,low for (F).

with the idea that responses adapt more to V_{max} than V_{min}, it is difficult to interpret from the slopes alone, as the difference in values (V_{max} - V_{min}) can change from block to block for *chosen value* responses.

We examined the relationship between slope value range using Adaptation Ratios (ARs). We defined ARs for three hypothetical scenarios: adaptation to maximum value (AR_{max}), adaptation to minimum and maximum (AR_{range}), or no adaptation (AR_{none}) (see Methods). ARs provide a measure of the degree of adaptation. If neurons adapt completely to the maximum and minimum values, $AR_{range} = 1$, whereas if they adapt to the maximum only, $AR_{max} = 1$. Note that AR_{none} is simply the ratio of slopes in the two conditions, which should be 1 if responses do not adapt. Since ARs are ambiguous for certain types of range transition, AR=1 does not prove that responses do adapt in a particular manner. However, if AR for a given hypothesis $\neq 1$, it indicates that the response does not adapt completely to the parameters of interest (or in the case of AR_{none}, that responses *do* adapt at least partially to the change in value). Table 3.2 summarizes ARs for each type of transition. A few results are worth noting. First, $AR_{none} < 1$ for all types of range transition, indicating that adaptation consistently occurs. AR_{max} also differs from 1 in nearly all conditions (the only exception occurs in a case where V_{max} changes alone, a transition where AR_{max} and AR_{range} are indistinguishable). The results are closer to adaptation to the range of values ($V_{max} - V_{min}$). However, $AR_{range} > 1$ for responses where the V_{min} changes alone or where V_{max} decreases, indicating that responses do not fully adapt to changes either maximum or minimum values. Overall, the results suggest that responses adapt to both maximum and minimum values, but that the dynamic range does not remap completely.

Analyses of *s* and AR measured changes in the gain of value encoding. However, as Fig.3.3 illustrates, changes in range are accompanied by a change in the overall activity level, which we

refer to as an offset. This offset can be quantified as a change in maximum and minimum responses. We calculated R_{min} and R_{max} using the tuning fit for each range block and found the difference in each value across different ranges (Fig.3.4d-f; Table 3.2). The results confirmed the impression given by the ARs. ΔR_{min} and ΔR_{max} were consistently higher in ranges where V_{min} and V_{max} were higher, regardless of how the range changed. Nevertheless, observed changes in R_{min} and R_{max} were lower than predicted for non-adapting responses. It is worth noting that distributions of ΔR_{min} and ΔR_{min} appear unimodal (Fig.3.4d-f, inset), suggesting a single group of partially adapting neurons rather than a mix of adapting and non-adapting cells.

Table 3.2. Metrics of adaptation in *offer value* and *chosen value* responses across six types of range transition. Columns 1-3: median Adaptation Ratios calculated for three hypotheses: 1) neurons adapt to max value only, 2) neurons adapt to both max and min, 3) neurons do not adapt. If a hypothesis is true, AR = 1. Columns 4-5: median normalized difference in R_{max} and R_{min} between range blocks. Nonzero values indicate a change in neural activity range between sessions (incomplete adaptation). Asterisks (*) indicate a significant deviation from 1 (columns 1-3) or from 0 (columns 4-5). Plus ($^{+}$) indicates that the median ΔR_{min} or ΔR_{max} differs from the prediction for non-adaptive coding. All $p < 0.01$, Wilcoxon signed rank test.

Transition Type	$\boldsymbol{AR_{max}}$	$\boldsymbol{AR_{range}}$	$\boldsymbol{AR_{none}}$	$\boldsymbol{\Delta R_{max}}$	$\boldsymbol{\Delta R_{min}}$
Increase Max	1.04	1.04	0.78*	0.17*,+	0.011
Decrease Max	1.13*	1.13*	0.74*	0.22*,+	0.060
Increase Min	0.83*	1.23*	0.83*	0.029	-0.20*,+
Decrease Min	0.88*	1.39*	0.88*	0.018	-0.19*,+
Increase Both	1.37*	1.04	0.86*	0.22*,+	0.17*,+
Decrease Both	1.27*	0.94	0.82*	0.17*,+	0.19*,+

3.3.4 Adaptation does not affect linearity of tuning

Previous work has found that value encoding in OFC is close to linear, but slightly convex on average (Rustichini et al. 2017). We asked whether range adaptation had any effect on this curvature. We fit each value-encoding response with separate quadratic and cubic regressions for each range condition. As in previous experiments, few responses showed significant quadratic or cubic terms (β_2: 10.6%, β_3: 4.9%; p<0.05, F-test). Across the population, quadratic terms were slightly positive on average (p = 5.8E-56, Wilcoxon signed rank test), while cubic terms were slightly negative (p = 1.6E-3, Wilcoxon signed rank test). The distribution of β_2 did not differ between high and low value ranges (Fig.3.5a; median values: 0.064, 0.61; p = 0.47, Wilcoxon rank sum test) and was slightly lower in the wide range (median: 0.017; p = 9.6E-9 vs. high range, 1.1e-10 vs. low range). However, this difference appeared to arise from the fact that the wide range included a greater number of distinct values, making the fits more constrained. To test this, we recalculated quadratic fits for the wide range using only the subset of values present in the low range. The distribution of β_2 from this subsampled fit did not differ from the high and low ranges (median $\beta_{2,\text{subsampled}}$ = 0.045; both p > 0.1). The distribution of β_3 did not differ across high, low, and wide conditions (Fig.3.5b; median values: -0.014, 1.8E-3, & -3.8E-3; all p > 0.1, Wilcoxon rank sum test).

The same pattern of results was found when we compared β_2 and β_3 for each response across blocks (Fig.3.5c-f). While values of β_2 varied substantially, coefficients for each response were correlated across blocks (see figure legend). This correlation suggests that β_2 may be a characteristic of each neuron's response function. As in the previous analysis, we found that β_2 was slightly higher in narrow ranges compared to the wide range (Fig.3.5e), though this was only significant for changes in V_{max} (median difference= 0.031, p = 1.4E-4, Wilcoxon signed rank

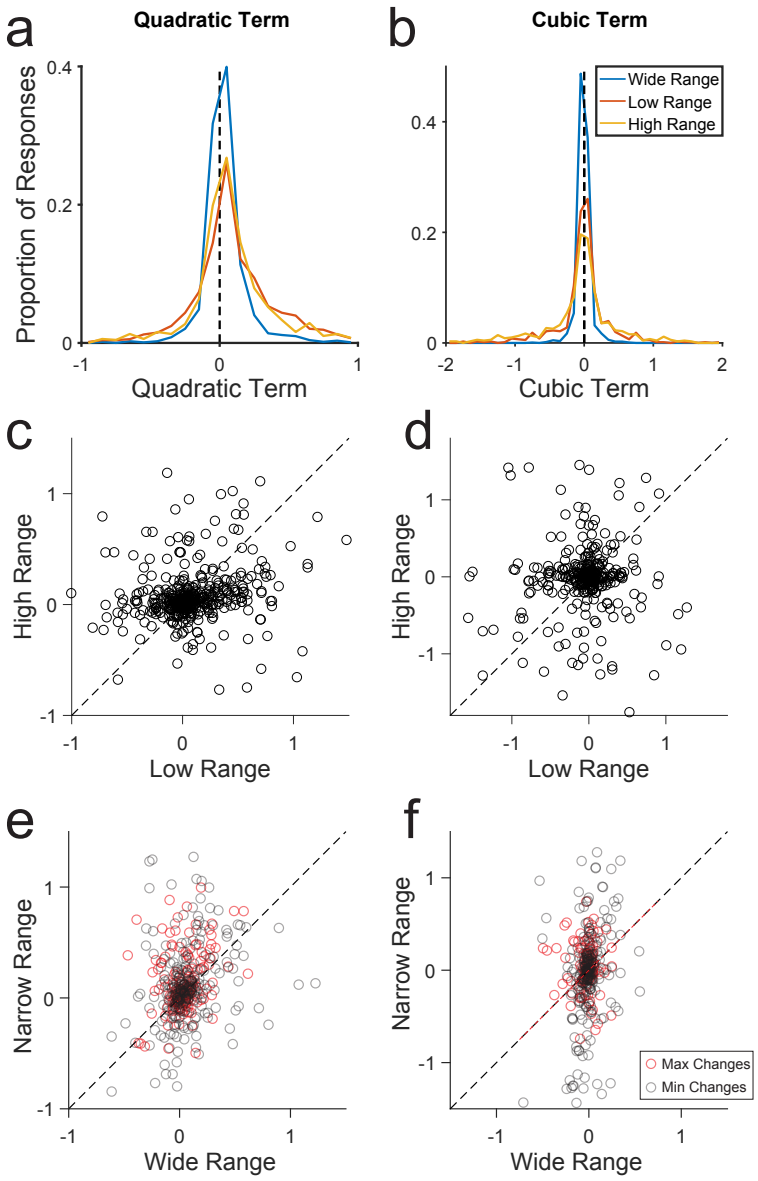

Figure 3.5 Quadratic and cubic tuning parameters. (A,B) Distribution of quadratic (A) and cubic (B) coefficients for all value encoding responses in wide, low, and high ranges. (C-F) Quadratic and cubic coefficients for individual responses across blocks. Each point represents one response. Dotted lines show y=x. Correlation (r) and p-values across each transition type: (C) r = 0.11, p = 1.6E-3; (D) r = 0.048, p = 0.33; (E) r = 0.39, p = 1.4E-4 (change in Vmax); r = 0.35, p = 1.1E-8 (change in Vmin); (F) r = - 0.12, p = 0.12 (change in Vmax); r = 0.24, p = 1.5E-4 (change in Vmin).

test). The effect disappeared when β_2 for the wide range was calculated with subsampled values ($p = 0.39$). Values of β_3 did not differ across any type of range transition (all $p > 0.1$) and did not show a consistent pattern of correlation across blocks. Taken together, these results show that adaptation alters the gain and offset of value-encoding responses, but not their overall functional form.

3.3.5 Adaptation is temporally complete

The observation of partial adaptation in value-encoding responses raises the possibility that adaptation was still ongoing during data collection. To test this, we divided each block in half and computed the tuning function of responses independently in the first and second parts. If adaptation was temporally incomplete, we would expect the response in the second half of Range 2 to show greater changes than the first. In contrast, tuning functions for the first and second halves of Range 2 are nearly identical for all transition types (Fig.3.6), although results were noisy for responses where the maximum value increased (Fig.3.6a). Statistical analysis confirmed that changes in the slope and intercept of the tuning function were present within the first half block of Range 2 (all $p < 0.01$). These results confirm that adaptation occurs relatively quickly after a change in value range, and the features of value adaptation we describe reflect responses at a steady state rather than an unfinished transition in encoding.

3.3.6 Offer value adaptation is influenced by the non-encoded range

The value adaptation task included some sessions the range of juices A and B changed in the same direction (congruent) and other sessions where they changed in opposite directions (non-congruent). This allowed us to ask whether value adaptation in one class of response was affected by changes in the non-encoded juice. We grouped *offer value* responses according to

whether they were recorded during a congruent or non-congruent change in range (n = 214 and 100 responses). We examined the changes in *s*, R_{min}, and R_{max} across blocks for each group (Fig.3.7; Table 3.3). Note that for noncongruent sessions, the total value range of the two juices is comparable across blocks, whereas for congruent sessions the total range changes substantially.

Responses adapted to V_{max} for both congruent and noncongruent transitions, but adaptation to V_{min} in noncongruent sessions was weak or absent. This effect could be seen in both the response gain and change in offset. *s* was significantly different following changes in V_{max} (p = 1.0E-4), but not V_{min} (p = 0.24), although the trend for V_{min} was in the expected direction (Fig.3.7de). When V_{min} and V_{max} changed together, *s* was shallower in the high range compared to the low range, consistent with adaptation to V_{max} only (Fig.3.7f). Median(ΔR_{min}) for when both V_{min} and V_{max} changed was 0.37, compared to a predicted value of 0.4 if neurons adapted to the maximum only (n.s., p = 0.33). However, when V_{min} changed alone, median(ΔR_{min}) was different from predictions for both full adaptation (predicted $\Delta R_{min} = 0$) and no adaptation (predicted $\Delta R_{min} = -0.4$), suggesting that weak adaptation to the V_{min} may still occur with noncongruent transitions. Nevertheless, adaptation to V_{min} was greatly reduced in the noncongruent condition, while adaptation to V_{max} was broadly similar across conditions. Since noncongruent transitions produced minimal change in the total value range, these results suggest that responses adapt to the maximum value of their encoded juice, but may adapt to the minimum of the total range (but see Discussion).

3.3.7 Baseline activity impairs simulated choice behavior

A previous study showed that choice performance improved monotonically with the degree of value adaptation (Rustichini and Padoa-Schioppa 2015). However, this study only considered

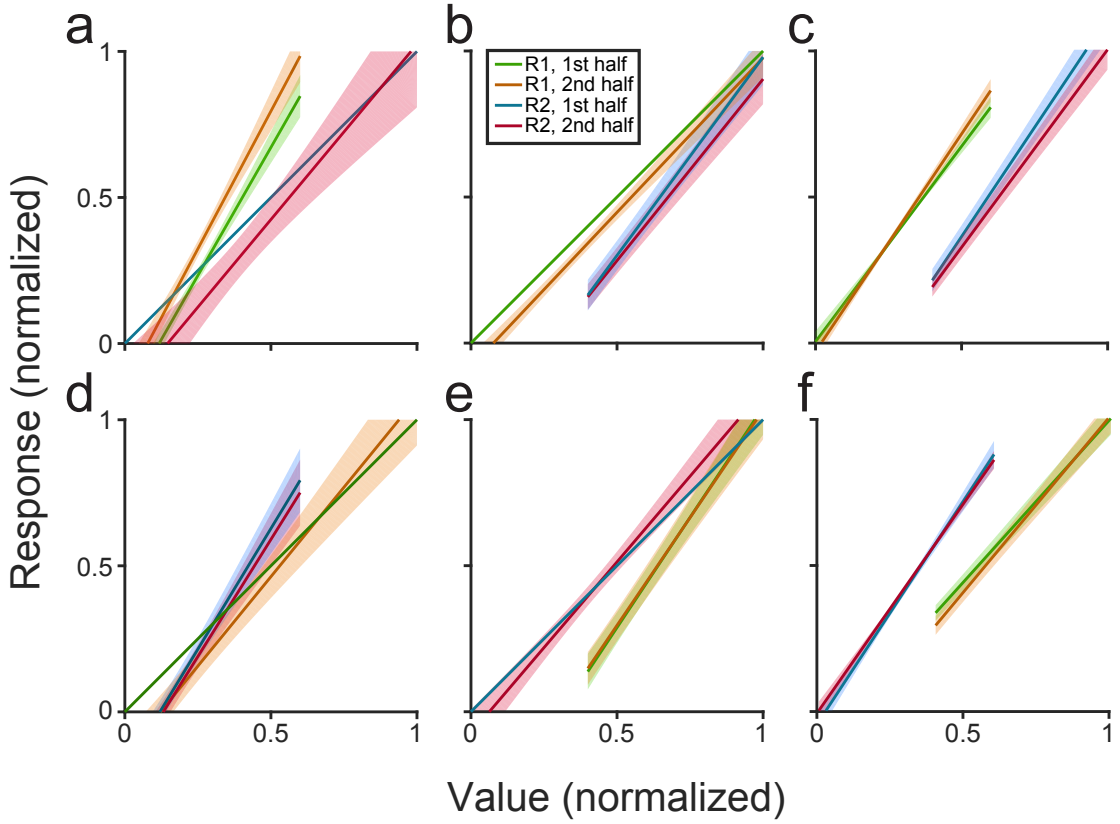

Figure 3.6 Tuning in offer value responses for the first and second half of each block. Transition types: (A-C) Increase in maximum (n = 38) (A), minimum (n = 64) (B), or both (n = 76) (C). (D-F) Decrease in maximum (n = 33) (D), minimum (n = 99) (E), or both (n = 53) (F). Shaded regions indicate SEM. Tuning functions are consistent across the early and late halves of the adapting range block. Colors indicate temporal progression: Range 1, first half (green); Range 1, second half (orange); Range 2, first half (blue); Range 2, second half (red). Responses were normalized to the first half of the wide range block for plotting purposes.

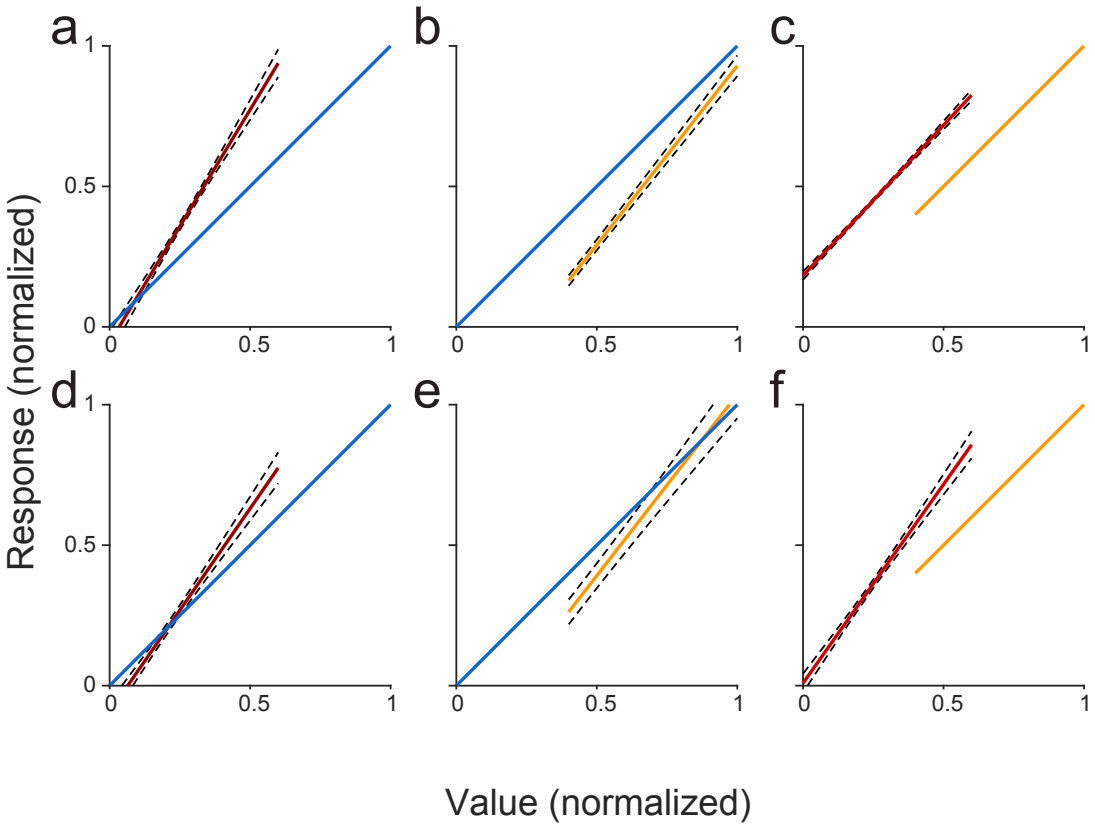

Figure 3.7 Adaptation in offer value neurons for congruent and incongruent transitions. The range of the two juices can change the same direction (A-C) or opposite directions (D-F). (A,D) Change in maximum value. (B,E). Change in minimum value. (C,F) Change in both. Neural responses and values are normalized to the wide range in cases where the maximum or minimum value changes alone (A,B,D,E) and normalized to the high range in cases where both change.

Table 3.3 Median changes in slope, R_{min} and R_{max} following congruent and non-congruent changes in juice range. We define Δs as s_{wide}/s_{narrow} for cases where the maximum or minimum values changes (rows 1-2) and as s_{high}/s_{low} for cases where both change (row 3). Asterisks (*) indicate a significant deviation from 1 (for s) or 0 (for ΔR). Plus ($^{+}$) indicates that the median ΔR_{min} or ΔR_{max} is different from the value predicted for non-adaptive coding. All $p<0.05$, Wilcoxon signed rank test.

Transition Type	***Congruent***			***Non-congruent***		
	Δs	ΔR_{max}	ΔR_{min}	Δs	ΔR_{max}	ΔR_{min}
ΔMax	0.62*	0.14^{+}	6.2E-3	0.72*	$0.33^{*,+}$	0.038^{+}
ΔMin	0.84*	0.065	$-0.20^{*,+}$	0.80	-0.038	$-0.26^{*,+}$
Shift	0.96	$0.24^{*,+}$	$0.25^{*,+}$	0.79*	$0.20^{*,+}$	0.37*

changes in the slope of encoding. Furthermore, the analysis was limited to instances where the minimum offer value was zero, and it assumed that neurons had zero baseline activity. Here we found that value-encoding responses adapt to the minimum as well as the maximum responses and that adaptation involves a shift in R_{min} as well as the slope of encoding. To interpret the behavioral effect of this shift, we need to consider how baseline response levels affect activity in decision-making circuits.

To explore this, we generated a simple linear model of a decision circuit (see Methods). We simulated a value-encoding population that contained 5,000 *offer value A* and 5,000 *offer value B* units. Each unit encoded the value of its preferred juice in a linear way, and trial-to-trial variability was correlated across units, with correlation levels estimated based on previous empirical results (Conen and Padoa-Schioppa 2015). We simulated the responses of this network to a series of choices between two options. The values of options were randomly determined on each trial. The decision was determined based on the activity of the two *offer value* pools. Thus,

on trials where the activity of *offer A* units exceeded that of *offer B* units, juice A was defined as the chosen option.

We examined the choice pattern of the simulated network for varying levels of baseline activity (R_{BL}). We considered two general scenarios: 1) each unit had a fixed $R_{max,}$ so increasing R_{BL} reduced the available dynamic range; or 2) each unit had a fixed activity range ($\Delta R = R_{max} - R_{BL}$), so increasing R_{BL} shifted the dynamic range up. The second scenario is analogous to the shift in R_{min} that we observed for range blocks with higher minimum value. For each scenario, we simulated choice activity for increasing levels of R_{BL}. To assess choice behavior, we calculated the fractional reward rate for every condition, defined as the chosen value divided by the maximum available value for each trial. The average fractional reward across each simulated session provided a metric of choice performance. Note that chance value for the reward fraction is >0.5, since the lower value option on each trial still has $V > 0$. Instead, chance level should be interpreted as the level of behavioral performance when $R_{BL} = R_{max}$, i.e. is the fraction of reward obtained when $R_{BL} = 1$ in scenario 1 (Fig.3.8a).

In both scenarios, reward acquisition decreased with increasing values of R_{BL} (Fig.3.8). This effect was stronger for simulations using a higher Fano factor (F). Despite this general pattern, the overall impairment was relatively minor for simulations where R_{max} could shift. The fractional reward level in this condition was >0.95 even for R_{BL} equal to or exceeding the total response range (Fig.3.8b). In the context of range adaptation, these results suggest that a shift in the offset of the tuning function may have little effect on behavior, whereas a change in ΔR may substantially alter choice performance.

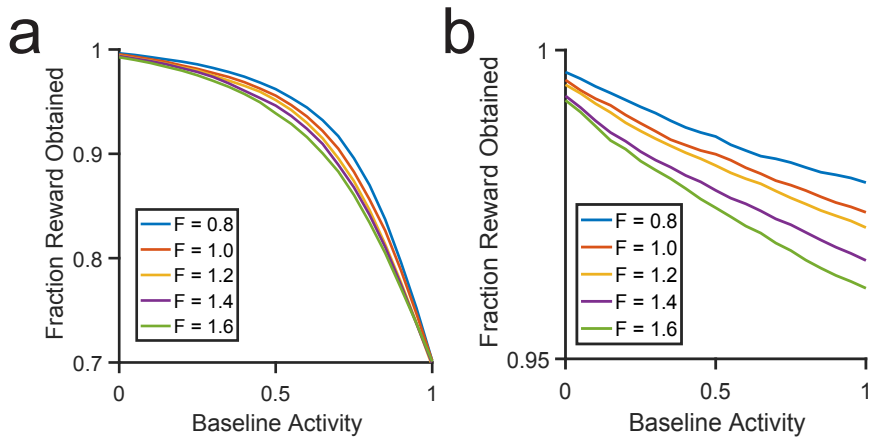

Figure 8. Choice simulation. Decrease in reward acquisition with baseline activity. Reward level is computed as a fraction of optimum outcome. (A) For neurons with a fixed maximum value, reward acquisition decreases substantially in a nonlinear manner as the baseline response increases. (B) For neurons with a fixed range, reward acquisition decreases mildly as baseline activity increases. Trace colors indicate results simulated for different Fano factors. Each curve shows the mean of 20 simulated sessions.

3.4 Discussion

In this study, we examined how OFC neurons adapt to changes in the value distribution during a juice choice task. We found that neurons adapted to changes in both maximum and minimum values. Notably, while responses showed consistently higher gain in blocks with a narrow (high or low) value range, neural activity range did not remap completely to the current value distribution. Instead, the range of activity shifted depending on the current range, creating an offset in the overall response level. The highest firing rates were not observed in blocks with a low value range, and the lowest firing rates were not observed during a high range. As a result, value encoding responses fall in an intermediate zone between fully adaptive coding and absolute value coding (no adaptation). Importantly, this result did not reflect an unfinished time course of adaptation, as tuning functions reached a steady state within the first half of each range block.

Although this experiment is the first to look explicitly at changes in response offset, previous studies have also reported intermediate adaptation in prefrontal areas. Kobayashi et al. observed range-dependent changes in the gain of value encoding neurons in several sub-regions of OFC (Kobayashi et al. 2010). While they divided neurons into as adapting, non-adapting, or partially adapting groups, their results were also consistent with a single, variable population of partially adapting responses. In human subjects, Burke et al. also found partial adaptation in the BOLD signal in ventromedial prefrontal cortex (vmPFC) using a decoding approach (Burke et al. 2016). Taken together, these findings suggest that partial adaptation may be a reliable characteristic of coding in prefrontal cortex.

3.4.1 Offsets in the activity range are inefficient

The presence of an offset in adapted tuning curves somewhat contradicts the predictions of a previous study, which showed that maximal linear adaptation was necessary for optimal choice behavior (Rustichini et al. 2017). The results of our simulation confirmed that increasing the offset of the activity range can impair decision making, particularly when this increase leads to a reduction of the dynamic range. Given this inefficiency, it is worthwhile to consider a few potential explanations for the presence of an offset.

One possibility is that neurons adapt to the range of received values rather than the range of offers. This hypothesis is consistent with the results from our analysis of noncongruent changes in range. When the juice ranges change in opposite directions, adaptation to the minimum value is limited or absent, while adaptation to the maximum value is preserved. Importantly, when juice ranges are noncongruent, low offer values for lower-range juice will never be chosen, as the higher-range minimum consistently outranks it. Thus, if adaptation depends on the received values of each juice, responses will never adapt to this low minimum. In contrast, when ranges are congruent, the minima of the two juices change together, ensuring that the minimum received values change across blocks. This interpretation is supported by results from an fMRI study by (Burke et al. 2016), which found that the BOLD signal in vmPFC adapted to the range of received – but not observed – outcomes. However, this explanation only accounts for adaptation to the minimum value. It cannot explain the offset in response to the maximum value or the fact that intermediate adaptation was also found in *chosen value* responses.

Alternatively, value adaptation may be affected by the overall task structure. Monkeys were highly trained on the range adaptation task, and they were familiar with all possible transitions between the high, low and wide ranges. While complete adaptation would allow for an efficient

representation of values within a block, it would limit the circuit's ability to respond when the value range changed. In contrast, intermediate adaptation reserves a portion of the dynamic range for new values that may appear after a transition. This interpretation suggests that value encoding depends on at least two components: a slow, learning-based process that draws on contextual knowledge; and a more rapid adaptive component that adjusts to the locally experienced value range.

Finally, intermediate adaptation may allow the circuit to maintain information about the current contextual value. Information about the current contextual value makes it possible to predict future reward expectations and affects subjects' motivation to engage in the task. Moreover, effective value comparison in an adapting network requires information about the distribution of available values as well as neural activity levels on a given trial. Without some mechanism for maintaining this information, signals are ambiguous across contexts and cannot guide behavior effectively (Fairhall et al. 2001; Rustichini et al. 2017). The differences in response offset that we observed in OFC may be used by the network to help distinguish the current value state.

3.4.2 Decoding adapted responses

The presence of adaptation in the decision circuit presents a puzzle. If *offer value* neurons adapt to the range of their encoded juice, then the decision process cannot rely on a direct comparison of firing rates for the two populations. In previous work, we proposed that the decision circuit could compensate for this change by adjusting the synaptic weights of neurons at the decoding stage (Rustichini and Padoa-Schioppa 2015; Rustichini et al. 2017). However, this mechanism is not sufficient if responses adapt to the minimum value as well as the maximum. Adaptation to the minimum value involves an additive component as well as a multiplicative one, which single scaling factor cannot adjust for. One possibility is that neurons downstream of *offer value* cells

may adjust their input/output relationship in a more complex way. For example, if noise in the synaptic currents of these neurons increased by some mechanism, that would increase the gain of response specifically to lower value inputs (Hô and Destexhe 2000; Chance et al. 2002).

Notably, this scaling problem does not exist if neurons adapt to the minimum value of both options as opposed to their preferred juice alone. Interestingly, our results are consistent with this hypothesis. When we analyzed noncongruent range transitions, we found that *offer value* responses adapted to the *maximum* value of their encoded juice, but that adaptation to the *minimum* value was reduced or absent. This result would be expected if neurons adapted to whichever minimum was lower across the two juices. However, this result has other possible interpretations (see above), and a more target experiment is necessary to distinguish between adaptation to the total minimum or to the chosen minimum in value-encoding cells.

3.4.3 Potential mechanisms of value adaptation

Value adaptation involves both an additive and a multiplicative component. While adaptation to the maximum can occur via a simple change in gain, adaptation to the minimum requires both a change in gain and a horizontal shift in the response function. When the difference between maximum and minimum values is constant, adaptation is purely horizontal: the slope of encoding remains the same, but responses remap to a new set of values. Although this study design does not allow us to investigate the physiological mechanism of adaptation directly, there are a few possibilities to consider. Additive changes in activity often arise from changes in hyperpolarization or shunting inhibition (Holt and Koch 1997; Chance et al. 2002). In the context of this study, shunting effects are slightly more probable than hyperpolarization, as we did not see any range-dependent effect on pre-trial activity. Alternate explanations, such as cell-intrinsic changes in membrane conductivity, generally involve a mixture of additive and multiplicative

effects, which is difficult to reconcile with the purely additive adaptation we observed during high-to-low range transitions (Sanchez-Vives et al. 2000a, 2000b). The multiplicative component of value adaptation could arise from several potential mechanisms. Changes in gain can be produced by both cell-intrinsic mechanisms, such as changes in ionic conductance (Higgs 2006; Díaz-Quesada and Maravall 2008; Mease et al. 2013), and by circuit-level changes in inhibitory activity (Olsen et al. 2012; Wilson et al. 2012; Natan et al. 2017) or the background level of synaptic activity (Chance et al. 2002). Short-term depression can also induce changes in gain. Though the time course of STD is generally faster than value adaptation, a longer component lasting tens of seconds has also been observed (Varela et al. 1997; Kohn 2007).

A recent study examining a more medial region of OFC found that adaptation to simultaneously presented values was best explained by a divisive normalization model (Yamada et al. 2018). The data from our study, which reflect a slower across-trial form of adaptation, do not appear to follow a similar model. Among other features, the divisive normalization model predicts a decrease in the maximum response in conditions with a higher value range, which we do not observe. Divisive normalization is a common form of adaptation in sensory regions (Valerio and Navarro 2003; Wark et al. 2007; Olsen et al. 2010; Beck et al. 2011; Ohshiro et al. 2011), and it is highly effective at maximizing sensory information across a wide variety of stimuli (Simoncelli and Schwartz 2001; Wainwright et al. 2001; Carandini and Heeger 2011). However, it may not be well-suited for contextual adaptation to changes in value, which should maximize high-reward choices rather than by maintain high resolution stimulus information (Rustichini et al. 2017).

3.4.4 Discrepancies in behavioral results

In this experiment, we observed range-dependent changes in both relative value and the steepness of choice behavior. The increase in relative value during higher-value blocks is consistent with a small nonlinearity in the utility function of the two juices, leading to a greater proportion of A choices when the values of both options increased. This type of nonlinearity in utility has been observed previously in primate decision making (Pastor-Bernier et al. 2017). The changes in steepness are somewhat more surprising, as they contradict results from previous work (Rustichini et al. 2017). A recent analysis of behavior across different ranges found that decision patterns were generally noisier during blocks with higher maximum values, consistent with the idea neurons encoded value with lower resolution during these blocks. The current study finds a change in the opposite direction: steeper encoding during the wider value range. This result may partially arise from differences in the relative value across blocks, which shifted choices toward juice A in the wide block. However, this explanation is not completely satisfactory. Experiments that more carefully match value matrices and decision patterns across blocks may be necessary to resolve this question.

In summary, we examined how the neuronal representation in the OFC adapted to changes in maximum and minimum of the value distribution. We found that both maximum and minimum values influence the gain of value encoding, but only partially, leading to an offset in neuronal activity levels across ranges and potentially limiting behavioral performance. Future work is necessary to explore the practical effects of this inefficiency on choice behavior.

3.5 References

Adibi M, **Mcdonald JS**, **Clifford CWG**, **Arabzadeh E**. Adaptation Improves Neural Coding Efficiency Despite Increasing Correlations in Variability. doi: 10.1523/JNEUROSCI.3449-

12.2013.

Beck JM, **Latham PE**, **Pouget A**. Marginalization in Neural Circuits with Divisive Normalization. *J Neurosci* 31: 15310–15319, 2011.

Benucci A, **Saleem AB**, **Carandini M**. Adaptation maintains population homeostasis in primary visual cortex. *Nat Neurosci* 16: 724–9, 2013.

Burke CJ, **Baddeley M**, **Tobler PN**, **Schultz W**. Partial Adaptation of Obtained and Observed Value Signals Preserves Information about Gains and Losses. *J Neurosci* 36: 10016–10025, 2016.

Cai X, **Padoa-Schioppa C**. Contributions of orbitofrontal and lateral prefrontal cortices to economic choice and the good-to-action transformation. *Neuron* 81: 1140–51, 2014.

Carandini M, **Heeger DJ**. Normalization as a canonical neural computation. *Nat Rev Neurosci* 13: 51–62, 2011.

Chance FS, **Abbott L.**, **Reyes AD**. Gain Modulation from Background Synaptic Input. *Neuron* 35: 773–782, 2002.

Conen KE, **Padoa-Schioppa C**. Neuronal variability in orbitofrontal cortex during economic decisions. *J Neurophysiol* 114: 1367–1381, 2015.

Cox KM, **Kable JW**. BOLD Subjective Value Signals Exhibit Robust Range Adaptation. *J Neurosci* 34: 16533–16543, 2014.

Dan Y, **Atick JJ**, **Reid RC**. Efficient coding of natural scenes in the lateral geniculate nucleus: experimental test of a computational theory. [Online]. *J Neurosci* 16: 3351–62, 1996. http://www.ncbi.nlm.nih.gov/pubmed/8627371 [22 Feb. 2018].

Díaz-Quesada M, **Maravall M**. Intrinsic mechanisms for adaptive gain rescaling in barrel cortex. *J Neurosci* 28: 696–710, 2008.

Diederen KMJ, **Spencer T**, **Vestergaard MD**, **Fletcher PC**, **Schultz W**. Adaptive Prediction Error Coding in the Human Midbrain and Striatum Facilitates Behavioral Adaptation and Learning Efficiency. *Neuron* 90: 1127–1138, 2016.

Elliott R, **Agnew Z**, **Deakin JFW**. Medial orbitofrontal cortex codes relative rather than absolute value of financial rewards in humans. *Eur J Neurosci* 27: 2213–2218, 2008.

Fairhall AL, **Lewen GD**, **Bialek W**, **De Ruyter van Steveninck RR**. Efficiency and ambiguity in an adaptive neural code. *Nature* 412: 787–792, 2001.

Fellows LK. Orbitofrontal contributions to value-based decision making: Evidence from humans with frontal lobe damage. *Ann N Y Acad Sci* 1239: 51–58, 2011.

Fellows LK, **Farah MJ**. The role of ventromedial prefrontal cortex in decision making: Judgment under uncertainty or judgment per se? *Cereb Cortex* 17: 2669–2674, 2007.

FitzGerald THB, **Seymour B**, **Dolan RJ**. The role of human orbitofrontal cortex in value comparison for incommensurable objects. *J Neurosci* 29: 8388–8395, 2009.

Gutnisky DA, **Dragoi V**. Adaptive coding of visual information in neural populations. *Nature* 452: 220–4, 2008.

Hardin J, **Garcia SR**, **Golan D**. A method for generating realistic correlation matrices. *Ann Appl Stat* 7: 1733–1762, 2013.

Hengen KB, **Lambo ME**, **Van Hooser SD**, **Katz DB**, **Turrigiano GG**. Firing Rate Homeostasis in Visual Cortex of Freely Behaving Rodents. *Neuron* 80: 335–342, 2013.

Higgs MH. Diversity of Gain Modulation by Noise in Neocortical Neurons: Regulation by the Slow Afterhyperpolarization Conductance. *J Neurosci* 26: 8787–8799, 2006.

Hô N, **Destexhe A**. Synaptic Background Activity Enhances the Responsiveness of Neocortical Pyramidal Neurons. *J Neurophysiol* 84: 1488–1496, 2000.

Holt GR, **Koch C**. Shunting Inhibition Does Not Have a Divisive Effect on Firing Rates. *Neural Comput* 9: 1001–1013, 1997.

Kennerley SW, **Behrens TEJ**, **Wallis JD**. Double dissociation of value computations in orbitofrontal and anterior cingulate neurons. *Nat Neurosci* 14: 1581–1589, 2011.

Kobayashi S, **Pinto de Carvalho O**, **Schultz W**. Adaptation of Reward Sensitivity in Orbitofrontal Neurons. *J Neurosci* 30: 534–544, 2010.

Kohn A. Visual adaptation: physiology, mechanisms, and functional benefits. *J Neurophysiol* 97: 3155–3164, 2007.

Krekelberg B, **van Wezel RJA**, **Albright TD**. Adaptation in Macaque MT Reduces Perceived Speed and Improves Speed Discrimination. *J Neurophysiol* 95: 255–270, 2006.

Lewicki MS. Efficient coding of natural sounds. (2002). doi: 10.1038/nn831.

Liu B, **Macellaio M V.**, **Osborne LC**. Efficient sensory cortical coding optimizes pursuit eye movements. *Nat Commun* 7: 12759, 2016.

Mease RA, **Famulare M**, **Gjorgjieva J**, **Moody WJ**, **Fairhall AL**. Emergence of adaptive computation by single neurons in the developing cortex. *J Neurosci* 33: 12154–70, 2013.

Natan RG, **Rao W**, **Geffen MN**. Cortical Interneurons Differentially Shape Frequency Tuning following Adaptation. *Cell Rep* 21: 878–890, 2017.

Ohshiro T, **Angelaki DE**, **DeAngelis GC**. A normalization model of multisensory integration. *Nat Neurosci* 14: 775–82, 2011.

Olsen SR, **Bhandawat V**, **Wilson RI**. Divisive Normalization in Olfactory Population Codes. *Neuron* 66: 287–299, 2010.

Olsen SR, **Bortone DS**, **Adesnik H**, **Scanziani M**. Gain control by layer six in cortical circuits

of vision. *Nature* 483: 47–52, 2012.

Ongur D, **Price J**. The Organization of Networks within the Orbital and Medial Prefrontal Cortex of Rats, Monkeys and Humans. *Cereb Cortex* 10: 206–219, 2000.

Padoa-Schioppa C. Range-Adapting Representation of Economic Value in the Orbitofrontal Cortex By Camillo Padoa-Schioppa Supplementary Figures. *J Neu* 29: 1404–14014, 2009.

Padoa-Schioppa C, **Assad JA**. Neurons in the orbitofrontal cortex encode economic value. *Nature* 441: 223–6, 2006.

Pastor-Bernier A, **Plott CR**, **Schultz W**. Monkeys choose as if maximizing utility compatible with basic principles of revealed preference theory. *Proc Natl Acad Sci* 114: E1766–E1775, 2017.

Peters J, **Büchel C**. Overlapping and distinct neural systems code for subjective value during intertemporal and risky decision making. *J Neurosci* 29: 15727–15734, 2009.

Raghuraman AP, **Padoa-Schioppa C**. Integration of Multiple Determinants in the Neuronal Computation of Economic Values. *J Neurosci* 34: 11583–11603, 2014.

Rich EL, **Wallis JD**. Decoding subjective decisions from orbitofrontal cortex. *Nat Neurosci* 19: 973–980, 2016.

Rudebeck PH, **Murray EA**. Dissociable effects of subtotal lesions within the macaque orbital prefrontal cortex on reward-guided behavior. *J Neurosci* 31: 10569–10578, 2011.

Rustichini A, **Conen KE**, **Cai X**, **Padoa-Schioppa C**. Optimal coding and neuronal adaptation in economic decisions. *Nat Commun* 8, 2017.

Rustichini A, **Padoa-Schioppa C**. A neuro-computational model of economic decisions. *J Neurophysiol* 114: 1382–1398, 2015.

Saez RA, **Saez A**, **Paton JJ**, **Lau B**, **Salzman CD**. Distinct Roles for the Amygdala and Orbitofrontal Cortex in Representing the Relative Amount of Expected Reward. *Neuron* 95: 70–77.e3, 2017.

Sanchez-Vives M V, **Nowak LG**, **McCormick DA**. Membrane mechanisms underlying contrast adaptation in cat area 17 in vivo. *J Neurosci* 20: 4267–4285, 2000a.

Sanchez-Vives M V, **Nowak LG**, **McCormick D a**. Cellular mechanisms of long-lasting adaptation in visual cortical neurons in vitro. *J Neurosci* 20: 4286–4299, 2000b.

Simoncelli EP (New YU, **Schwartz O (New YU**. Natural sound statistics and divisive normalization in the auditory system [Online]. *Adv. Neural Inf. Process. Syst. 13 Proc. 2000 Conf.* http://books.google.com/books?hl=en&lr=&id=Mgs2FwtgNxwC&oi=fnd&pg=PA166&dq=Natural+sound+statistics+and+divisive+normalization+in+the+auditory+system&ots=EJ2L-qjzeD&sig=JdmPOT2u02GUUx_S0E0-WhSwb5U.

Soltani A, **De Martino B**, **Camerer C**. A Range-Normalization Model of Context-Dependent Choice: A New Model and Evidence. *PLoS Comput Biol* 8: e1002607, 2012.

Tobler PN, **Fiorillo CD**, **Schultz W**. Adaptive coding of reward value by dopamine neurons. *Science* 307: 1642–5, 2005.

Valerio R, **Navarro R**. Optimal coding through divisive normalization models of V1 neurons. In: *Network: Computation in Neural Systems*. 2003, p. 579–593.

Varela JA, **Sen K**, **Gibson J**, **Fost J**, **Abbott LF**, **Nelson SB**. A quantitative description of short-term plasticity at excitatory synapses in layer 2/3 of rat primary visual cortex [Online]. *J Neurosci* 17: 7926–7940, 1997. http://www.ncbi.nlm.nih.gov/entrez/query.fcgi?cmd=Retrieve&db=PubMed&dopt=Citation&list_uids=9315911.

Wainwright MJ, **Schwartz O**, **Simoncelli EP**. Natural Image Statistics and Divisive Normalization: Modeling Nonlinearities and Adaptation in Cortical Neurons. *Stat. Theor. brain.* .

Wark B, **Lundstrom BN**, **Fairhall A**. Sensory adaptation. *Curr. Opin. Neurobiol.* 17: 423–429, 2007.

Wilson NR, **Runyan CA**, **Wang FL**, **Sur M**. Division and subtraction by distinct cortical inhibitory networks in vivo. *Nature* 488: 343–8, 2012.

Xie J, **Padoa-Schioppa C**. Neuronal remapping and circuit persistence in economic decisions. *Nat. Neurosci.* 2016.

Yamada H, **Louie K**, **Tymula A**, **Glimcher PW**. Free choice shapes normalized value signals in medial orbitofrontal cortex. *Nat Commun* 9, 2018.

Chapter 4: Adaptation and Noise Correlation in Choice Behavior

In this document, I presented two experiments investigating noise correlation and value adaptation in of OFC networks during decision-making. I found that noise correlation levels were low but unbalanced between different pools of *offer value* pools. After accounting for another known source of choice variability, I found that the noise correlations and choice probabilities measured in OFC were consistent with a decision rule that placed uniform weights on all *offer value* responses. The interaction between this decoding scheme and the pattern of noise correlations limits the information available to the decision-making circuit.

Neural adaptation partially compensates for this limitation. Intuitively, increases in the gain of neural encoding increase performance by enhancing the sensitivity of neuronal responses, increasing the signal-to-noise ratio. However, if the network is uncorrelated, this effect does not necessarily persist at the population level, as the variability of individual responses can be reduced by pooling. In the presence of noise correlations, variability can persist even when responses are combined across a large population. The robustness of this effect depends on both the structure of correlations and the nature of the decoder. In the case of a uniform pooling model, any unbalanced correlation across two competing value-encoding populations leads to noise in the net activity level.

Working with a collaborator, we recently developed a theoretical model to assess the effect of gain adaptation on decision-behavior in the presence of noise correlations (Rustichini et al. 2017). We considered a linear pooling model in which a decision was made by taking the difference in the summed activity of two value-encoding populations. The firing rate of each unit

was a Poisson variable with the mean response proportional to the offer value for the preferred juice. To derive the choice pattern from the model analytically, we approximated each response as a Gaussian. This allowed us to estimate the variance of the population activity in the presence of correlated noise. Both the analytical approach and simulation results showed that noise correlations added stochasticity to the decision pattern, reducing total reward acquisition. Gain adaptation ameliorated this effect, increasing the signal-to-noise ratio of the population response. This result remained true even when decoding required unequal rescaling of read-out weights for the two populations, an adjustment that was necessary maintain consistency in relative values when different options were drawn from unequal value distributions. Furthermore, performance improved monotonically with the degree of gain adaptation, such that the optimal behavioral improvement arose when the slope of encoding was inversely proportional to the value range.

This model considered only changes in the maximum value and assumed that both the minimum value and minimum response were zero. The simulation results I presented in Chapter 3 partially fill this gap, showing that a nonzero response to the minimum value leads to suboptimal choice. However, this analysis did not address the question of how the decision circuit might compensate for differences in the minimum value when making comparisons. While both the model above and the simulations in Chapter 3 can use synaptic rescaling to compensate for differences in the maximum value of options, this adjustment cannot account for differences in the minimum. As discussed in Chapter 3, one possibility is that the circuit adapts to the overall minimum rather than the minimum of each juice. Alternatively, the decoder could effectively subtract the minimum response from its output function and add a downstream bias term to compensate for differences in the minimum.

Despite these uncertainties, the general principles of the (Rustichini et al. 2017) model apply to transitions in the minimum value as well as the maximum. Increasing gain allows for higher resolution value-representations despite the information-limiting effects of noise correlation. Notably, I found only intermediate adaptation to both maximum and minimum values. This finding suggests that while adaptation in OFC does partially compensate for the effects of correlations, the effect is suboptimal. Furthermore, the behavioral effects I observed in Chapter 3 do not align with the predictions of the model for improved performance in narrow-adapted conditions. This finding presents a puzzle that is relatively common in studies of adaptation. Studies of sensory adaptation find effects on the level of both neurons and behavior, but connecting the two directly is often a challenge (Kohn 2007; Solomon and Kohn 2014). Increases in the resolution of single-neuron representations do not always extend to the population level or map onto to behavior in a straightforward way (Solomon and Kohn 2014). Part of the complexity may arise from the existence of several simultaneous adaptation processes affecting behavior at different levels of processing.

4.1 Conclusion

The work presented here provides a more detailed understanding of responses orbitofrontal cortex, and particularly two features of the network that may respectively limit and enhance information processing during decision making. First, I show that noise correlations in OFC have a range-limited structure that interacts with a correlation-blind decoding algorithm to limit information content in the neural population. Second, I find that value-encoding responses in OFC adapt to both maximum and minimum values, a process that permits greater resolution of value encoding in a correlated network. However, this adaptation involves only partial remapping of the dynamic range. The partial nature of adaptation may impose additional limits

on value representation in OFC. Future work will be needed to clarify the relationship between adaptation and choice behavior, and to predict the effects of adaptation and noise correlations in a biophysically realistic model of choice.

4.2 References

Kohn A. Visual Adaptation: Physiology, Mechanisms, and Functional Benefits. *J Neurophysiol* 97: 3155–3164, 2007.

Rustichini A, **Conen KE**, **Cai X**, **Padoa-Schioppa C**. Optimal coding and neuronal adaptation in economic decisions. *Nat Commun* 8, 2017.

Solomon SG, **Kohn A**. Moving Sensory Adaptation beyond Suppressive Effects in Single Neurons. *Curr Biol* 24: R1012–R1022, 2014.